Alfvén-wave regulated Cosmic-ray Hydrodynamics

MASTER THESIS

in

Physics

at the

Institute of Physics and Astronomy
Faculty of Science
University of Potsdam

Submitted by:
Timon Thomas

Supervised by:
Prof. Dr. Christoph Pfrommer

1. Referee:
Prof. Dr. Christoph Pfrommer

2. Referee:
apl. Prof. Dr. Achim Feldmeier

Potsdam, 16 July 2018

Abstract

Cosmic rays are pervasive in different astrophysical environments, where they significantly contribute to the emerging dynamics. They interact predominantly with the ambient medium by small-scale electromagnetic waves, which loose energy through wave-damping processes and heat the surrounding plasma. As a dilute population of charged particles with high energies, their transport cannot described by ordinary hydrodynamic. The scattering between cosmic rays and Alfvén waves enables us to reduce the full kinetic dynamics of the bulk of cosmic rays into a special hydrodynamical framework. Furthermore, as the scattering by Alfvén waves isotropizes the cosmic ray distribution in the rest frame of the Alfvén waves, they are effectively transport with the same velocity as the waves. This effect is called cosmic ray streaming and is described in the energy equation of cosmic ray hydrodynamics. Current numerical solutions of this equation and in particular the implementation of this effect struggle to correctly capture this effect in a consistent manner. In this work we develop a new hydrodynamic transport theory, which adds the flux of cosmic rays as a new dynamical variable. We consider both, pitch-angle scattering and momentum diffusion as realizations of the scattering between cosmic rays and Alfvén waves. This allows us to describe the evolution of cosmic ray energy with a formulation that is Galilean-invariant and energy conserving. We highlight similarities and differences between our derivation and that of radiation hydrodynamics because both resemble each other very closely. The inclusion of Alfvén waves as a new fluid allows us to describe cosmic ray hydrodynamics in a self regulated manner. We demonstrate this using numerical simulations of a few explanatory scenarios.

Zusammenfassung

Kosmische Strahlung ist in verschiedenen astrophysikalischen Umgebungen allgegenwertig, wo sie signifikant zur entstehenden Dynamik beiträgt. Sie interagiert überwiegend mittels kleinskaliger elektromagnetischer Wellen mit dem umgebendem Medium, welches durch Wellendämpfungprozesse geheizt wird. Als eine verdünnte Population von geladenen Partikeln mit hoher Energie kann ihr Transport nicht durch die übliche Hydrodynamik beschrieben werden. Die Streuung kosmischer Strahlen mit Alfvén-Wellen ermöglicht es uns, die volle kinetische Dynamik der Mehrheit der kosmischen Strahlung in einem speziellem hydrodynamischem Bild zu beschreiben. Da die Streuung die Verteilung der kosmischen Strahlung im Ruhesystem der Alfvén-Wellen isotropisiert, werden diese effektiv mit derselben Geschwindigkeit transportiert, wie die Wellen. Dieser Effekt wird Strömung kosmischer Strahlen genannt, und ist in der Energiegleichung kosmischer Strahlen modelliert. Gegenwertige numerische Lösungen dieser Gleichung und insbesondere die Implementationen dieses Effekts haben große Probleme, diesen Effekt korrekt und konsistent zu erfassen. In dieser Arbeit entwickeln wir eine neue hydrodynamische Transporttheorie, welche den Fluss kosmischer Strahlen als eine neue dynamische Variable hinzufügt. Wir berücksichtigen Anstellwinkelstreuung und Impulsdiffusion als Realisierung der Streuung zwischen kosmischen Strahlen und Alfvénwellen. Dies erlaubt es uns, die Energiedynamik kosmischer Strahlung Galilei-invarant und Energie erhaltend zu beschreiben. Wir heben Gemeinsamkeiten und Unterschiede zwischen unserer Herleitung und derer der Strahlungshydrodynamik hervor, da beide eine große Ähnlichkeit besitzen. Die Aufnahme der Alfvén-Wellen als ein neues Fluid, erlaubt uns die Hydrodynamik kosmischer Strahlen in einer selbstregulierten Weise zu beschreiben. Wir zeigen dies durch numerische Simulationen einiger beispielhafter Szenarien.

Most of the presented results are based on Thomas and Pfrommer (2018), which was submitted to MNRAS. I use the present work to explain the used arguments in greater detail and to add omitted calculations, especially in the appendix.

Contents

1 Introduction

Cosmic rays (CRs) are charged particles with large kinetic energies (MeV to EeV). They constitute a non-thermal collisionless particle population that interacts with their surroundings predominantly through electromagnetic fields. As in most astrophysical scenarios the assumptions of magnetohydrodynamics (MHD) and its refinements are applicable, they mostly influenced by a large-scale magnetic field. This field and their charged nature forces them to spiral around field lines. In a collective effect CRs can amplify additional small-scale Alfvén waves whenever CRs deviate from isotropy (Lerche, 1967; Kulsrud and Pearce, 1969). These waves scatter the CR efficiently and thus alter the propagation of CRs. The mere scattering of CRs causes them to spatially diffuse in the same manner as collision between molecules causes Brownian motion. In contrast to Brownian motion, diffusion is anisotropic and directed along the magnetic field lines because of the CRs' gyro motion. Furthermore, the scattering by Alfvén waves causes the CRs to be essentially transported with the waves rather than with the surrounding gas. This effect is called CR streaming and is described in the energy equation of CR hydrodynamics (CRHD) (Zweibel, 2017). Another side-effect of the interaction between CRs and Alfvén waves, a manifestation of the second order Fermi process (Fermi II), can de- or accelerate CRs. Therefore, there is a constant exchange of energy between CRs and Alfvén waves as long as the later are amplified. In contrast to the CRs themselves, these Alfvén waves are capable of efficiently interacting with the thermal medium and heat it via various plasma kinetic effects. This heating and the pressure provided by CRs influence different astrophysical environments.

The first order Fermi (Fermi I) process accelerates particles at collisionless magnetized shocks. A few thermal particles get rapidly scattered on both sides of the shock and gain energy by an effectively recoil-free scattering event at the other (approaching) side, which causes a subsequent crossing of the shock front. This scattering-crossing cycle repeats itself until the scattered particles eventually exit this process. They now have higher energy as the surrounding pool of ordinary thermal particles. Since this process can be mapped onto a diffusion process, it is commonly referred to as diffusive shock acceleration (DSA). The presence of CRs at the shock can modify the local shock structure and even introduce a CR mediated shock precursor (Drury and Völk, 1981; Völk and McKenzie, 1981; McKenzie and Bond, 1983; Jones, 1993).

On the largest scales, these shocks can be situated within relativistic jets from active galactic nuclei or are situated between jets and the intracluster medium (ICM). Once cooling gas falls onto a super-massive black holes, relativistic jets can drive outflows from the center of a galaxy cluster into the ICM. The produced CR are abundant enough such that the subsequent heating of the ICM by Alfvén waves can explain the high temperatures observed even though radiative cooling should be very effective (Guo and Oh, 2008; Wiener et al., 2013; Jacob and Pfrommer, 2017).

In the evolution of disk galaxies CRs have an important role. There, the main sources of CRs are shocks of supernova remnants (SNRs) (Blasi, 2013), wind termination shocks (Seo et al., 2018), and clusters of massive stars (Aharonian et al., 2018). After the latter form or the first supernovae (SNs) explode, CRs are transported along the toroidal magnetic field of the galaxy. As the density of CRs increases and the magnetic field is amplified by a galactic dynamo, the Parker instability buoyantly rises overcritical bubbles of CRs from the galactic plane (Parker,

1966; Rodrigues et al., 2016). This tears the toroidal magnetic field apart and enables CRs to escape into the circumgalatic medium (CGM). In this process, gas is entrained by CRs and is either expelled from or falls back unto the galaxy in fountain flows (Uhlig et al., 2012). During the further evolution of a typical galaxy, SN and wind bubbles of massive star cluster open up the magnetic fields perpendicular to disk. CRs moving along those field lines build up pressure support against gravity and hinder gas from collapsing. This suppresses star formation and can lunch powerful galactic winds (Breitschwerdt et al., 1991, 1993; Hanasz et al., 2013; Booth et al., 2013; Salem and Bryan, 2014; Recchia et al., 2016; Girichidis et al., 2016; Wiener et al., 2017).

Aside of localized versions of the above global galactic effects, low-to-intermediate energy CRs ($\lesssim$ 1GeV) contribute to the dynamics of the interstellar medium (ISM) trough their ionization capabilities. Since dense cold molecular clouds are effectively shielded against UV radiation, CRs are one of main sources of ionization in those environments (Padovani and Galli, 2013). The altered chemistry changes the initial conditions of star formation. In consequence, permeating CRs can even affect star formation in CR dominated ultra luminous infrared galaxies on a global level (Papadopoulos et al., 2011).

Inside the solar system the gyroradii of CRs below ~10 GeV are small enough to be affected by interplanetary magnetic fields and the solar wind. This solar modulation alters the properties of the low-energy CR distribution, such that terrestrial and most of the space-bound CR flux measurements do not reliably probe the properties of CRs in the galactic environment (Potgieter, 2013). The outermost boundary for those effects is expected to be at 100-150 AU, outside of the bow wave/heliopause of the solar wind. Currently the most promising prospect for in situ measurements of the interstellar flux of CRs is the Voyager I probe, which currently travels at a distance of 142 AU away from the Sun. In 2012, Voyager I saw an increase in Galactic and a decrease in heliospheric particle fluxes (Cummings et al., 2016). Since then, Voyager I likely observes low-energy Galactic CRs from our local environment in the ISM. The CR subsystems onboard of the probe are still functional and expected to be so for a few years. Comparing the ground/orbital CR measurements with those of Voyager allows to gain insight into the galactic transport of CRs (Aloisio et al., 2015). We here explicitly exclude a discussion of CR dynamics inside the solar system from our work and focus on those in the ISM, CGM, and ICM.

To understand the emerging dynamics in all those environments a precise description of CR transport is crucial. Current attempts to numerically model these systems struggle to capture CR diffusion and streaming in a numerical consistent, stable, and efficient way. Standard finite-volume methods for simulating CR streaming fail due to a numerical instability. A proposed alternative is to regularize the critical terms (Sharma et al., 2010). This regularization cast the energy equation of CRHD into a nonlinear anisotropic diffusion equation. Numerical implementation of this differential equation type is possible but computationally expensive (Sharma et al., 2010; Meyer et al., 2014; Vaidya et al., 2017, R. Pakmor private communication). To overcome the above problems, Jiang and Oh (2018) propose to describe CR transport with equations similar to those of radiation hydrodynamics (RHD) but miss to give a derivation for their approach. They show numerically that their ad-hoc ansatz is indeed capable of mimicing CR transport. Here, we pick up and refine their idea, in order to develop a new macroscopic transport theory for CRs, which captures the diffusion and streaming effects in a self-regulated framework. We achieve this by deriving a new equation for the flux of CR energy and coupling

both CR energy and flux equations to the energy equations of Alfvén waves. Both are linked through approximative descriptions of pitch-angle scattering and the energy transfer between both participants. Our new formalism restores the old CR transport equation in the asymptotic limit. As the overall derivation is highly inspired by the corresponding way to derive the equations of RHD, we frequently highlight similarities and show up differences between both CRHD and RHD.

We use Heaviside Lorentz units throughout this work and denote $\boldsymbol{ab}$ as the dyadic product of vectors $\boldsymbol{a}$ and $\boldsymbol{b}$.

2 Preliminaries

We recall some of the required basic theory concerning the motions of charged particles and MHD known from textbooks. See for example Sturrock (1994), Kulsrud (2004), and Zank (2014).

2.1. Motion of charged particles

Consider a particle of charge q subject to electromagnetic forces provided by a large-scale magnetic field $\boldsymbol{B}$, small-scale magnetic field $\delta\boldsymbol{B}$, and small-scale electric field $\delta\boldsymbol{E}$. We postpone the definition of the differences between large and small scales. The particle position $\boldsymbol{x}$, its velocity $\boldsymbol{v}$, and its momentum $\boldsymbol{p}$ change according to the relativistically-correct form of Newton's equations:

$$\frac{\mathrm{d}\boldsymbol{x}}{\mathrm{d}t} = \boldsymbol{v}, \tag{2.1}$$

$$\frac{\mathrm{d}\boldsymbol{p}}{\mathrm{d}t} = q\left[\delta\boldsymbol{E} + \frac{\boldsymbol{v}}{c} \times (\boldsymbol{B} + \delta\boldsymbol{B})\right]. \tag{2.2}$$

Both momentum and velocity of the particle are linked by $\boldsymbol{p} = \gamma m\boldsymbol{v}$, where $\gamma = 1/\sqrt{1 - v^2/c^2}$ is the Lorentz factor of the particle.

Let us restrict this situation further and assume that the small-scale fields have small amplitude: $\delta B \ll B$, $\delta E \sim 0$ and that the large-scale magnetic field is aligned with the z axis $\boldsymbol{B} = B\boldsymbol{z}$. In this case, the forces exerted by these fields are small perturbations compared to the forces provided by $\boldsymbol{B}$. We can solve the equations of motion to first order by ignoring the contribution of the small-scale fields. The solution is the

$$\text{unperturbed orbit of a particle:} \begin{cases} x(t) &= \dfrac{v\sqrt{1-\mu^2}}{\Omega}\sin(\Omega t), \\ y(t) &= \dfrac{v\sqrt{1-\mu^2}}{\Omega}\cos(\Omega t), \\ z(t) &= v\mu t, \end{cases} \tag{2.3}$$

where

$$\Omega = \frac{qB}{\gamma mc} \tag{2.4}$$

is the particle's gyrofrequency and the projection of the velocity onto the magnetic field direction μ is called the pitch-angle. The particle's speed v, Ω, and μ are constants of motions in the unperturbed orbit. This trajectory is clearly oversimplified but nevertheless instructive: the particle moves in a helical motion around the large-scale magnetic field. The elapsed time during one complete gyration is given by $2\pi/\Omega$. The typical length scale associated with the gyromotion is $v\,\Omega$ and of the order 0.25 AU for 1GeV protons under ISM conditions ($B = 1\ \mu$G).

We can relax some of our assumptions: consider a magnetic field that slowly changes compared to the gyromotion, meaning that the time and length scale on which $\boldsymbol{B}$ changes are larger than many gyrotimes and -radii. Then, the true particle orbit must change in comparison to the unperturbed orbit in (2.3). Since these changes are slow, the particle will approximately remain in a helical motion even if $\boldsymbol{B}$ differs from $B\boldsymbol{z}$. Consequently, the definitions of Ω and μ remain useful but we have to define them locally: the new orbits are fully described by the local gyro-frequency $qB(x,t)/(\gamma mc)$ and the local pitch-angle $\mu = \boldsymbol{v}\cdot\boldsymbol{b}$, where $\boldsymbol{b} = \boldsymbol{B}/B$ is the direction of the magnetic field.

We can even include the small-scale electromagnetic fields: assume that these fields vary on scales comparable or smaller than the respective values of the gyromotion and are of stochastic nature. Then a single particle will see permanently varying fields. Consequently, these fields will change the particle's Ω and μ over the course of its motion. However, on scales much larger then the gyromotion, the ensemble of particles will not be affected because the ensemble-averaged ($\langle\cdot\rangle$) small-scale fields and hence the associated forces vanish:

$$\langle\delta\boldsymbol{B}\rangle = \langle\delta\boldsymbol{E}\rangle = 0. \tag{2.5}$$

To be mathematically more precise, we can define the large-scale fields as the mean of the total fields and use both terms interchangeably:

$$\boldsymbol{B} = \langle\boldsymbol{B}_{\rm total}\rangle = \langle\boldsymbol{B} + \delta\boldsymbol{B}\rangle, \tag{2.6}$$
$$\boldsymbol{E} = \langle\boldsymbol{E}_{\rm total}\rangle = \langle\delta\boldsymbol{E}\rangle = 0, \tag{2.7}$$

while the deviations from the mean fields are the small-scale fields. The gyrofrequencies and pitch-angles can be defined in the same way as ensemble averages.

Individual trajectories may become complicated, while properties of the whole population remain meaningful. Hence, we now switch to a statistical description of particles. The phase space motion of the distribution of particles is the governed by Boltzmann's equation:

$$\frac{\partial f}{\partial t} + \frac{\mathrm{d}\boldsymbol{x}}{\mathrm{d}t}\cdot\frac{\partial f}{\partial \boldsymbol{x}} + \frac{\mathrm{d}\boldsymbol{p}}{\mathrm{d}t}\cdot\frac{\partial f}{\partial \boldsymbol{p}} = 0, \tag{2.8}$$

where $f = f(\boldsymbol{x},\boldsymbol{p})$ is the number of particles in a phase space parcel of size $\mathrm{d}\boldsymbol{x}\times\mathrm{d}\boldsymbol{p}$ centered around $(\mathbf{x},\mathbf{p})$. Inserting the equations of motion gives:

$$\frac{\partial f}{\partial t} + \boldsymbol{v}\cdot\frac{\partial f}{\partial \boldsymbol{x}} + q\left(\frac{\boldsymbol{v}}{c}\times\boldsymbol{B}\right)\cdot\frac{\partial f}{\partial \boldsymbol{p}} = \left.\frac{\partial f}{\partial t}\right|_{\rm scatt}, \tag{2.9}$$

where we separated the contributions of small-scale fields into the term $\left.\frac{\partial f}{\partial t}\right|_{\rm scatt}$. Both CRs and thermal gas particles are described by this *Vlasov*-equation. In the following, we treat both particle species separately.

Particles in the thermal gas have lower energies (eV to keV scales for thermal particles compared to MeV to EeV scales for CRs) but larger number densities (scales of $n_{\rm thermal}\sim 1\mathrm{cm}^{-3}$ compared to $n_{\rm CR}\sim 10^{-10}\mathrm{cm}^{-3}$). We describe the thermal gas as a fluid and use the standard approximation of ideal MHD for it.The fluid approximation is valid as long as binary-collisions between particles are faster than any time of interest. In this case, Boltzmann's

H-theorem guaranties that the momentum distribution of the particles is highly unstructured and is approximatively given by the Maxwell-Boltzmann distribution:

$$f_{\text{thermal}}(\boldsymbol{v}) = C \exp[-m/(k_{\text{B}}T)(\boldsymbol{v} - \boldsymbol{u})^2], \tag{2.10}$$

where k_{B} is Boltzmann's constant, T is the temperature of the gas, and C is a normalization constant. The quantity $\boldsymbol{u} = \boldsymbol{u}(x, t)$ is the bulk or mean velocity of the thermal gas. Therefore, the whole distribution of thermal particles can be described by a normalization constant, the temperature, and the bulk velocity. In the following we describe the thermal distribution through those three quantities. In the following, we use the letter f for the distribution of CRs.

Boltzmann's theorem is not valid for CRs because these particles do not scatter rapidly with themselves; hence, we cannot assume that CRs follow a Maxwell-Boltzmann distribution. Surprisingly measurements of the CR distribution show that the momentum distribution of CRs is highly unstructured, too. Although, there are minor features contained in the CR distribution, like the CR ankle and knee, the energy carrying bulk of CRs can be approximated by a powerlaw $f(p) \propto p^{-\alpha}$. The powerlaw index α can vary between 4.0 and 4.7 when measured directly at Earth or theoretically inferred for the DSA mechanism.

2.2. Equations of MHD

The three equations of ideal MHD are:

$$\frac{\partial \rho}{\partial t} + \boldsymbol{\nabla} \cdot (\rho \boldsymbol{u}) = 0, \tag{2.11}$$

$$\frac{\partial \rho \boldsymbol{u}}{\partial t} + \boldsymbol{\nabla} \cdot (\rho \boldsymbol{u}\boldsymbol{u} + P\mathbf{1} - \boldsymbol{B}\boldsymbol{B}) = \boldsymbol{f}, \tag{2.12}$$

$$\frac{\partial \varepsilon}{\partial t} + \boldsymbol{\nabla} \cdot [\boldsymbol{u}(\varepsilon + P) - (\boldsymbol{u} \cdot \boldsymbol{B})\boldsymbol{B}] = \boldsymbol{u} \cdot \boldsymbol{f}, \tag{2.13}$$

where $\varepsilon = \rho \boldsymbol{u}^2/2 + \varepsilon_{\text{th}} + \varepsilon_{\text{B}}$ is total energy density, $\varepsilon_{\text{B}} = \boldsymbol{B}^2/2$ is the magnetic energy, $\varepsilon_{\text{th}} = P_{\text{th}}/(\gamma_{\text{th}} - 1)$ is the thermal energy density, P_{th} is the thermal pressure, P is the total (thermal + magnetic) pressure, γ_{th} is the adiabatic index, ρ is the density of the gas, and $\boldsymbol{f}$ are external force densities. We shortly describe the physical meaning of these equations: The

continuity equation in eq. (2.11) states that the total mass is conserved. When all particle sinks and sources are neglected, this is equivalent to the conservation of the total number of particles constituting the gas. As the density can be linked with the normalization constant in eq. (2.10), the continuity equation evolves one of the defining parameters of the Maxwell-Boltzmann distribution. The

equation of motion in eq. (2.12) is the macroscopic version of Newton's second law. It states that the total momentum inside the fluid is conserved up to external forces acting on the gas. The Lorentz force is included by the contributions due to the magnetic pressure $\boldsymbol{B}^2/2$ to the total pressure and magnetic tension $\boldsymbol{B}\boldsymbol{B}$. Note that this equation merely evolves the mean velocity of the gas and not that of individual particles. The

energy equation in eq. (2.13) describes how the total energy evolves. It states that energy is conserved up to work $\boldsymbol{v} \cdot \boldsymbol{f}$ done by external forces. As total energy depends on the thermal energy which by itself depends on the gas temperature, this yields the third and last parameter of the Maxwell-Boltzmann distribution. We can thus fully describe the thermal gas by those three equations.

These equations are incomplete, since no equation states the dynamics of the magnetic field. We here resort to the approximation of ideal MHD and assume infinite conductivity of the gas. It follows that the evolution of the magnetic field is fully described by two equations:

$$\frac{\partial \boldsymbol{B}}{\partial t} + \boldsymbol{\nabla} \cdot (\boldsymbol{B}\boldsymbol{u} - \boldsymbol{u}\boldsymbol{B}) = 0, \tag{2.14}$$

$$\boldsymbol{\nabla} \cdot \boldsymbol{B} = 0, \tag{2.15}$$

where the first equation is the ideal MHD version of Faraday's induction law and the second equation states the absence of magnetic monopoles.

As our main interest lays in the dynamics of CRs, we assume that the solution of these equations are given through numerical or other methods. As CRs interact indirectly with the thermal gas, we show in sec. 3.6.1 how those equations have to be modified to account for the presence of CRs. To this end, we derive additional forces $\boldsymbol{f}$ that are exerted on the gas.

2.3. Alfvén waves

A particular useful technique to analyze the mathematical structure of nonlinear partial differential equations, such as those of ideal MHD, is to linearize them. The first step in this linearization is to introduce small perturbations in all relevant quantities:

$$\rho \mapsto \rho + \delta\rho \qquad \boldsymbol{B} \mapsto \boldsymbol{B} + \delta\boldsymbol{B} \tag{2.16}$$

$$\boldsymbol{u} \mapsto 0 + \delta\boldsymbol{u} \qquad P_{\mathrm{th}} \mapsto P_{\mathrm{th}} + \delta P_{\mathrm{th}} \tag{2.17}$$

and neglecting any external forces. We assume that the perturbations reside on an uniform background gas and take all quantities without a δ to be constant. This situation is approximatively realized if we focus on length scales smaller than the scales on which the actual quantities of MHD change. Thus our the depicted situation is local in Nature. Furthermore, we assume that the sound velocity is constant and that, consequently,

$$\delta P_{\mathrm{th}} = c_{\mathrm{s}}^2 \delta\rho, \tag{2.18}$$

where c_{s} is the isothermal sound speed.

Inserting those replacements into the MHD equations and ignoring all terms that are at least quadratic in a perturbation yields:

$$\frac{\partial \delta\rho}{\partial t} = \rho \boldsymbol{\nabla} \cdot \delta\boldsymbol{u}, \tag{2.19}$$

$$\rho \frac{\partial \delta\boldsymbol{u}}{\partial t} = -c_{\mathrm{s}}^2 \boldsymbol{\nabla}\delta\rho + (\boldsymbol{\nabla} \times \delta\boldsymbol{B}) \times \boldsymbol{B}, \tag{2.20}$$

$$\frac{\partial \delta\boldsymbol{B}}{\partial t} = -\boldsymbol{\nabla} \times (\delta\boldsymbol{u} \times \boldsymbol{B}). \tag{2.21}$$

Taking the time derivative of eq. (2.20) and inserting the other two equations yields:

$$\frac{\partial^2 \delta \boldsymbol{u}}{\partial t^2} = c_\mathrm{s}^2 \boldsymbol{\nabla}\boldsymbol{\nabla} \cdot \delta \boldsymbol{u} - \{\boldsymbol{\nabla} \times [\boldsymbol{\nabla} \times (\delta \boldsymbol{u} \times \boldsymbol{v}_\mathbf{a})]\} \times \boldsymbol{v}_\mathbf{a} \tag{2.22}$$

where the Alfvén vector is $\boldsymbol{v}_\mathbf{a} = \boldsymbol{b} v_\mathrm{a}$ and the Alfvén velocity is

$$v_\mathrm{a} = B/\sqrt{\rho}. \tag{2.23}$$

As these equations are linear in all perturbations, we can express their solutions in terms of the Fourier transform of all occurring quantities. We use the following definition of the Fourier transformation:

$$a(\boldsymbol{x}, t) = \int_{\mathbb{R}} \mathrm{d}\omega \int_{\mathbb{R}^3} \mathrm{d}\boldsymbol{k}\; a(\boldsymbol{k}, \omega)\, e^{i(\omega t - \boldsymbol{k}\cdot\boldsymbol{x})}, \tag{2.24}$$

where $a \in \{\delta\rho, \delta\boldsymbol{u}, \delta\boldsymbol{B}\}$. The new functions $a(\boldsymbol{k}, \omega)$ are called Fourier components of $a(\boldsymbol{x}, t)$.

The most convenient way to express the linearized equations in terms of the Fourier components is to use the replacements:

$$\frac{\partial}{\partial t} \mapsto \mathrm{i}\omega \qquad\qquad \boldsymbol{\nabla} \mapsto -\mathrm{i}\boldsymbol{k}, \tag{2.25}$$

which can be derived from eq. (2.24). Inserting this replacements into the linearized MHD equation links ω and $\boldsymbol{k}$ through a set of coupled linear equations. Those equations can be solved for ω and yield an expression for $\omega = \omega(\boldsymbol{k})$. Only the Fourier components which fulfill this *dispersion relation* have a physical meaning. Any other combination of ω and $\boldsymbol{k}$ do not lead to an approximate solution of the MHD equation and are thus useless for physical models. We reduce the Fourier decomposition to:

$$a(\boldsymbol{k}, \omega) = \delta(\omega - \omega(\boldsymbol{k}))\, a(\boldsymbol{k}), \tag{2.26}$$

and hence have:

$$a(\boldsymbol{x}, t) = \int_{\mathbb{R}} \mathrm{d}\boldsymbol{k}\; a(\boldsymbol{k})\, e^{i(\omega(\boldsymbol{k})t - \boldsymbol{k}\cdot\boldsymbol{x})}, \tag{2.27}$$

Finally, inserting eqs. (2.25) into eq. (2.22) and using Grassmann's identities gives:

$$\omega^2 \delta\boldsymbol{u} = c_\mathrm{s}^2 \boldsymbol{k}\boldsymbol{k} \cdot \delta\boldsymbol{u} - \boldsymbol{v}_\mathbf{a} \cdot [\delta\boldsymbol{u}\,(\boldsymbol{k}\cdot\boldsymbol{v}_\mathbf{a}) - \boldsymbol{v}_\mathbf{a}\,(\boldsymbol{k}\cdot\delta\boldsymbol{u})]\,\boldsymbol{k} + (\boldsymbol{v}_\mathbf{a}\cdot\boldsymbol{k})\,[\delta\boldsymbol{u}\,(\boldsymbol{k}\cdot\boldsymbol{v}_\mathbf{a}) - \boldsymbol{v}_\mathbf{a}\,(\boldsymbol{k}\cdot\delta\boldsymbol{u})] \tag{2.28}$$

This equation in ω, $\boldsymbol{k}$ and $\delta\boldsymbol{u}$ contains all the information of the dispersion relation. We can eliminate $\delta\boldsymbol{u}$ by requiring that the waves are incompressible ($\boldsymbol{k}\cdot\delta\boldsymbol{u} = 0$, and therefore do not introduce a density perturbation) and that the velocity perturbation is perpendicular to the mean magnetic field ($\boldsymbol{B}\cdot\delta\boldsymbol{u} = 0$). Inserting this into eq. (2.28) yields the dispersion relation of Alfvén waves:

$$\omega^2 = (\boldsymbol{v}_\mathbf{a}\cdot\boldsymbol{k})^2. \tag{2.29}$$

The Fourier decomposition in eq. (2.27) integrates over multiple Fourier components and consequently over multiple Alfvén waves. Under most circumstances, these waves tend to have

larger amplitudes at smaller wave numbers and follow approximatively a powerlaw: $|\boldsymbol{a}(k)| \propto k^{-q}$. In our theory this behavior has two different physical reasons: for Alfvén waves in the large-scale magnetic field this distribution is a result of nonlinear wave-mode couplings and the resulting turbulent cascade of energy. For small-scale waves this is also true but is further supported by another idea. Because CRs are charged particles they can generate electromagnetic fields and in particular Alfvén waves on their on gyro scale (Lerche, 1967). The latter effect is caused by a plasma-kinetic instability: the gyroresonant instability. As the momentum distribution of CRs is a powerlaw, the waves produced by them is likely to be one too.

Even though the large-scale magnetic field has an inherent turbulent structure, we shall assume that we understand its evolution and hence know $\boldsymbol{B}(\boldsymbol{x}, t)$. We cannot assume this for the small scales. We need to describe them in a statistical way because we do the same for particles that generate the waves. We introduce the statistics of Alfvén waves as follows: the linearized equations of MHD do not contain any restrictions on the correlations between two modes at $\boldsymbol{k}$ and $\boldsymbol{k}'$. Therefore, it is common practice to assume that they are uncorrelated (Tautz and Shalchi, 2010):

$$\langle a(\boldsymbol{k}) a^*(\boldsymbol{k}') \rangle = |a(\boldsymbol{k})|^2 \delta(\boldsymbol{k} - \boldsymbol{k}'), \tag{2.30}$$

where $\langle\rangle$ is the average over realizations. This can be understood in practical terms: as two Alfvén waves do not influence each other by virtue of the linearized MHD equations, we have to adopt the most general assumptions concerning their correlation. Any correlation between the waves would have a physical reasoning supporting this correlation. Indeed, localized and interaction nonlinear Alfvén waves have to be correlated due to their shared history. Even temporal correlations between two waves can occur and alter the interaction between CRs and Alfvén waves (Teufel and Schlickeiser, 2002; Shalchi, 2009).

The cascade of uncorrelated wave modes is the mathematical description of a stochastic population of Alfvén waves which we will refer to as the *Alfvénic turbulence*. As a consequence of the stochasticity, we continue to describe the waves in terms of their Fourier components $a(\boldsymbol{k})$ rather then in their real-space realizations $a(\boldsymbol{x}, t)$.

We can further restrict our pool of waves due to a plasma-kinetic effect named linear Landau damping. This effect does not occur in our dispersion relation, as we modeled the gas hydrodynamically. Consider an oblique Alfvén wave (relative to mean magnetic field). These waves can couple to magnetosonic waves, which couple to thermal particles. Through this coupling the thermal plasma can now interact and exchange energy with the Alfvén wave. The particles mostly extract energy and effectively damp these wave (Foote and Kulsrud, 1979). We discard all oblique waves and reduces the dispersion relation of Alfvén waves to:

$$\omega = \pm v_\mathrm{a} k, \tag{2.31}$$

where $k = \boldsymbol{k} \cdot \boldsymbol{b}$. These waves are non-dispersive as their resulting phase and group velocities coincide. From the two signs in eq. (2.31) we know that there are two distinct propagation modes: parallel Alfvén waves either co- or counter-propagate along the mean magnetic field. To simplify our discussion, we drop the term "parallel" and simply call these waves "Alfvén waves" if no confusion is possible.

By counting the dependent equations and MHD quantities, we can conclude that there are 2 linearly independent quantities. This degeneracy is present only for parallel propagting Alfvén waves. In this case, one branch of the magnetosonic waves algebraically coincides with the

geniue, the *shear*, Alfvén waves and is called a *pseudo* Alfvén wave. Both parallel propagting waves have the same dispersion relation and are incompressible but have different directions of the magnetic field perturbations $\delta\boldsymbol{B}$. Because $\delta\boldsymbol{B} \perp \boldsymbol{B}$ holds for both waves, we name them by their polarization direction. If $\boldsymbol{B} \parallel \boldsymbol{z}$ we call

$$\delta B^{\mathrm{R}}(k) = \delta B^{x}(k) - i\delta B^{y}(k), \tag{2.32}$$

$$\delta B^{\mathrm{L}}(k) = \delta B^{x}(k) + i\delta B^{y}(k) \tag{2.33}$$

the right- and left-hand polarized components. The magnetic energy contained in the, e.g., right-handed Alfvén waves is, using eq. (2.30):

$$\varepsilon_{\mathrm{a}}^{\mathrm{R}}(x,t) = \left\langle \frac{\delta B^{\mathrm{R}} \delta B^{\mathrm{R}*}}{2} \right\rangle (x,t) \tag{2.34}$$

$$= \frac{1}{2} \int_{-\infty}^{\infty} \mathrm{d}k \int_{-\infty}^{\infty} \mathrm{d}k' \left\langle \delta B^{\mathrm{R}}(k) \delta B^{\mathrm{R}*}(k') \right\rangle e^{i[(\omega(k)-\omega(k'))t-(k-k')z]} \tag{2.35}$$

$$= \frac{1}{2} \int_{-\infty}^{\infty} \mathrm{d}k \, |B^{\mathrm{R}}(k)|^2, \tag{2.36}$$

where we had to take the ensemble average since energy is an actual physical observable and hence shared between all realizations. Furthermore, as the magnetic field itself is a physical quantity it must be real valued such that the reality condition $\delta\boldsymbol{B}(k) = \delta\boldsymbol{B}^*(-k)$ holds. Defining the spectra of waves as $I^{\mathrm{R,L}}(k) = |B^{\mathrm{R,L}}(k)|^2$ and inserting both definitions yields our final expression for the magnetic wave energy. There are two wave polarizations and two wave propagations; such that we can define four different wave energies:

$$\varepsilon_{\mathrm{a},\pm}^{\mathrm{R,L}}(x,t) = \int_{0}^{\infty} \mathrm{d}k \, I_{\pm}^{\mathrm{R,L}}(k), \tag{2.37}$$

where $I_{\pm}^{\mathrm{R,L}}(k)$ are the respective intensities.

3 Theory of Cosmic Ray Hydrodynamics

In this section we are going to derive and discuss our new hydrodynamical equations. In a first step we calculate moments of the Vlasov equation until most of its dynamics is captured by two more simplified equations. We proceed with a discussion of the stochastic scattering between CRs and the Alfvénic turbulence. Adopting a *grey*-like assumption on the wave spectra, we are able to incorporate the effects of microscopic scattering into our macroscopic equations. We discuss how our new theory relates to currently established theories throughout our derivation.

3.1. Derivation of the CR Fluid equations

Integration of the full Vlasov-equation (2.9) is unfeasible in a tractable analytical manner. To overcome the complexity of 7 coupled dimensions, several approximations can be made. As described above, we assume that the electromagnetic perturbations are small (i.e. $\delta B \ll B$). Therefore, the typical time scales on which the perturbations become dynamically important are larger than the particle's gyrofrequency. In this time hierarchy, the hydrodynamic time scale is even large. This is the time scale on which the whole CR population can influence hydrodynamic properties of the thermal gas. As our main-interest lies in those hydrodynamical scales, we can approximate processes on time scales well below. We do so by stepping the hierarchy backwards and conclude that the time scale of a single CR revolution cannot not affect the hydrodynamical picture of the CR population. We can thus average the Vlasov-equation over a CR gyro-orbit.

The remaining phase space dynamics of CRs are described by a gyro-averaged form of the Vlasov-Equation, the so called focused transport equation (Skilling, 1975; Isenberg, 1997; Zank et al., 2000):

$$\begin{aligned} &\frac{\partial f}{\partial t} + (\boldsymbol{u} + \mu v \boldsymbol{b}) \cdot \boldsymbol{\nabla} f \\ &\quad + \left[\frac{1-3\mu^2}{2} (\boldsymbol{b} \cdot \boldsymbol{\nabla} \boldsymbol{u} \cdot \boldsymbol{b}) - \frac{1-\mu^2}{2} \boldsymbol{\nabla} \cdot \boldsymbol{u} \right] p \frac{\partial f}{\partial p} \\ &\quad + \left[v \boldsymbol{\nabla} \cdot \boldsymbol{b} + \mu \boldsymbol{\nabla} \cdot \boldsymbol{u} - 3\mu (\boldsymbol{b} \cdot \boldsymbol{\nabla} \boldsymbol{u} \cdot \boldsymbol{b}) \right] \frac{1-\mu^2}{2} \frac{\partial f}{\partial \mu} = \left. \frac{\partial f}{\partial t} \right|_{scatt} . \end{aligned} \tag{3.1}$$

In this equation a mixed coordinate system is used: while $\boldsymbol{x}$ and t are measured in the lab frame, the particle momentum p and velocity v are measured in the comoving frame with the gas, which propagates with a local non-relativistic velocity $\boldsymbol{u}$. The cosine of the particle pitch-angle $\mu = \boldsymbol{v} \cdot \boldsymbol{b}/v$ is measured with respect to the unit vector along the local magnetic field $\boldsymbol{b}$. For an extensive discussion of the occurring pseudo-forces see le Roux and Webb (2012).

There are multiple ways to tackle the remaining complexity of this equation: the *Chapman-Enskog* expansion, where the fast (scattering) and slow (hydrodynamic) time scales are treated separately, or the *moment*-expansion, where the transport equation is expanded in moments of one of its coordinates.

The first method is the standard way to derive various forms of the diffusion equation and is the common choice to describe CR transport (Skilling, 1971; Zweibel, 2013). The pitch-angle

scattering time scale is assumed to be the fast time scale, whereas the actual time scale of the hydrodynamical system is treated as slow. Usually this expansion results in a diffusion equation. In general, the order of the Chapman-Enskog expansion, determines whether one faces normal diffusion (e.g. heat-equation-type diffusion $\partial_t q = \partial_{xx} q$) or more sophisticated mathematical forms of physical diffusion (e.g. hyper-diffusion $\partial_t q = \partial_{xxxx} q$, Malkov and Sagdeev (2015)). The assumed separation between the time scales has to be checked *a posteriori*, as it not *a priori* clear that the resulting *apparent* diffusion velocity remains physical.

The Chapman-Enskog expansion is used in RHD as an approximation in the optically thick limit (Mihalas and Weibel Mihalas, 1984): there, photons scatter rapidly such that any preferred direction of the photon distribution is lost on the slow time scale. On a microscopic level individual photons move at the speed of light, but their bulk velocity is frozen to the gas velocity. Relative to this velocity, the photons diffuse in all directions. But there are some problems concerning the validity of the diffusion approximation in RHD: if it is used in the optically thin limit light can diffuse at velocities exceeding the speed of light. In addition, and more practically, there are no shadows in the diffusion approximation, as light is expected to be scattered efficiently on a global level and thus around any obstacle.

Both RHD problems are partially cured if one uses the second, the moment method. The characteristic feature of this method is the expansion in one or more dynamically important coordinates to describe the dynamics. This is accomplished in practice by choosing suitable functions $h_i(\boldsymbol{x}, \boldsymbol{p})$ such that there exist expansion coefficients f_i with:

$$f(t, \boldsymbol{x}, \boldsymbol{p}) = \sum_{i=0}^{\infty} f_i(t)\, h_i(\boldsymbol{x}, \boldsymbol{p}). \tag{3.2}$$

The burden of solving eq. (3.1) or similar equations is transfered towards finding solutions of differential equations that evolve f_i. In general, the expansion functions are chosen such that the resulting equations for the f_i's are easier to solve. The evolution equations for the coefficients can be obtained by inserting eq. (3.2) into the original differential equation and subsequently integrating it. This procedure results in a set of differential equations:

$$\frac{\partial f_i}{\partial t} = ... \qquad i = 0, 1, 2, ... \tag{3.3}$$

In RHD, the expansion coordinate is the propagation direction of photons $\boldsymbol{n}$. This results into moments of the angular distribution of radiation (Mihalas and Weibel Mihalas, 1984). For example, to first order this approach leads to the two-stream approximation, where light is expected to move either parallel or anti-parallel to a preferred direction. This refined description of photon propagation restores shadows behind obstacles.

The downside of this method is that one usually faces a closure problem. An infinite number of moments and their evolution equations are needed to close the system (3.3). There are, again, different ways to tackle this problem: the most practical is to truncate the expansion after a certain order and neglect contributions from higher moments. This results in the case of radiative transfer in the so called Eddington-approximation, where only the 1 and $\boldsymbol{n}$ moments are considered. We will use an similar expansion as the basis for our description of cosmic ray transport.

While this solution to the closure problem is simple, it is also wrong: Zank et al. (2000) shows that the order of truncation determines the global features of the solution. In the end,

one has to check whether the neglected moments are indeed small and if the truncation was justified.

3.1.1. Pitch-Angle Moments

We use the moment-method to derive macroscopic equations from (3.1). This route is as old as the first descriptions of cosmic ray transport and was frequently revisited (Klimas and Sandri, 1971; Earl, 1973; Zank et al., 2000; Litvinenko and Schlickeiser, 2013). We here recall the excellent derivation of Zank (2014) for completeness and to introduce our notation. CRs are mostly scattered in pitch-angle rather than momentum, since the former process does not require an energy exchange between the scattering agent and the CR. Therefore, we expect pitch-angle scattering to be more dynamically important. We expand the focused transport equation in moments of the pitch-angle μ by using (scaled) Legendre polynomials P_n as our expansion functions:

$$\begin{aligned} f &= f_0\,\mathrm{P}_0(\mu) + f_1\,\mathrm{P}_1(\mu) + f_2\,\mathrm{P}_2(\mu) + ... \\ &= f_0 + f_1\,3\mu + f_2\,5\frac{1-3\mu^2}{2} + ... \end{aligned} \tag{3.4}$$

This expansion has the usual interpretation that is known, e.g., from electrostatics: f_0 represents the monopole of the distribution and contains the information about the integrated quantities of the distribution. The first moment f_1 is the dipole and is the skewness of f in our preferred direction along the mean magnetic field $\boldsymbol{b}$. Finally, f_2 is the quadrupole moment while $f_3, f_4, ...$ are higher-order poles.

The Legendre polynomials are best suited for the analysis of (3.1), due to their relation to the scattering operator: one of the most basic scattering operators describes pitch-angle scattering by:

$$\left.\frac{\partial f}{\partial t}\right|_{\mathrm{scatt}} = \frac{\partial}{\partial \mu}\left[\frac{1-\mu^2}{2}\nu(\mu,p)\frac{\partial f}{\partial \mu}\right], \tag{3.5}$$

where $\nu(\mu, p)$ is the scattering coefficient. The Legendre polynomials are eigenfunctions of this scattering operator if and only if the scattering coefficient is independent of μ and p. In this case

$$\frac{\partial}{\partial \mu}\left[\frac{1-\mu^2}{2}\nu(p)\frac{\partial \mathrm{P}_n}{\partial \mu}\right] = -\frac{n(n+1)}{2}\nu(p)\mathrm{P}_n. \tag{3.6}$$

To further proceed, we truncated the expansion (3.4) after the first order and continue with:

$$f = f_0 + f_1 3\mu. \tag{3.7}$$

Because of this fundamental assumption we circumvent the closure problem. It is valid in the case of rapid pitch-angle scattering causing only small anisotropies of the CR distribution. A more thoughtful a posteriori justification is given later.

Inserting this ansatz into eq. (3.1) and taking the zeroth and first μ-moments of this equation results in equations for both the isotropic and anisotropic distribution. For completeness, we

explicitly calculate all term-by-term integrals in the Appendix A.1. The differential equation for the isotropic part reads:

$$\frac{\partial f_0}{\partial t} + \boldsymbol{u}\cdot\boldsymbol{\nabla} f_0 + \boldsymbol{\nabla}\cdot(v\boldsymbol{b}f_1) - \frac{1}{3}(\boldsymbol{\nabla}\cdot\boldsymbol{u})p\frac{\partial f_0}{\partial p} = \left.\frac{\partial f_0}{\partial t}\right|_{\text{scatt}}. \tag{3.8}$$

The new equation for the anisotropy in the CR-distribution reads:

$$\frac{\partial f_1}{\partial t} + \frac{v}{3}\boldsymbol{b}\cdot\boldsymbol{\nabla} f_0 + \boldsymbol{u}\cdot\boldsymbol{\nabla} f_1 + \left[-\frac{2}{5}(\boldsymbol{b}\cdot\boldsymbol{\nabla}\boldsymbol{u}\cdot\boldsymbol{b}) - \frac{1}{5}\boldsymbol{\nabla}\cdot\boldsymbol{u}\right]p\frac{\partial f_1}{\partial p} + \left[\frac{1}{5}\boldsymbol{\nabla}\cdot\boldsymbol{u} - \frac{3}{5}(\boldsymbol{b}\cdot\nabla\boldsymbol{u}\cdot\boldsymbol{b})\right]f_1 = \left.\frac{\partial f_1}{\partial t}\right|_{\text{scatt}}. \tag{3.9}$$

A more careful expansion would use eigenfunctions of the scattering operator with a pitch-angle dependent scattering rate $\nu(\mu)$. These eigenfunctions exist and form an orthogonal set of functions in virtue of the Sturm-Lioville theory for most cases. In general, this would give us different expansion functions (but most likely polynomials), which would differ from the Legendre polynomials. The only advantage of this approach would be, that we did not need to assume pitch-angle independence of the scattering coefficient and would capture the dynamics more accurately. Since we cutoff the expansion after the first order and assume small anisotropies, we do not expect an overall change of the presented theory. Further, this more rigorous treatment would obfuscate the derivation and cast our results inherently dependent on the actual functional form of ν. Our compromise to expand f as if the scattering coefficient is independent of pitch-angle mediates between physical clarity and mathematical correctness.

3.1.2. Fluid equations

To gain insight into the macroscopic evolution of the CR population, we take appropriate moments of the phase space eqs. (3.8) and (3.9). We here focus on the thermodynamic description of CRs and thus integrate the distribution multiplied by the relativistic kinetic energy $T(p) = \sqrt{p^2c^2 + (mc^2)^2} - mc^2$ to get the total CR energy density

$$\varepsilon_{\text{cr}} = \int \mathrm{d}^3p\, T(p) f(p,\mu) = \int_0^\infty \mathrm{d}p\, 4\pi p^2 T(p) f_0(p). \tag{3.10}$$

Closely related, the CR-pressure can be defined as

$$P_{\text{cr}} = \int \mathrm{d}^3p\, \frac{pv}{3} f(p,\mu) = \int_0^\infty \mathrm{d}p\, \frac{4\pi}{3} p^2 pv f_0(p). \tag{3.11}$$

All higher moments of the Legendre-polynomial expansion vanish and only the isotropic part of distribution contributes to both quantities. Both pressure and energy obey an equation of state:

$$P_{\text{cr}} = (\gamma_{cr} - 1)\varepsilon_{\text{cr}} \tag{3.12}$$

with $\gamma_{cr} = 4/3$ in the ultra-relativistic limit. By analogy, similar expressions for the anisotropic distribution can be defined:

$$f_{\rm cr} = \int_0^\infty \mathrm{d}p\, 4\pi p^2 T(p) v f_1(p), \tag{3.13}$$

$$K_{\rm cr} = \int_0^\infty \mathrm{d}p\, 4\pi p^2 \frac{pv}{3} v f_1(p) \tag{3.14}$$

The macrophysical meaning of both equations is evident: because $f_{\rm cr}$ is the μv-moment of the CR energy density, it is the CR energy flux along the magnetic field. Respectively, $K_{\rm cr}$ is the CR pressure flux along the magnetic field lines. Again, an equation of state links both quantities, which coincides in the ultra-relativistic limit with that of CR energy density and flux:

$$K_{\rm cr} = (\gamma_{cr} - 1) f_{\rm cr}. \tag{3.15}$$

To finally get a macroscopic evolution equation for the CRs, we multiply eqs. (3.8) and (3.9) by $T(p)v$ and integrate over the momentum space. To close the resulting equations, we take the ultra-relativistic limit ($v = c$) of terms, which cannot be expressed in $\varepsilon_{\rm cr}$, $P_{\rm cr}$, $f_{\rm cr}$ or $K_{\rm cr}$. This only needs to be done in terms containing the derivative along the magnetic field. We arrive at

$$\boxed{\frac{\partial \varepsilon_{\rm cr}}{\partial t} + \boldsymbol{\nabla} \cdot (\boldsymbol{u}(\varepsilon_{\rm cr} + P_{\rm cr}) + \boldsymbol{b} f_{\rm cr}) = \boldsymbol{u} \cdot \boldsymbol{\nabla} P_{\rm cr} + \left.\frac{\partial \varepsilon_{\rm cr}}{\partial t}\right|_{\rm scatt}} \tag{3.16}$$

and

$$\boxed{\frac{\partial f_{\rm cr}}{\partial t} + \boldsymbol{\nabla} \cdot (\boldsymbol{u} f_{\rm cr}) + \frac{c^2}{3} \boldsymbol{b} \cdot \nabla \varepsilon_{\rm cr} = -(\boldsymbol{b} \cdot \boldsymbol{\nabla} \boldsymbol{u}) \cdot (\boldsymbol{b} f_{\rm cr}) + \left.\frac{\partial f_{\rm cr}}{\partial t}\right|_{\rm scatt}}. \tag{3.17}$$

We used the equations of state (3.15) to write eq. (3.17) in this compact form.

Except for the term containing $f_{\rm cr}$, the interpretation of eq. (3.16) is as usual: the CR energy is a conserved quantity, which is convected with the gas. Thus CRs are subject to adiabatic gains or loses whether the gas is expanding or contracting. The interpretation of eq. (3.17) is not as straightforward: in an uniform magnetic field $f_{\rm cr}$ convected with the gas but, in general, the first term of the right hand side prevents this interpretation. It accounts for changes of the flux due to a spatial varying MHD environment. This term is a combined consequence of our local pitch-angle definition and our comoving formulation, as pitch-angles constantly change in disordered magnetic fields.

The third term describes more directly the transport mechanism of CRs. This term is known from radiative transfer, as it is the projected counterpart of a term appearing in the Eddington-approximation. Consider the toy model of a CR population with globally vanishing flux but locally varying density where all CRs have the same energy and all gas quantities are uniform. In this case, because the flux is zero, the CR anisotropy is zero everywhere, too. Thus, at every point the same number of CRs are moving with and against the direction of the magnetic field. This situation has to change after an instant of time, as we can see by focusing on an isolated parcel: due to the local gradient in the number of CRs, the number of CRs that move from one direction into the parcel cannot be the same number of CRs that enter from the other direction. In consequence, there are now more CRs moving in the opposite direction of the CR gradient. This corresponds to an increase in anisotropy and in flux as well.

3.2. Cosmic Ray Scattering

So far, we have only accounted for the dynamics imposed by the large-scale magnetic field. As the small-scale magnetic fields are turbulent, we have to describe their interaction with stochastic methods. A simple and effective method to handle the stochasticity is to introduce diffusions terms into the Vlasov-equation.

CRs are affected by the Lorentz-force of small-scale electromagnetic fields in two ways: 1) by pitch-angle scattering, where the magnetic component can change the pitch-angle of a CR but cannot increase the particle momentum or its energy, and 2) by momentum diffusion, where the Fermi-II process stochastically accelerates charged particles through the electric component of the turbulence. Introducing a corresponding diffusion term for each possible combination of μ and p in eq. (3.1) gives:

$$\left.\frac{\partial f}{\partial t}\right|_{\text{scatt}} = \frac{1}{p^2}\frac{\partial}{\partial p}p^2\left(D_{pp}\frac{\partial f}{\partial p} + D_{p\mu}\frac{\partial f}{\partial \mu}\right) + \frac{\partial}{\partial \mu}\left(D_{\mu\mu}\frac{\partial f}{\partial \mu} + D_{p\mu}\frac{\partial f}{\partial p}\right), \tag{3.18}$$

where $D_{\mu\mu}$, D_{pp} and $D_{\mu p} = D_{p\mu}$ are diffusion coefficients.

Correctly evaluating the diffusion coefficients is challenging. Each CR samples the electromagnetic fields on its own trajectory. The resulting forces differ from particle to particle. Furthermore, due the scattering, these trajectories are complicated and non-analytic and CRs can interact or resonate with many different Alfvén waves. This limits any analytic approach to describe CR scattering. Therefore, we have to proceed with an approximation. In the quasi-linear theory (QLT) the electromagnetic turbulence is sampled along the unperturbed orbits of eq. (2.3). This is approximately true as we assume that the perturbation of the Alfvén waves are small and the actual particle trajectory diverge only slightly from the unperturbed orbit.

A way to check these assumption is to simulate true orbits of CRs in predefined Alfvénic turbulence and calculate the diffusion coefficients of the CR distribution afterwards. This is done for pitch-angle scattering in Tautz et al. (2013), where the QLT is shown to be in a good agreement with the numerical results.

In QLT the resonance between Alfvén waves and CRs becomes a sharp δ-resonance: specific waves of frequency ω resonate with the CRs of velocity v, pitch-angle μ and gyrofrequency Ω that fulfill the resonance condition:

$$\omega - k\mu v + n\Omega = 0 \qquad n = ..., -1, 0, +1, ... \tag{3.19}$$

Note that this is a gyroresonance which is Doppler-shifted into the frame of the CR. The sign of n determines whether CRs interact with waves of right-handed ($n > 0$) or left-handed ($n < 0$) polarization. The main resonances of interest for pitch-angle scattering are $n = \pm 1$ while higher harmonics can be neglected for purely parallel propagating waves (Schlickeiser, 1989):

$$\omega - k\mu v \pm \Omega = 0 \tag{3.20}$$

We can interpret the condition from a wave and from a particle perspective: if we fix a wave with particular ω, then eq. (3.20) reveals which CRs are able to resonate and hence interact with it. As eq. (3.20) depends nonlinearly on the particle properties, this condition is fulfilled for CRs of different energies and pitch-angles. If we instead consider a fixed particle momentum, the condition can be manipulated such that it singles out the resonant wave frequencies.

We derive in sec. 2.3 the dispersion relation (2.31) for Alfvén waves:

$$\omega = \begin{cases} +kv_\mathrm{a} & \text{for co-propagating waves, and} \\ -kv_\mathrm{a} & \text{for counter-propagating waves.} \end{cases} \tag{3.21}$$

By inserting this into eq. (3.20), we see that there are 4 combinations of signs that are able to fulfill the resonance condition: CRs resonate with co-propagating waves

$$\begin{cases} +\dfrac{v_\mathrm{a}}{v} < \mu & \text{of right-handed polarization,} \\ \mu < +\dfrac{v_\mathrm{a}}{v} & \text{of left-handed polarization,} \end{cases}$$

and with counter-propagating waves

$$\begin{cases} -\dfrac{v_\mathrm{a}}{v} < \mu & \text{of right-handed polarization,} \\ \mu < -\dfrac{v_\mathrm{a}}{v} & \text{of left-handed polarization.} \end{cases}$$

Therefore, there are always two waves of different polarizations and propagation directions that interact with a given CR.

By rearranging eq. (3.20) for k we see that the *resonant wave number* is the same for resonances of different polarizations but equal wave propagation directions:

$$k_{\mathrm{res},\pm} = \frac{\Omega}{\mu v \mp v_\mathrm{a}}. \tag{3.22}$$

In the limit $\mu \to \pm v_\mathrm{a}/v$, the denominator of eq. (3.22) vanishes and $k_{\mathrm{res},\pm} = \infty$. Because there are no waves with this wavenumber, CRs with $\mu = \pm v_\mathrm{a}/v$ seem to be unable to scatter. This introduces a sink in pitch-angle space as every CRs would get pitch-angle scattered until it approaches this μ-value. After a few scattering times, the whole CR population thus gyrates almost perpendicular to the mean magnetic field. This apparent process is the manifestation of the 90°-problem. It is a result of the initial QLT-assumption of unperturbed gyro-orbits. In reality, even the smallest amount of scattering alters CR orbits compared to the unperturbed one. This broadens the resonance between CRs and Alfvén waves. In consequence, this introduces additional scattering from waves neighboring the sharp resonance wave number $k_{\mathrm{res},\pm}$. Hence, even CRs with $\mu = \pm v_\mathrm{a}/v$ get scattered by Alfvén waves (Shalchi, 2005). Successor theories of QLT which do not suffer from this problem are developed in Shalchi and Schlickeiser (2005); Tautz et al. (2008) with a standard reference book by Shalchi (2009). Nevertheless, we are mostly interested in hydrodynamic CR transport and, as we will show later, therein only pitch-angle averaged scattering coefficients are important. These quantities are very well described in the QLT limit (see, e.g., figures of Tautz et al., 2013).

We subsume the different handedness of the resonant polarization-types into a definition and introduce the resonant wave energy

$$R_\pm(k_{\mathrm{res},\pm}) = I_\pm^\mathrm{L}(-k_{\mathrm{res},\pm}) + I_\pm^\mathrm{R}(k_{\mathrm{res},\pm}), \tag{3.23}$$

and set $I_\pm^{\mathrm{L,R}}(k) = 0$ for negative arguments $k < 0$. Through this definition, $R_\pm$ returns the intensity of the correct polarization state for a given propagation direction (see Fig. 3.1).

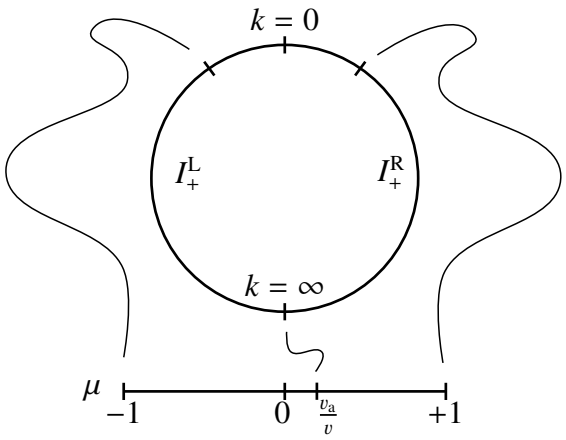

Figure 3.1.: On the definition of resonant wave energy for co-propagating Alfvén waves. Any given CR resonates with only one resonant wave polarization state of left- (L) or right-(R) handedness (see text). At $\mu = v_a/v$ the resonant wave number $k_{res,+}$ becomes singular as the denominator in eq. (3.22) vanishes. Moving μ over this point, $k_{res,+}$ switches its sign which physically corresponds to a change of the polarization state of the resonant wave type. Hence, the point $k = \infty$ connects both wave types by their resonance with CRs of $\mu = v_a/v$. Mathematically this procedure is called Alexandroff compactification and enables us to topologically identify the k-space as a circle. Figure from Thomas and Pfrommer (2018).

By analogy, we define a total wave power spectrum that contains all power carried by co- and counter-propagating waves via:

$$E_\pm(k) = I_\pm^L(k) + I_\pm^R(k). \tag{3.24}$$

This enables us to define the total Alfvén wave energy density:

$$\varepsilon_{a,\pm} = \int_0^\infty \mathrm{d}k\, E_\pm(k). \tag{3.25}$$

With these definitions in place, the *scattering frequency* at which Alfvén waves scatter CRs is given by (Skilling, 1975; Schlickeiser, 1989):

$$\nu_\pm(p,\mu) = \pi\Omega \frac{|k_{res,\pm}| R(k_{res,\pm})}{\varepsilon_B} \tag{3.26}$$

Deriving the corresponding diffusion coefficients is challenging. Every possible combination of $\delta\boldsymbol{E}$ and $\delta\boldsymbol{B}$ correlations needs to be linked using dispersion properties of Alfvén waves and contribute to these coefficients. Even just sketching the derivation would highly obscure the present analysis; hence, we simply cite the results (Schlickeiser, 1989; Dung and Schlickeiser,

1990):

$$D_{\mu\mu} = \frac{1-\mu^2}{2}\left[\left(1-\mu\frac{v_\mathrm{a}}{v}\right)^2 \nu_+ + \left(1+\mu\frac{v_\mathrm{a}}{v}\right)^2 \nu_-\right], \tag{3.27}$$

$$D_{\mu p} = \frac{1-\mu^2}{2} p \frac{v_\mathrm{a}}{v}\left[\left(1-\mu\frac{v_\mathrm{a}}{v}\right)\nu_+ - \left(1+\mu\frac{v_\mathrm{a}}{v}\right)\nu_-\right], \tag{3.28}$$

$$D_{pp} = \frac{1-\mu^2}{2} p^2 \frac{v_\mathrm{a}^2}{v^2}(\nu_+ + \nu_-). \tag{3.29}$$

Contrary to the currently preferred convention to express the diffusion coefficients directly in terms of the resonant wave energy (used, e.g., by Dung and Schlickeiser, 1990), we express these coefficients in terms of $\nu_\pm$. The algebraic advantage of our convention will become apparent later.

The rest of this work is devoted to the approximative analysis of eq. (3.18) together with these coefficients.

3.3. Cosmic Ray Diffusion

In this section we treat the scattering in its non-relativistic limit. With this we show how to derive a hydrodynamic form of the scattering terms that result in a set of transport equations resembling the dynamics of the usual CR diffusion equation. In the next section this derivation is expanded to a more precise model. This results in equations which capture the diffusion as a limiting case.

In the limit $v_\mathrm{a}/v \to 0$ all terms except the pitch-angle diffusion term drop out of eqs. (3.27) to (3.29). This limit has thus a simple interpretation: as all momentum altering terms vanish, CRs solely interact with the magnetic component of the Alfvén waves. The remaining scattering term in eq. (3.18) is given in eq. (3.5) with $\nu(\mu, p) = \nu_+(\mu, p) + \nu_-(\mu, p)$ being the total scattering coefficient. To calculate how this scattering influences the evolution of CR energy we have to take the first moment of this equation, which results in

$$\begin{aligned}\left.\frac{\partial \varepsilon_\mathrm{cr}}{\partial t}\right|_\mathrm{scatt} &= \int_0^\infty \mathrm{d}p 2\pi p^2 T(p) \int_{-1}^1 \mathrm{d}\mu \frac{\partial}{\partial\mu}\left[\frac{1-\mu^2}{2}\nu(\mu,p)\frac{\partial f}{\partial\mu}\right] \\ &= \int_0^\infty \mathrm{d}p 2\pi p^2 T(p)\, \frac{1-\mu^2}{2}\nu(\mu,p)\frac{\partial f}{\partial\mu}\bigg|_{\mu=-1}^{\mu=1} \\ &= 0\end{aligned} \tag{3.30}$$

As expected, there are no gains or loses of CR energy due to interactions with the magnetic turbulence. The corresponding equation for the effect of scattering on the CR flux density is

calculated by taking the second moment of (3.5). We get:

$$\begin{aligned}\left.\frac{\partial f_{\rm cr}}{\partial t}\right|_{\rm scatt} &= \int_0^\infty {\rm d}p 2\pi p^2 T(p) v \int_{-1}^1 {\rm d}\mu\, \mu \frac{\partial}{\partial \mu}\left[\frac{1-\mu^2}{2}\nu(\mu,p)\frac{\partial f}{\partial \mu}\right] \\ &= -\int_0^\infty {\rm d}p\, 2\pi p^2 T(p) v \int_{-1}^1 {\rm d}\mu\, \frac{1-\mu^2}{2}\nu(\mu,p)\frac{\partial f}{\partial \mu} \\ &= -\frac{3}{2}\int_0^\infty {\rm d}p\, 4\pi p^2 T(p) v \int_{-1}^1 {\rm d}\mu\, \frac{1-\mu^2}{2}\nu(\mu,p) f_1 \\ &= -\int_0^\infty {\rm d}p\, 4\pi p^2 T(p) v \nu(p) f_1 \\ &= -\bar{\nu}_{\rm T} f_{\rm cr}, \end{aligned} \tag{3.31}$$

where we introduce the energy-averaged scattering coefficient as

$$\bar{\nu}_{\rm T} = \frac{1}{f_{\rm cr}}\int_0^\infty {\rm d}p\, 4\pi p^2 T(p)\nu(p) f_1(p), \tag{3.32}$$

where $\nu(p)$ is the pitch-angle-averaged scattering coefficient (with 3/2 for normalization reasons):

$$\nu(p) = \frac{3}{2}\int_{-1}^1 {\rm d}\mu\, \frac{1-\mu^2}{2}\nu(p,\mu). \tag{3.33}$$

3.3.1. Relation to the Diffusion and Telegraph Equations

We are now able to show, that our formulation is a superset of the usual diffusive-transport approximations. The approaches taken in standard works of Skilling (1971) and Schlickeiser (1989) are the same: both authors use the Chapman-Enskog expansion of the Fokker-Planck equation to separate different contributions by their corresponding order in $O(v_{\rm a}/v)$ and $O(\bar{\nu}_T v_{\rm a}/v)$.

Expanding eq. (3.9) to lowest order in the two numbers v/L, where L is a typical CR gradient length, and $\bar{\nu}_{\rm T}$ results in

$$\frac{v}{3}\boldsymbol{b}\cdot\boldsymbol{\nabla} f_0 = -\bar{\nu}_{\rm T} f_1. \tag{3.34}$$

This links the macroscopic gradient to the local anisotropy of cosmic rays. It is further an approximation of the steady state of eq. (3.9). By inserting this equation back into eq. (3.8) results in the usual diffusion equation for the distribution f. To derive a similar equation we would have to take the appropriate moments of the diffusion equation in f. We skip this step and use this expansion directly for the energy density and flux equations. In the latter one, the lowest order Chapman-Enskog expansion reads

$$\frac{c}{3}\boldsymbol{b}\cdot\boldsymbol{\nabla}\varepsilon_{\rm cr} = -\bar{\nu}_{\rm T} f_{\rm cr}. \tag{3.35}$$

Inserting this back into the equation for the total energy (3.16) results in:

$$\frac{\partial \varepsilon_{\rm cr}}{\partial t} + \boldsymbol{\nabla}\cdot(\boldsymbol{u}(\varepsilon_{\rm cr}+P_{\rm cr}) - \bar{\kappa}\boldsymbol{b}\boldsymbol{b}\cdot\boldsymbol{\nabla}\varepsilon_{\rm cr}) = \boldsymbol{u}\cdot\boldsymbol{\nabla}P_{\rm cr}, \tag{3.36}$$

which perfectly coincides with the known diffusion equation (see e.g. Zweibel, 2017) when we identify

$$\bar{\kappa} = \frac{c^2}{3\bar{\nu}_\mathrm{T}} \tag{3.37}$$

as the diffusion coefficient. Thus our new formulation in terms of CR energy density and flux is a superset of the widely used diffusion approximation.

We can further connect our set of equation to the telegraph equation. For $\boldsymbol{u} = \mathbf{0}$, we obtain, after differentiating eq. (3.16) with respect to t and eq. (3.17) with respect to z,

$$\frac{1}{\bar{\nu}_\mathrm{T}} \frac{\partial^2 \varepsilon_\mathrm{cr}}{\partial^2 t} + \frac{\partial \varepsilon_\mathrm{cr}}{\partial t} = \boldsymbol{\nabla} \cdot (\bar{\kappa} \boldsymbol{b}\boldsymbol{b} \cdot \boldsymbol{\nabla} \varepsilon_\mathrm{cr}) \tag{3.38}$$

The telegraph equation is hyperbolic with characteristic speeds $= \pm c/\sqrt{3}$, and is a compromise between the wave and diffusion equations. The fundamental solution of eq. (3.38) contains two wavefronts $\delta(x \pm c/\sqrt{3})$ with a normalization, decaying with a characteristic time of $2/\nu$ (Malkov and Sagdeev, 2015). These singular features were the starting point of a recent debate concerning the validity of the telegrapher approximation for CR transport: direct numerical simulations of (3.1) do not show any wavefronts (Litvinenko and Noble, 2013, 2016). Hence the hyperbolic approach to model the CRs cannot be applied in the 'ballistic' regime $t \lesssim 2/\bar{\nu}_\mathrm{T}$. In the 'diffusive' regime (almost no anisotropy and $t \gtrsim 2/\bar{\nu}_\mathrm{T}$) both the diffusive and telegrapher treatments correctly reproduce the expected behavior of the Fokker-Planck-equation (FPE). In cases, where intrinsic anisotropy is present, the telegraph equation captures features in the solution of the FPE correctly, which are inherently smeared out in the diffusive solution (Litvinenko and Noble, 2016; Tautz and Lerche, 2016).

3.3.2. Justification of the Assumption

From eq. (3.34) we see that to order of magnitude

$$f_1 \simeq \frac{1}{3} \frac{c}{\bar{\nu}_T L} f_0 \tag{3.39}$$

where L is, again, a typical CR-scaleheight. If we take the mean free path of CRs λ as the maximal average length they travel until they get pitch-angle scattered, we can identify this quantity as the Knudsen number $\mathsf{Kn} = \lambda/L$ and hence have

$$\frac{f_1}{f_0} \simeq \mathsf{Kn}. \tag{3.40}$$

The Knudsen number tells us, whether a fluid approximation ($\simeq$ tracing out the particle momentum by taking appropriate moments) is valid or whether we have to consider the dynamics in a kinetic approach. Inserting eq. (3.37) into the definition yields

$$\mathsf{Kn} \simeq \frac{\bar{\kappa}}{cL} = \cdot 10^{-4} \frac{\kappa_{28}}{L_\mathrm{kpc}}, \tag{3.41}$$

where we scaled this to the typical galactic diffusion coefficient $\kappa_{28} = \bar{\kappa}/(10^{28}\,\mathrm{cm^2\,s^{-1}})$ used in the literature (Blasi and Amato, 2012) and scaled the scaleheight to $L_{\mathrm{kpc}} = L/(1\mathrm{kpc})$. Hence at scales of kpc CRs undergo frequent scattering, such that the fluid description and our expansion are valid on this scale. On the contrary, if we are interested in scales $\lesssim 10\,\mathrm{pc}$ the CR fluid approximation breaks down and CRs need to be treated in the full phase space.

3.4. Cosmic Ray Streaming

The presented model in the last section is too simplified. By only accounting for $O(1)$ in $\nu v_\mathrm{a}/v$ terms, there is no energy transfer between CRs and Alfvén waves. Thus, every initially present wave energy is quickly damped and CRs remain unscattered. This would cast our derivation of hydrodynamic equation useless, because CRs cannot be described as as a fluid without an scattering.

As we show in this section, order $O(1)$ is too low and we have to consider terms of order $O(\nu v_\mathrm{a}^2/v^2)$ to correctly capture the interaction between CRs and Alfvén waves[1]. This higher order introduces momentum diffusion and hence energy transfer between waves and CRs. In the relevant cases the energy transfer is a formal sink of particle energy, which needs to be a source of wave energy. The produced waves scatter CRs and our hydrodynamical theory remains valid. We thus keep all terms in eqs. (3.27) to (3.29).

Directly calculating moments of CR scattering as the resonant wave spectrum and hence ν are inherently energy dependent. The presented procedure in the last section proves to be challenging and different averaged forms of the scattering coefficients have to be introduced to close the transport equation. A feasible solution to this formal problem is the *grey* approximation known from RHD. Therein all absorption/scattering coefficients all treated as constant values over a certain energy range of interest. This enables calculation of energy moments but is only valid if there are no special features in the absorption/scattering coefficients.

To directly translate this idea to CRs, we would have to assume that the scattering frequency ν is constant. From the definition in eq. (3.26) is this algebraically impossible. Even casting eq. (3.26) to become independent of k_res would require a wave spectrum $I \propto k^{-1}$, which results in a diverging total energy density $\varepsilon_{\mathrm{a},\pm}$. Additionally, the gyrofrequency Ω in front of the definition is energy dependent and cannot be removed by any special choice of I. We adopt a more complex but also more physically correct variant of grey approximation. For this we focus our analysis on a typical CR with characteristic velocity $v' = c = \text{const.}$ and gyrofrequency Ω'. To embrace the idea of a grey transport, we treat the scattering as if all CR would have this velocity and gyrofrequency. Formally, we replace all occurring gyrofrequencies and velocities in the scattering terms by those of the typical CR:

$$v \to c, \tag{3.42}$$

$$\Omega = \Omega(p) \to \Omega' = \text{const.} \tag{3.43}$$

[1] One may wonder why such an high order theory is necessary to get a satisfying results. Mihalas and Klein (1982) answers this question in RHD by noting that *'exact consistency of various forms of the energy equation for a radiating fluid requires retention of all v/c terms affecting the radiation field'*.

We further use an isospectral ansatz for the wave intensities:

$$I_{\pm}^{\mathrm{L}}(k) = H(k - k'_{\mathrm{min},\pm})\, C_{\pm} \frac{1}{k^q}, \tag{3.44}$$

$$I_{\pm}^{\mathrm{R}}(k) = H(k - k'_{\mathrm{min},\mp})\, C_{\pm} \frac{1}{k^q}, \tag{3.45}$$

where $k'_{\mathrm{min},\pm} = \Omega/(v \mp v_{\mathrm{a}})$ are the minimal resonant wave numbers and $C_{\pm}$ are normalization constants to be determined. This ansatz is physically plausible: the choice $q = 5/2$ would correspond to a Goldreich-Sridhar-type energy spectrum predicted for Alfvén waves in the inertial regime of MHD turbulence (Goldreich and Sridhar, 1995). This would correspond to a justifiable approach but is not applicable as we are interested in waves that are driven at the injection scale. Indeed, theoretical arguments including different aspects of CR-Alfvén wave dynamics come to the conclusion that $q = 0.8$ to 2.0 for the bulk of resonant wave numbers (Lazarian and Beresnyak, 2006; Yan and Lazarian, 2011; Lithwick and Goldreich, 2001).

Continuing and inserting our ansatz into the definition in eq. (3.25) results in:

$$C_{\pm} = (q-1) \frac{\varepsilon_{\mathrm{a},\pm} \Omega'^{q-1}}{(v' + v_{\mathrm{a}})^{q-1} + (v' - v_{\mathrm{a}})^{q-1}}. \tag{3.46}$$

Adopting our replacements and the isospectral intensity into eq. (3.26) yields finally:

$$\nu_{\pm} = \pi \Omega' \frac{\varepsilon_{\mathrm{a},\pm}}{\varepsilon_B} (q-1) \frac{|\mu v' \mp v_{\mathrm{a}}|^{q-1}}{(v' + v_{\mathrm{a}})^{q-1} + (v' - v_a)^{q-1}}. \tag{3.47}$$

We restrict ourself to the case $q = 2$, which is algebraically convenient and a compromise between a Goldreich-Sridhar-type energy spectrum and the inferred values of q. With this we can calculate the pitch-angle-averaged scattering coefficient to

$$\bar{\nu}_{\pm} = \frac{3}{2} \int_{-1}^{1} \mathrm{d}\mu \frac{1-\mu^2}{2} \nu_{\pm} = \frac{3\pi}{8} \Omega' \frac{\varepsilon_{\mathrm{a},\pm}/2}{\varepsilon_B} \left(1 + \frac{2 v_{\mathrm{a}}^2}{v'^2}\right). \tag{3.48}$$

To calculate the influence of scattering on CR dynamics we have to evaluate the integrals

$$\left.\frac{\partial \varepsilon_{\mathrm{cr}}}{\partial t}\right|_{\mathrm{scatt}} = \int_0^{\infty} \mathrm{d}p\, 2\pi p^2 T(p) \int_{-1}^{1} \mathrm{d}\mu \left.\frac{\partial f}{\partial t}\right|_{\mathrm{scatt}} \tag{3.49}$$

for the CR energy density and

$$\left.\frac{\partial f_{\mathrm{cr}}}{\partial t}\right|_{\mathrm{scatt}} = \int_0^{\infty} \mathrm{d}p\, 2\pi p^2 T(p) v \int_{-1}^{1} \mathrm{d}\mu\, \mu \left.\frac{\partial f}{\partial t}\right|_{\mathrm{scatt}} \tag{3.50}$$

for the CR energy flux density. The complete calculation is carried out in the Appendix A.2. We here state the results. For the CR energy density integral we obtain:

$$\left.\frac{\partial \varepsilon_{\mathrm{cr}}}{\partial t}\right|_{\mathrm{scatt}} = -3 \frac{v_a}{c^2} (\bar{\nu}_+ - \bar{\nu}_-) K_{\mathrm{cr}} + 4 \frac{v_a^2}{c^2} (\bar{\nu}_+ + \bar{\nu}_-) P_{\mathrm{cr}} \tag{3.51}$$

$$= -\frac{v_a}{3\kappa_+} \left[f_{\mathrm{cr}} - v_a(\varepsilon_{\mathrm{cr}} + P_{\mathrm{cr}})\right] + \frac{v_a}{3\kappa_-} \left[f_{\mathrm{cr}} + v_a(\varepsilon_{\mathrm{cr}} + P_{\mathrm{cr}})\right], \tag{3.52}$$

while the CR energy flux integral evaluates to:

$$\left.\frac{\partial f_{\rm cr}}{\partial t}\right|_{\rm scatt} = -(\bar{\nu}_+ + \bar{\nu}_-) f_{\rm cr} + v_a(\bar{\nu}_+ - \bar{\nu}_-)(\varepsilon_{\rm cr} + P_{\rm cr}) \tag{3.53}$$

$$= -\frac{c^2}{3\kappa_+}\left[f_{\rm cr} - v_a(\varepsilon_{\rm cr} + P_{\rm cr})\right] - \frac{c^2}{3\kappa_-}\left[f_{\rm cr} + v_a(\varepsilon_{\rm cr} + P_{\rm cr})\right], \tag{3.54}$$

where we define the spatial diffusion coefficients by:

$$\kappa_\pm = \frac{c^2}{3\bar{\nu}_\pm}. \tag{3.55}$$

In both equations the first line is the direct algebraic results of the calculation. The second line emphasizes the symmetric properties of the scattering process with respect to the wave frames.

Let us give a few remarks concerning these terms and their dynamics:

- Eqs. (3.52) and (3.54) are Galilean invariant: only the flux in the respective wave frame $f_{\rm cr} \pm v_{\rm a}(\varepsilon_{\rm cr} + P_{\rm cr})$ determines the magnitude of pitch-angle scattering and energy transfer. Any lower-order approximation in $v_{\rm a}/v$ loses this property.
- If the bulk of CRs are isotropic in one wave frame, corresponding to $f_{\rm cr} = \pm v_a(\varepsilon_{\rm cr} + P_{\rm cr})$, the scattering contribution of the corresponding wave type vanishes. This results becomes evident by switching into one of the Alfvén waves frame: there the Alfvén wave consists purely of a magnetic component. Accordingly, waves and CRs only interact via pitch-angle scattering

  $$\left.\frac{\partial f}{\partial t}\right|_{\rm scatt,wave} = \frac{\partial}{\partial \mu}\left(\frac{1-\mu^2}{2}\nu(p,\mu)\frac{\partial f}{\partial \mu}\right)\Bigg|_{\rm wave}. \tag{3.56}$$

  For an isotropic distribution $\partial_\mu f|_{\rm wave} = 0$ holds and hence no scattering takes place.
- Consider the following scenario where CRs are transported at a velocity greater than the Alfvén velocity:

  $$|f_{\rm cr}| \geq v_{\rm a}(\varepsilon_{\rm cr} + P_{\rm cr}). \tag{3.57}$$

  In this case, CRs lose energy by virtue of eq. (3.52) to one of the wave types. This in turn will increase the scattering coefficient $\bar{\nu} \propto \varepsilon_{\rm a}$ and thus lead to stronger scattering of CRs. This will continue until the CRs become isotropic in the corresponding wave frame. This is the manifestation of the CR self-confinement idea. Formally speaking CRs dynamically enforce that in equilibrium,

  $$|u_{\rm st}| = \left|\frac{f_{\rm cr}}{\varepsilon_{\rm cr} + P_{\rm cr}}\right| \lesssim v_{\rm a} \tag{3.58}$$

  and thus CR stream at most at the Alfvén speed. Translating this back into the distribution components $f_{0,1}$, this states that the Knudsen number is

  $$\mathsf{Kn} = \left|\frac{f_1(p)}{f_0(p)}\right| \lesssim \frac{v_{\rm a}}{v} \ll 1, \tag{3.59}$$

  for most momenta. Hence, CRs are sufficiently confined such that their anisotropy is small. We use this assumption a priori as our initial building block to expand the full distribution in its first two moments only. We can now justify this presumption a posteriori.

- We derive the preceding argument macroscopically for the macroscopic quantities $\varepsilon_{\rm cr}$ and $f_{\rm cr}$. On a microscopic level this certainly changes. As CRs with low and intermediate energies ($T \lesssim 200$ GeV) carry the bulk of CR pressure for distributions with $\propto f^{-\alpha}$, $\alpha > 4$, this argument holds for them. This is the energy range, for which resonant CRs sufficiently amplify Alfvén waves such that the argument even holds microscopically. For CRs at higher energies, which have a much lower number density, the scattering by self-provided Alfvén waves is not sufficient to efficiently scatter. These high-energy CRs contribute little to the total amount of energy contained in CRs such that hydrodynamically only low- and intermediate-energy CRs are of interest.
- We use eq. (3.43) as a grey approximation in our derivation. A more correct non-grey approximation would be possible by introducing momentum-averaged scattering coefficients. To account for the different momentum integrals, we would have to introduce 7 of those averaged coefficients. This zoo of new coefficients would obfuscate the derivation and thus is ignored in this exploratory work.
- We use a handful of approximations to derive our new transport equations. Nonetheless this approximation/derivation is compatible with previous studies: to connect our equations to previous work, we use the Chapman-Enskog expansion in the scattering terms. Doing so in eq. (3.17) in combination with eq. (3.54) where the fast time scales are given by L/c and κ/c^2 yields

$$f_{\rm cr} = -\frac{1}{\bar{\nu}_+ + \bar{\nu}_-}\frac{c^2 \boldsymbol{b}}{3} \cdot \boldsymbol{\nabla}\varepsilon_{\rm cr} + v_a \frac{\bar{\nu}_+ - \bar{\nu}_-}{\bar{\nu}_+ + \bar{\nu}_-}(\varepsilon_{\rm cr} + P_{\rm cr}). \tag{3.60}$$

This is the equilibrium flux of CRs when CR inertia and pseudoforces can be neglected. In practice, the actual time-dependent flux is near this equilibrium flux when CRs are efficiently scattered. Back-inserting this into eq. (3.16) results in

$$\begin{aligned}\frac{\partial \varepsilon_{\rm cr}}{\partial t} + \boldsymbol{\nabla} \cdot [(\boldsymbol{u} + u_{\rm st}\boldsymbol{b})(\varepsilon_{\rm cr} + P_{\rm cr}) - \kappa \boldsymbol{b}\boldsymbol{b} \cdot \boldsymbol{\nabla}\varepsilon_{\rm cr}] = \\ +(\boldsymbol{u} + u_{\rm st}\boldsymbol{b}) \cdot \boldsymbol{\nabla} P_{\rm cr} + 4\frac{\bar{\nu}_+\bar{\nu}_-}{\bar{\nu}_+ + \bar{\nu}_-}\frac{v_{\rm a}^2}{c^2}(\varepsilon_{\rm cr} + P_{\rm cr}),\end{aligned} \tag{3.61}$$

where

$$\boldsymbol{v}_{\rm st} = v_a \frac{\bar{\nu}_+ - \bar{\nu}_-}{\bar{\nu}_+ + \bar{\nu}_-}\boldsymbol{b} \tag{3.62}$$

is the streaming velocity and

$$\kappa = \frac{c^2}{3(\bar{\nu}_+ + \bar{\nu}_-)} \tag{3.63}$$

is the total diffusion coefficient.
This equation coincides with the streaming-diffusion equation, modified by the inclusion of the last term (Ko, 1992; Zweibel, 2017; Pfrommer et al., 2017). This term accounts for the Fermi II process. This process always transfers energy from Alfvén waves to CRs since both $\bar{\nu}_+$ and $\bar{\nu}_-$ are positive.

3.5. Alfvénic Turbulence

The result in the last section shows that it is crucial to know $\bar{\nu}_\pm$ to correctly understand the scattering and hence the transport CRs. In particular, the relative balance between $\bar{\nu}_+$ and $\bar{\nu}_-$ regulates the streaming velocity and thus the macroscopic transport of energy. Since $\bar{\nu}_\pm \propto \varepsilon_{\mathrm{a},\pm}$ it is sufficient to know how the energy contained in Alfvén waves evolves to correctly evaluate $\nu_\pm$ in our grey approximation. In this section we recall the fluid equations of the macroscopic transport of Alfvén wave energy and account for their interaction with CRs and the thermal gas. To this end, we calculate the growth of wave energy by the gyro-resonant instability with the same methods as we do for CR scattering. By reviewing the primary damping mechanisms of waves, we formally couple the waves to the thermal gas.

3.5.1. Transport of Alfvén Waves

The macroscopic transport equation for the energy contained in a single wave mode can be calculated using the action principle of Whitham (1961). Neglecting all nonlinear terms, this results in (Dewar, 1970; Jacques, 1977):

$$\frac{\partial E_\pm(k)}{\partial t} + \boldsymbol{\nabla} \cdot [(\boldsymbol{u} \pm v_\mathrm{a}\boldsymbol{b})\, E_\pm(k)] + \frac{1}{2}(\boldsymbol{\nabla}\cdot\boldsymbol{u})E_\pm(k) = \Gamma_\pm(k)E_\pm(k), \tag{3.64}$$

where $\Gamma_\pm(k)$ are growth and damping rates of a single wave mode.

The interpretation of the hyperbolic part of this equation is straightforward: Alfvén wave energy is transported with the total Alfvén velocity $\boldsymbol{u} + v_\mathrm{a}\boldsymbol{b}$ and is subject to adiabatic changes with respect to the gas frame.

The hydrodynamic formulation can be obtained by integrating over all wave-numbers, which yields with the definition of eq. (3.25) (Ko, 1992):

$$\frac{\partial \varepsilon_{\mathrm{a},\pm}}{\partial t} + \boldsymbol{\nabla} \cdot [(\boldsymbol{u} \pm v_a\boldsymbol{b})\, \varepsilon_{\mathrm{a},\pm}] + \frac{1}{2}(\boldsymbol{\nabla}\cdot\boldsymbol{u})\varepsilon_{\mathrm{a},\pm} = S_{\mathrm{gri},\pm} - L_{\mathrm{a},\pm}, \tag{3.65}$$

where we separated the total contributions of the gyro-resonant instability

$$S_{\mathrm{gri},\pm} = \int_0^\infty \mathrm{d}k\, \Gamma_{\mathrm{gri},\pm}(k) R_\pm(k), \tag{3.66}$$

and other loss processes

$$L_{\mathrm{a},\pm} = \int_0^\infty \mathrm{d}k\, \Gamma_{\mathrm{loss},\pm}(k) E_\pm(k). \tag{3.67}$$

into different terms. We are now calculating these hydrodynamic terms, based on the respective growth and damping rates Γ.

3.5.2. Gyroresonant Instability

The gyroresonant instability dynamically links CRs and Alfvén waves. It is the conceptional inverse of momentum-diffusion. Trigged by any residual anisotropy of CRs in the wave frame,

this instability transfers energy between CRs and waves as a collective plasma-kinetic effect. On a microscopic level these waves are excited as CRs gyrate around the mean magnetic field. They can thus resonantly interact with electromagnetic fields of the same frequency as their gyrofrequency.

The growth rate of this process is given by (see e.g. Kulsrud and Pearce, 1969):[2]

$$\Gamma_{\pm,\mathrm{st}} = \pm\pi\frac{\Omega^2 v_\mathrm{a}}{\varepsilon_\mathrm{B}}\int \mathrm{d}^3p\frac{1-\mu^2}{2}p\left(\frac{\partial f}{\partial\mu}+\frac{\boldsymbol{b}\cdot\boldsymbol{u}_\pm}{c}p\frac{\partial f}{\partial p}\right)\delta\left((\mu v\mp v_\mathrm{a})k-\Omega\right), \tag{3.68}$$

where $\boldsymbol{u}_\pm$ are the wave velocities relative to the reference frames. As the comoving frame is our reference frame, these velocities are given by $\boldsymbol{u}_\pm = \pm v_\mathrm{a}\boldsymbol{b}$. Performing the momentum integral yields the actual growth-/damping-rate of a single wave mode. The resulting expression depends on the Doppler shifted CR-anisotropy $\partial_\mu f \pm p v_\mathrm{a}/c\partial_p f$, evaluated at the momenta corresponding to gyro-resonance.

We are here interested in the growth/damping of the total wave energy density. For this it is inconvenient to evaluate the momentum integral directly. Employing our approximation of sec. 3.4, we calculate eq. (3.66) to:

$$S_{\mathrm{gri},\pm} = \pm\frac{v_\mathrm{a}}{3\kappa_\pm}\left[f_\mathrm{cr}\mp v_\mathrm{a}(\varepsilon_\mathrm{cr}+P_\mathrm{cr})\right]. \tag{3.69}$$

The actual evaluation of both integrals is presented in the Appendix A.3.

By comparing this equation to eq. (3.52), we conclude that CR scattering and gyro-instability conserves the energy in our theory. Again, this is owning to our approximation up to order $O(\bar{v}v_\mathrm{a}^2/c^2)$. Any lower-order theory is energy non-conserving, as the same terms in the CR energy and Alfvén wave-energy equations appear formally at different orders.

3.5.3. Wave Damping Processes

Wave damping processes transfer energy from Alfvén waves to the thermal gas. Consequently, these processes indirectly link CRs to the thermal gas. There is a variety of different phenomena that can drain energy from the waves. Here we focus on the most important processes.

Ion Neutral Damping

Friction between ions and neutrals was the first damping process considered for counteracting the gyroresonant instability (see Appendix C of Kulsrud and Pearce, 1969). It becomes important in situations where there is a non-negligible amount neutrals present in the thermal gas. When ions and neutrals drift with respect to each other, friction between the two species de- and accelerates both species until they reach a dynamical equilibrium. Furthermore, ions are subject to the Lorentz force provided by the Alfvén waves. In the case when the friction and Lorentz forces can cancel each other, energy is transfered from the waves to the ions and neutrals. In the end this process thermalizes wave energy and heats the gas.

[2] Most old literature sources describe the wave growth in their own wave frames and/or neglect the momentum derivative of f, due to the $u_\pm/c$ factor in front of it. For an energy conserving result up to order $u_\pm^2/c^2$ it is necessary to fully account for the Doppler shift between wave and reference frame, as it is done here.

We here consider a plasma composed of ions (i), neutral hydrogen (H) and neutral helium (He). This situation is analyzed in detail by Soler et al. (2016). Let us first define the friction coefficients between species β and β' (Braginskii, 1965):

$$\alpha_{\beta\beta'} = n_\beta \, n_{\beta'} \, m_{\beta\beta'} \, \sigma_{\beta\beta'} \frac{4}{3} \sqrt{\frac{8 k_\mathrm{b} T}{\pi m_{\beta\beta'}}}, \tag{3.70}$$

where T is the temperature (we assume that all plasma components are in local thermal equilibrium), m_β is particle mass of species β, $m_{\beta\beta'} = m_\beta m_{\beta'}/(m_\beta + m_{\beta'})$ is the reduced mass, k_B is Boltzmann's constant, $\sigma_{\beta\beta'}$ is the momentum transfer cross section given by $\sigma_{iH} \approx 10^{-18}\mathrm{m}^2$ and $\sigma_{iHe} \approx 3 \times 10^{-19}\mathrm{m}^2$. With this definition, the rate at which Alfvén waves transfer energy to the gas is given by:

$$\Gamma_\mathrm{in} = \frac{1}{2} \left(\frac{\alpha_\mathrm{iH}}{\rho_\mathrm{i}} + \frac{\alpha_\mathrm{iHe}}{\rho_\mathrm{i}} \right), \tag{3.71}$$

where ρ_i is the mass density of ions. In comparison to Soler et al. (2016) we neglect any higher-order contribution of $\alpha_{\beta\beta'}$ to this rate. Because Γ_in is independent of wave number, we can readily calculate the total loss term by ion-neutral damping to

$$L_{\mathrm{in},\pm} = \Gamma_\mathrm{in} \, \varepsilon_{\mathrm{a},\pm}. \tag{3.72}$$

This process operates efficiently when neutrals are abundant as $\alpha_{iH}, \alpha_{iHe} \propto n_\mathrm{neutrals}$. Thus neutral damping can be important in dense cold HI regions like in molecular clouds.

Nonlinear Landau Damping

As the name suggest, nonlinear Landau damping is a second-order process consisting of two participating waves. Consider two Alfvén waves with wave numbers and frequencies, $k_{1,2}$ and $\omega_{1,2}$. They form together a beat wave that travels at speed,

$$v_\mathrm{beat} = \frac{\omega_1 - \omega_2}{k_1 - k_2} \tag{3.73}$$

and drives a second-order magnetic pressure gradient that couples to a second-order ion sound wave which in turn induces a longitudinal electric field (Hollweg, 1971). Charged particles in the thermal gas can interact with this electric field, when the approximate gyroresonance

$$v_\mathrm{th} \approx v_\mathrm{beat} \tag{3.74}$$

is fulfilled. Note that this is a gyroresonace between three participants as opposed to the CR gyroresonace in sec. 3.2. Here a thermal particle resonates with the beat wave of two magnetic perturbations, whereas in the CR gyro-resonance the particle resonates solely with a single wave. The description of the associated transfer of energy is done in detail by Lee and Völk (1973). Their full theory can be condensed and simplified for various astrophysical environments (Miller, 1991).

We can categorize pairs of Alfvén waves by their propagation direction along the mean magnetic field: they either propagate in the same direction or anti-parallel to each other. Nonlinear

Landau damping between anti-parallel propagating waves is in general weaker (Miller, 1991) such that we focus only on the damping of two waves propagating in the same direction. For this case $v_{\rm beat} = v_{\rm a}$ and the resonance condition in eq. (3.74) boils down to: $v_{\rm th} \approx v_{\rm a}$. This condition is fulfilled in plasmas with a high value $\beta_{\rm plasma}$ by protons and other ions, whereas in low $\beta_{\rm plasma}$ plasmas only electrons can mediate the damping.

The rate at which waves lose energy by nonlinear Landau Damping is given by (Völk and McKenzie, 1981):

$$\Gamma_{\rm nll,\pm}(k) = \frac{\sqrt{\pi}}{8}\frac{v_{\rm th}}{\varepsilon_{\rm B}} k \int_0^k {\rm d}k'\, E_\pm(k')., \tag{3.75}$$

and is genuinely nonlinear through its dependence on $E_\pm(k)$. Nevertheless, we can insert this rate into eq. (3.67) and formally perform the integration to

$$L_{\rm nll,\pm} = \alpha \varepsilon^2_{\rm a,\pm} \tag{3.76}$$

where the damping coefficient is given by,

$$\alpha = \frac{\sqrt{\pi}}{8}\frac{v_{\rm th}}{\varepsilon_B}\langle k\rangle, \tag{3.77}$$

with an averaged wave number (Völk and McKenzie, 1981):

$$\langle k\rangle = \frac{1}{\varepsilon^2_{\rm a,\pm}} \int_0^\infty {\rm d}k\, k E_\pm(k) \int_0^k {\rm d}k'\, E_\pm(k'), \tag{3.78}$$

which has to be of order as the CR gyroradius, as the first integral gives a larger weight to waves with lower wavenumbers.

There is a small inconsistency in our theory. We assumed in sec. 3.4 a special algebraic form for $E_\pm(k)$ in order to calculate the scattering terms. If we now insert eqs. (3.44) and (3.45) with our choice $q = 2$ into eq. (3.78), the integral diverges at large wavenumbers. This is a formal problem of our isospectral assumption for the intensities $I^{\rm L,R}_\pm$. In reality, these spectra are not applicable for large wave numbers. There, only a few CRs resonate and the driving of waves by the gyroresonant instability becomes weak. As driving becomes sub-dominant, all sorts of damping become more important and the CR generated turbulence must enter its inertia regime until it reaches its dissipation scales for larger wave numbers. There, our assumption of isospectral intensities breaks down. In the end, eq. (3.78) can be safely evaluated because the spectrum must become harder.

Turbulent Wave Damping

In the energy eq. (3.64) any nonlinear interaction is assumed to be small. Nevertheless, in MHD turbulence and hence in Alfvénic turbulence energy is transfered to larger wavenumbers by virtue of a cascade mediated by mode coupling. Lazarian and Beresnyak (2006) and Farmer and Goldreich (2004) argue that the contributions of this cascade to the dynamical evolution of $\varepsilon_{\rm a,\pm}$ cannot be neglected. We follow this suggestion and correct our simplified equations by including the nonlinear damping of a single mode by an effective damping rate.

The main difference between HD and MHD turbulence is the high anisotropy of the cascade along the mean magnetic field. Consider a localized and elongated Alfvén wave packet with parallel wavenumber k and perpendicular wavenumber $k_\perp$. This wave is sheared perpendicular to the mean magnetic field through the Lorentz force during its propagation. This leaves the wave distorted (Lithwick and Goldreich, 2001). Consequently, the energy is transfered to larger k and smaller $k_\perp$. This process is thus energy conserving but removes energy from a specific wave number k.

This damping operates on eddy turnover time scales and is minimized at the largest injection scale. As the gyro-instability drives Alfvén waves, this scale is given by the gyro-radius of CRs: $r_\mathrm{L} \approx 1/k_\mathrm{min}$. The associated damping rate is given by (Farmer and Goldreich, 2004; Zweibel, 2013):

$$\Gamma_\mathrm{turb} \approx v_\mathrm{a} k_\mathrm{min} \sqrt{\frac{k_\mathrm{mhd,turb}}{k_\mathrm{min}}}, \tag{3.79}$$

where $k_\mathrm{mhd,turb}$ is the wavenumber at which the large-scale magnetic field is driven. Integrating over the wave spectrum yields a total wave damping of

$$L_\mathrm{turb,\pm} = \Gamma_\mathrm{turb} \varepsilon_\mathrm{a,\pm}. \tag{3.80}$$

Turbulent Linear Landau Damping

So far we assumed that the Alfvén waves are purely propagating parallel to the mean magnetic field lines. This mean magnetic field is turbulent and hence constantly changes its directions. Strong curvature in the magnetic field can shift the wave propagation mode from a parallel one to a slightly oblique one. By Ohm's law this obliquity introduces a small electric field component of the wave along $\boldsymbol{B}$. Thermal particles get accelerated by this field and thus the thermal gas is heated.

Because this effect again depends on the actual nature of turbulence, we treat it only approximately. The rate at which energy is lost can be written as (Zweibel, 2017):

$$\Gamma_\mathrm{ll} \approx -\frac{\sqrt{\pi}}{4} v_\mathrm{a} k_\mathrm{\parallel,min} \sqrt{\beta_\mathrm{plasma} \frac{k_\mathrm{MHD,turb}}{k_\mathrm{\parallel,min}}}. \tag{3.81}$$

Because this rate is independent of k, we can readily integrate it over the wave spectrum to get a total wave energy loss term of

$$L_\mathrm{ll,\pm} = \Gamma_\mathrm{ll} \varepsilon_\mathrm{a,\pm}. \tag{3.82}$$

By comparing eqs. (3.81) and (3.79), we conclude that both loss processes introduced by the MHD turbulence have approximately the same strength (e.g., turbulent linear Landau damping is more dominate when $\beta_\mathrm{plasma} \gtrapprox 16/\pi \approx 5$).

3.6. CR-MHD Equations

So far, we treat the MHD quantities as passive external components of our theory. As discussed in the last section, CRs and the thermal gas interact indirectly through electromagnetic fields.

To account for this coupling we combine MHD and CR fluid equations in this section to a combined set of CR MHD equations.

3.6.1. Coupling to the thermal gas

The most dominant interaction between both particle species is through the Lorentz force mediated by the large scale magnetic field. To formally describe this we rewrite the momentum equation in (2.12) in its original form:

$$\frac{\partial(\rho \boldsymbol{u})}{\partial t} + \boldsymbol{\nabla} \cdot (\rho \boldsymbol{u}\boldsymbol{u} + P_{\mathrm{th}}\mathbf{1}) = \frac{\boldsymbol{j}_{\mathrm{gas}} \times \boldsymbol{B}}{c} + \boldsymbol{f}_{\mathrm{ponder}}, \tag{3.83}$$

where j_{gas} is the current of the gas and $\boldsymbol{f}_{\mathrm{ponder}}$ is the pondermotive force density.

A fully correct CR transport theory in the limit $O(v_{\mathrm{a}}^2/v^2)$ would introduce a variety of MHD inertia terms into the comoving eq. (3.1) (Zank, 2014). We implicitly neglected these and thus assumed a coupling between CRs and thermal particles in the Newtonian limit. To be consistent, we have to formally describe the momentum and energy balance between the two in the same limit.

In the Newtonian limit the CR fluid is an ordinary fluid and can be described by a momentum equation similar to the one for the thermal gas. In particular, we have for the momentum component parallel to the magnetic field:

$$\rho_{\mathrm{cr}} \left(\frac{\partial \boldsymbol{u}_{\mathrm{cr}}}{\partial t} \right)_{\perp} + \rho_{\mathrm{cr}} \left(\boldsymbol{u}_{\mathrm{cr}} \cdot \boldsymbol{\nabla} \boldsymbol{u}_{\mathrm{cr}} \right)_{\perp} + \boldsymbol{\nabla}_{\perp} P_{\mathrm{cr}} = \frac{\boldsymbol{j}_{\mathrm{cr}} \times \boldsymbol{B}}{c}. \tag{3.84}$$

Because CRs have a low number- and hence mass-density, they exhibit low inertia. They are thus strongly affected by any macroscopic force. Consequently, they try to reach a force equilibrium between forces exerted by themselves and external ones. We can neglect both inertia terms in eq. (3.84) and proceed with the force balance:

$$\boldsymbol{\nabla}_{\perp} P_{\mathrm{cr}} = \frac{\boldsymbol{j}_{\mathrm{cr}} \times \boldsymbol{B}}{c}. \tag{3.85}$$

Both momentum equations are linked by the occurring Lorentz forces and Ampere's law

$$\boldsymbol{\nabla} \times \boldsymbol{B} = \frac{\boldsymbol{j}_{\mathrm{gas}} + \boldsymbol{j}_{\mathrm{cr}}}{c}. \tag{3.86}$$

Replacing j_{gas} in eq. (3.83) and combining the result with the CR force balance yields an expression for the Lorentz force exerted on the gas:

$$\boldsymbol{f}_{\mathrm{Lorentz}} = \frac{\boldsymbol{j}_{\mathrm{gas}} \times \boldsymbol{B}}{c} = \boldsymbol{\nabla} \times \boldsymbol{B} \times \boldsymbol{B} - \boldsymbol{\nabla}_{\perp} P_{\mathrm{cr}}. \tag{3.87}$$

The dynamics of CRs along the magnetic field is extensively discussed in sec. (3.4). We obtain a definition for CR momentum parallel to the mean magnetic field by rewriting the definition of the CR energy flux density in eq. (3.13) in the ultra-relativistic limit:

$$\rho_{\mathrm{cr}} u_{\mathrm{cr},\parallel} = \frac{1}{c^2} f_{\mathrm{cr}}. \tag{3.88}$$

Our derivation of scattering is done in the semi-relativistic limit of (v^2/c^2). This implies that our descriptions of energy and hence momentum transfer between Alfvén waves and CRs are valid on short time scales. To get a consistent treatment, we have to describe all participants of the total momentum balance at the same order. Since we couple MHD and CR quantities in the $O(1)$ limit, we have to downgrade the CR dynamics to this order. We do so by using the Chapman-Enskog expansion of eq. (3.17), to get the force balance along the mean magnetic field in the $O(1)$ limit:

$$\frac{1}{3}\nabla_{\parallel}\varepsilon_{\mathrm{cr}} = \left.\frac{\partial(\rho_{\mathrm{cr}}u_{\mathrm{cr},\parallel})}{\partial t}\right|_{\mathrm{scatt}}, \tag{3.89}$$

or equivalently, using the equation of state (3.12):

$$\nabla_{\parallel}P_{\mathrm{cr}} = \left.\frac{\partial(\rho_{\mathrm{cr}}u_{\mathrm{cr},\parallel})}{\partial t}\right|_{\mathrm{scatt}}. \tag{3.90}$$

The scattering and hence the momentum transfer happens between Alfvén waves and CRs. But the amplification of Alfvén waves induces a dielectric current which can then interact with the thermal gas (Achterberg, 1981). The force density exerted on the thermal gas by this effect is called ponderomotive force density and is given by:

$$\boldsymbol{f}_{\mathrm{ponder}} = -\boldsymbol{\nabla}\left(P_{\mathrm{a},+} + P_{\mathrm{a},-}\right) - \nabla_{\parallel}P_{\mathrm{cr}}. \tag{3.91}$$

By the first law of thermodynamics, each conservative force is accompanied by a work done on the surroundings. For the thermal gas we can derive the associated work terms by multiplying eq. (3.83) by $\boldsymbol{u}$ and using the continuity equation. This yields the equation for the mechanical energy:

$$\frac{1}{2}\frac{\partial\left(\rho\boldsymbol{u}^2\right)}{\partial t} + \boldsymbol{\nabla}\cdot\left[\rho\boldsymbol{u}\left(\frac{\boldsymbol{u}^2}{2}\right)\right] = w_{\mathrm{th}} + w_{\mathrm{ponder}} + w_{\mathrm{lorentz}}, \tag{3.92}$$

where the volume work done by each of the forces are:

$$\begin{aligned}
\text{thermal gas pressure:} \quad & w_{\mathrm{th}} &&= -\boldsymbol{u}\cdot\boldsymbol{\nabla}P_{\mathrm{th}}, \\
\text{ponderomotive force:} \quad & w_{\mathrm{ponder}} &&= -\boldsymbol{u}\cdot\boldsymbol{\nabla}(P_{\mathrm{a},+} + P_{\mathrm{a},-}) - \boldsymbol{u}\cdot\nabla_{\parallel}P_{\mathrm{cr}}, \\
\text{Lorentz force:} \quad & w_{\mathrm{lorentz}} &&= +\boldsymbol{u}\cdot(\boldsymbol{\nabla}\times\boldsymbol{B}\times\boldsymbol{B}) - \boldsymbol{u}\cdot\boldsymbol{\nabla}_{\perp}(P_{\mathrm{cr}}).
\end{aligned} \tag{3.93}$$

The above arguments heavily depend on the $O(1)$ limit while we described scattering of CRs up to $O(v_{\mathrm{a}}^2/c^2)$. This inconsistency can be removed also by treating both the couplings to the second order. As we formulate CR hydrodynamics in the gas rest frame, this would require a more sophisticated handling of the geometric transport terms to correctly account for the change into a non-inertial frame. Indeed, even the first order ($O(v_{\mathrm{a}}/c)$) adds terms proportional to $\mathrm{d}\boldsymbol{u}/\mathrm{d}t$ and $\mathrm{d}\boldsymbol{b}/\mathrm{d}t$, where $\mathrm{d}/\mathrm{d}t = \partial/\partial t + \boldsymbol{u}\cdot\boldsymbol{\nabla}$ is the convective derivative (Zank, 2014). This would not only obfuscate our theory but also precludes a transparent analytical and numerical analysis of the resulting equations. We refrain from doing so and leave possible improvements for subsequent work. Nevertheless, this limits the applicability of our theory to cases where the relevant time scale Tc/v_{a} is larger than the shortest scattering time scale $c^2/v_{\mathrm{a}}^2/\nu$ considered.

3.6.2. Full set of CR-MHD Equations

Because equations describing the thermal gas and CRs are scattered throughout this work, we collect them here to provide an overview. The equations for ideal MHD coupled to non-thermal CR and Alfvén wave populations are given by:

$$\frac{\partial \rho}{\partial t} + \boldsymbol{\nabla} \cdot (\rho \boldsymbol{u}) = 0 \tag{3.94}$$

$$\frac{\partial \rho \boldsymbol{u}}{\partial t} + \boldsymbol{\nabla} \cdot (\rho \boldsymbol{u}\boldsymbol{u} + P_{\mathrm{tot}} \mathbf{1} - \boldsymbol{B}\boldsymbol{B}) = 0 \tag{3.95}$$

$$\frac{\partial \boldsymbol{B}}{\partial t} + \boldsymbol{\nabla} \cdot (\boldsymbol{B}\boldsymbol{u} - \boldsymbol{u}\boldsymbol{B}) = 0 \tag{3.96}$$

$$\frac{\partial \varepsilon}{\partial t} + \boldsymbol{\nabla} \cdot [\boldsymbol{u}(\varepsilon + P) - (\boldsymbol{u} \cdot \boldsymbol{B})\boldsymbol{B}] = -\boldsymbol{u} \cdot \boldsymbol{\nabla}(P_{\mathrm{cr}} + P_{\mathrm{a},+} + P_{\mathrm{a},-}) + L_{\mathrm{a},+} + L_{\mathrm{a},-}. \tag{3.97}$$

The total and gas pressures are given by:

$$P_{\mathrm{tot}} = P_{\mathrm{th}} + \frac{\boldsymbol{B}^2}{2} + P_{\mathrm{cr}} + P_{\mathrm{a},+} + P_{\mathrm{a},-}, \tag{3.98}$$

$$P = P_{\mathrm{th}} + \frac{\boldsymbol{B}^2}{2}, \tag{3.99}$$

where P_{th} is the thermal pressure, P_{cr} is the CR pressure and $P_{\mathrm{a},\pm}$ are the ponderomotive pressures due to presence of Alfvén waves. The total energy density contained in the large scale magnetic field and the thermal gas is

$$\varepsilon = \frac{\rho \boldsymbol{u}^2}{2} + \varepsilon_{\mathrm{th}} + \varepsilon_B, \tag{3.100}$$

where $\varepsilon_{\mathrm{th}}$ and $\varepsilon_B = \boldsymbol{B}^2/2$ are the thermal and magnetic energy densities. $L_{\mathrm{a},\pm}$ are the source terms of thermal energy due to Alfvén wave energy losses as detailed in sec. 3.5. All pressures and energy densities are related by the respective equations of states:

$$P_{\mathrm{th}} = (\gamma_{\mathrm{th}} - 1)\varepsilon_{\mathrm{th}}, \qquad \gamma_{\mathrm{th}} = \frac{5}{3}, \tag{3.101}$$

$$P_{\mathrm{cr}} = (\gamma_{\mathrm{cr}} - 1)\varepsilon_{\mathrm{cr}}, \qquad \gamma_{\mathrm{cr}} = \frac{4}{3}, \tag{3.102}$$

$$P_{\mathrm{a},\pm} = (\gamma_{\mathrm{a}} - 1)\varepsilon_{\mathrm{a},\pm}, \qquad \gamma_{\mathrm{a}} = \frac{3}{2}. \tag{3.103}$$

These equations describe how all MHD quantities evolve in the presence of CRs and Alfvén waves. Our contribution to the full system are the equation describing the evolution of the CR and Alfvén waves energies. Collecting the corresponding eqs.(3.16), (3.17), (3.52), and (3.54)

gives:

$$\frac{\partial \varepsilon_{\rm cr}}{\partial t} + \boldsymbol{\nabla} \cdot [\boldsymbol{u}(\varepsilon_{\rm cr} + P_{\rm cr}) + \boldsymbol{b} f_{\rm cr}] = \boldsymbol{u} \cdot \boldsymbol{\nabla} P_{\rm cr} - \frac{v_{\rm a}}{3\kappa_+}\left[f_{\rm cr} - v_{\rm a}(\varepsilon_{\rm cr} + P_{\rm cr})\right] + \frac{v_{\rm a}}{3\kappa_-}\left[f_{\rm cr} + v_{\rm a}(\varepsilon_{\rm cr} + P_{\rm cr})\right], \tag{3.104}$$

$$\frac{\partial f_{\rm cr}}{\partial t} + \boldsymbol{\nabla} \cdot (\boldsymbol{u} f_{\rm cr}) + \frac{c^2}{3}\boldsymbol{b} \cdot \nabla \varepsilon_{\rm cr} = -(\boldsymbol{b} \cdot \boldsymbol{\nabla} \boldsymbol{u}) \cdot (\boldsymbol{b} f_{\rm cr}) - \frac{c^2}{3\kappa_+}\left[f_{\rm cr} - v_{\rm a}(\varepsilon_{\rm cr} + P_{\rm cr})\right] - \frac{c^2}{3\kappa_-}\left[f_{\rm cr} + v_{\rm a}(\varepsilon_{\rm cr} + P_{\rm cr})\right], \tag{3.105}$$

$$\frac{\partial \varepsilon_{\rm a,\pm}}{\partial t} + \boldsymbol{\nabla} \cdot [\boldsymbol{u}(\varepsilon_{\rm a,\pm} + P_{\rm a,\pm}) \pm v_{\rm a} \boldsymbol{b} \varepsilon_{\rm a,\pm}] = \boldsymbol{u} \cdot \boldsymbol{\nabla} P_{\rm a,\pm}\left[f_{\rm cr} \mp v_{\rm a}(\varepsilon_{\rm cr} + P_{\rm cr})\right] - L_{\rm a,\pm}. \tag{3.106}$$

Our closure of the CR-Alfvénic subsystem is a grey approximation for the CR diffusion coefficient:

$$\frac{1}{\kappa_\pm} = \frac{9\pi}{8}\frac{\Omega'}{c^2}\frac{\varepsilon_{\rm a,\pm}/2}{\varepsilon_B}\left(1 + \frac{2v_{\rm a}^2}{c^2}\right), \tag{3.107}$$

where $\Omega' = Z'eB/(\gamma' mc)$ is the relativistic gyro frequency of typical member of the CR population with charge Z' and characteristic Lorentz factor γ' and particle rest mass m.

We can check the physical plausibility of our set of equations by the following argument: the total energy density contained in the thermal gas, magnetic fields, CRs, and Alfvén waves is given by

$$\varepsilon_{\rm tot} = \frac{\rho \boldsymbol{u}^2}{2} + \varepsilon_{\rm th} + \varepsilon_B + \varepsilon_{\rm cr} + \varepsilon_{\rm a,+} + \varepsilon_{\rm a,-}. \tag{3.108}$$

By adding all of the above energy equations, we see that the total energy $E_{\rm tot} = \int \mathrm{d}^3 x\, \varepsilon_{\rm tot}$ is conserved as its density follows a conservation law:

$$\frac{\partial \varepsilon_{\rm tot}}{\partial t} + \boldsymbol{\nabla} \cdot \boldsymbol{F}_{\rm tot} = 0, \tag{3.109}$$

where the total energy flux is given by:

$$\boldsymbol{F}_{\rm tot} = \boldsymbol{u}(\varepsilon_{\rm tot} + P_{\rm tot}) + \boldsymbol{b}[f_{\rm cr} + v_{\rm a}(\varepsilon_{\rm a,+} - \varepsilon_{\rm a,-}) - (\boldsymbol{u} \cdot \boldsymbol{B})\, B]. \tag{3.110}$$

This is a necessary result, as we excluded any external sources of CR/thermal/Alfvén wave energy and solely focused on the transport of CRs and Alfvén waves. Consequently, there are only processes that exchange energy among the subsystems.

3.7. Relation to Radiation Hydrodynamics

We briefly recall the derivation of the equations of radiation hydrodynamics. We describe radiation by its specific intensity $I = I(\boldsymbol{x}, \boldsymbol{n}, \nu)$, which is defined as the energy that is radiated

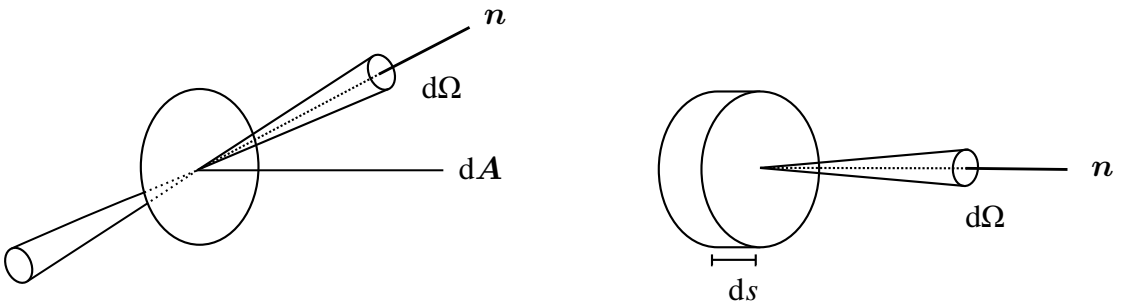

Figure 3.2.: On the definition of the specific intensity I and its scattering in a slab of length ds .

through a surface d$\boldsymbol{A}$ at a point $\boldsymbol{x}$ into a solid angle dν along the direction $\boldsymbol{n}$ in the frequency interval dν while dt elapses (see Fig. 3.2):

$$\mathrm{d}E \;= I(\boldsymbol{x}, \boldsymbol{n}, \nu)\, \boldsymbol{n} \cdot \mathrm{d}\boldsymbol{A}\, \mathrm{d}\Omega\, \mathrm{d}\nu\, \mathrm{d}t \tag{3.111}$$

We can define the first 2 direction moments of radiation as

$$\begin{bmatrix} J \\ \boldsymbol{H} \end{bmatrix} = \frac{1}{4\pi} \int \mathrm{d}\Omega \begin{bmatrix} 1 \\ \boldsymbol{n} \end{bmatrix} I(\boldsymbol{n}), \tag{3.112}$$

where J is the mean intensity and $\boldsymbol{H}$ is the monochromatic flux.

After neglecting true absorption and thermal sources of radiation, the *transfer equation* for radiation written in its specific intensity reads:

$$\frac{1}{c}\frac{\partial I}{\partial t} + \boldsymbol{n} \cdot \boldsymbol{\nabla} I = \frac{1}{c}\frac{\partial I}{\partial t} + \frac{\partial I}{\partial s} = \sigma\,(S - I)\,, \tag{3.113}$$

where $\sigma = \sigma(\boldsymbol{n})$ is the scattering coefficient and S is the source function, which accounts for radiation that is scattered from a direction $\boldsymbol{n}'$ into the ray that is directed along $\boldsymbol{n}$.

Scattering is mediated by the particles of the thermal gas. For processes such as Thomson scattering the interaction itself and hence the scattering coefficient are isotropic in the frame of the thermal gas. In contrast, the transfer equation is completely written in lab frame. In this frame scattering is highly anisotropic because the boost between lab and comoving frame induces an additional directional dependence of the scattering. This directional dependence introduces another difficulty while solving the equation. There are two possible ways of how to proceed (Mihalas and Weibel Mihalas, 1984): For the first possibility, we would have to reformulate the complete transfer equation in the comoving frame of the gas. This would remove the strong $\boldsymbol{n}$ dependence of the right hand side. Nevertheless, we would get many pseudoforces and other terms from the transformed space and time derivatives because the whole equation would have to be transformed. This is done in Buchler (1979) where the comoving transfer equation is used to derive the comoving equations of radiation hydrodynamics in full extent. We use a similar procedure in the main text to get a transport equation for CRs and the corresponding scattering in the comoving frame. For the sake of simplicity, here we use another procedure for radiation which relies on an expansion of the right hand side in the small value $\boldsymbol{u}/c$. We cite the transformed transfer equation from Mihalas and Klein (1982) in order $O(u/c)$

to proceed with:

$$\frac{1}{c}\frac{\partial I}{\partial t} + \boldsymbol{n}\cdot\boldsymbol{\nabla} I = \sigma_0\,(J - I) + \sigma_0\frac{\boldsymbol{n}\cdot\boldsymbol{u}}{c}\left(2J - \nu\frac{\partial J}{\partial \nu} + I\right) - \sigma_0\frac{\boldsymbol{u}}{c}\cdot\left(\boldsymbol{H} - \nu\frac{\partial \boldsymbol{H}}{\partial \nu}\right), \tag{3.114}$$

where quantities with a subscript 0 are measured in the comoving frame. We further use the original *grey*-approximation and neglect any frequency dependence, i.e., $\sigma_0 = \text{const}$ (which is given, e.g., for Thomson scattering).

We now approximate this equation through the first two thermodynamical moments in $\boldsymbol{n}$. Thus, we define the radiation energy density

$$E_{\text{rad}} = \int_0^\infty \mathrm{d}\nu \int \mathrm{d}\Omega\, I/c = \frac{4\pi}{c}\int_0^\infty \mathrm{d}\nu\, J \tag{3.115}$$

and the flux density of radiation energy as

$$\boldsymbol{F}_{\text{rad}} = \int_0^\infty \mathrm{d}\nu \int \mathrm{d}\Omega\, \boldsymbol{n} I = 4\pi\int_0^\infty \mathrm{d}\nu\, \boldsymbol{H}. \tag{3.116}$$

Similar to the derivation in the main text, we calculate the evolution equations for these quantities by taking appropriate moments of eq. (3.114). Integrating eq. (3.114) over solid angle and frequency gives:

$$\frac{\partial E_{\text{rad}}}{\partial t} + \boldsymbol{\nabla}\cdot\boldsymbol{F}_{\text{rad}} = -\frac{\sigma_0}{c}\boldsymbol{u}\cdot\boldsymbol{F}_{\text{rad}}. \tag{3.117}$$

Surprisingly, this equation contains a source term of radiation energy even though we neglected any true absorption and other sources of radiation. This term accounts for the different frames and is a consequence of the $O(u/c)$ expansion. Only the energy in comoving frame should be conserved by the scattering but not the radiation energy E_{rad} in the lab-frame.

Taking the $c\boldsymbol{n}$ moment requires care. We use the original Eddington-approximation to proceed and assume that

$$I(\boldsymbol{n}) = I_0 + \boldsymbol{n}\cdot\boldsymbol{I_1}. \tag{3.118}$$

Thus, we can decompose the intensity into a characteristic direction and an isotropic part. Using

$$\int \mathrm{d}\Omega\, \boldsymbol{n}\boldsymbol{n} = \frac{4\pi}{3}\mathbf{1}, \tag{3.119}$$

we evaluate the $c\boldsymbol{n}$-moment of eq. (3.114) to

$$\frac{\partial \boldsymbol{F}_{\text{rad}}}{\partial t} + c^2\boldsymbol{\nabla}\cdot\mathbf{P}_{\text{rad}} = -c\sigma_0\left[\boldsymbol{F}_{\text{rad}} - \boldsymbol{u}\cdot(E_{\text{rad}}\mathbf{1} + \mathbf{P}_{\text{rad}})\right], \tag{3.120}$$

where the radiation pressure tensor is given by: $\mathbf{P}_{\text{rad}} = E_{\text{rad}}\mathbf{1}/3$. We justify the Eddington approximation from this equation in some limits: if the scattering is strong, the right-hand side dominates and radiation evolves towards isotropy in the comoving frame. This in turn allows us to expand the intensity into its directional components because $|\boldsymbol{I_1}| \sim |\boldsymbol{u}|/v$. As the near-isotropy of radiation implies that higher directional moments become less import, the expansion in eq. (3.118) is justified. Furthermore, if the photon inertia is dynamically less important in

comparison to their scattering, we can use the Chapman-Enskog expansion in eq. (3.120). This yields $\boldsymbol{F}_{\mathrm{rad}} \approx \boldsymbol{u} E_{\mathrm{rad}} + \boldsymbol{u} \cdot \mathbf{P}_{\mathrm{rad}} = 4\boldsymbol{u} E_{\mathrm{rad}}/3$, which corresponds to a flux of a relativistic fluid with $\gamma_{\mathrm{rad}} = 4/3$. This flux corresponds to a boosted flux $\boldsymbol{F}_{\mathrm{rad}}|_{\mathrm{gas}} = 0$ in the gas frame.

Inserting this flux into the radiation energy eq. (3.117) yields a nonvanishing source term on the right-hand side. However, this implies that radiation energy is lost even in the apparent equilibrium case. This surprising results was not discussed by Mihalas and Klein (1982) and contradicts the inherent necessity of elastic scattering to be energy conserving. This flaw is partially corrected by Lowrie et al. (1999). They give a Galilean-invariant result for eqs. (3.117) and (3.120) in their eqs. (32a) and (32b).

Our derivation of the CR equations was highly inspired by the one presented here. Any step taken to transform from RT to RHD has a corresponding analogy in the main text, where we derive our equations of CRHD from the Vlasov-equation. Thus, unsurprisingly, both eqs. (3.117) and (3.117) carry a strong resemblance with our CR equivalents in eqs. (3.104) and (3.105).

4 Numerics of Cosmic Ray Hydrodynamics

Analysis of eqs. (3.106), (3.105), and (3.104) is rather difficult due to its nonlinear nature. In the previous section, we inferred some general features concerning the general propagation of CRs using asymptotical arguments. We use this section to introduce a finite volume method and apply it in a few numerical simulation to substantiate those claims.

To this end, we cast our equations in the standard form for hyperbolic equations with source terms and then describe a general-purpose algorithm to integrate equations of this form. The actual equations for the CR dynamics can then be obtained by inserting the specific terms.

We focus our attention on a constant background medium ($\rho = \text{const}$, $T = \text{const}$, $\boldsymbol{u} = 0$) where the magnetic field is directed along the x-axis ($\boldsymbol{B} = B_0$, $\boldsymbol{x} = \text{const}$). In this setting, we are able to investigate the dynamics of CRs in an isolated manner. As laid out in sec. 3.6, the CR and MHD equations are non-trivially coupled. This complicates the analysis of the emerging dynamics. We assume that the magnetized background medium is at rest and postpone studies of the dynamical impact of CRs to furture work. As such, our choice of MHD quantities remain constant for all times.

4.1. Finite Volume Method

In this simplified scenario the equations have numerical standard form:

$$\frac{\partial \boldsymbol{U}}{\partial t} + \frac{\partial \boldsymbol{F}(\boldsymbol{U})}{\partial x} = \boldsymbol{S}(\boldsymbol{U}), \tag{4.1}$$

where the state and flux vectors are given by

$$\boldsymbol{U} = \begin{bmatrix} \varepsilon_{\mathrm{cr}} \\ f_{\mathrm{cr}} \\ \varepsilon_{\mathrm{a},+} \\ \varepsilon_{\mathrm{a},-} \end{bmatrix}, \quad \boldsymbol{F}(\boldsymbol{U}) = \begin{bmatrix} f_{\mathrm{cr}} \\ c^2 \varepsilon_{\mathrm{cr}}/3 \\ +v_{\mathrm{a}} \varepsilon_{\mathrm{a},+} \\ -v_{\mathrm{a}} \varepsilon_{\mathrm{a},-} \end{bmatrix}, \tag{4.2}$$

while the sources are given by

$$\boldsymbol{S}(\boldsymbol{U}) = \begin{bmatrix} -\frac{v_{\mathrm{a}}}{3\kappa_+}\left(f_{\mathrm{cr}} - v_{\mathrm{a}}\gamma_{\mathrm{cr}}\varepsilon_{\mathrm{cr}}\right) + \frac{v_{\mathrm{a}}}{3\kappa_-}\left(f_{\mathrm{cr}} + v_{\mathrm{a}}\gamma_{\mathrm{cr}}\varepsilon_{\mathrm{cr}}\right) \\ -\frac{c^2}{3\kappa_+}\left(f_{\mathrm{cr}} - v_{\mathrm{a}}\gamma_{\mathrm{cr}}\varepsilon_{\mathrm{cr}}\right) - \frac{c^2}{3\kappa_-}\left(f_{\mathrm{cr}} + v_{\mathrm{a}}\gamma_{\mathrm{cr}}\varepsilon_{\mathrm{cr}}\right) \\ +\frac{v_{\mathrm{a}}}{3\kappa_+}\left(f_{\mathrm{cr}} - v_{\mathrm{a}}\gamma_{\mathrm{cr}}\varepsilon_{\mathrm{cr}}\right) - \alpha\varepsilon_{\mathrm{a},+}^2 + S_{\mathrm{inj}} \\ -\frac{v_{\mathrm{a}}}{3\kappa_-}\left(f_{\mathrm{cr}} + v_{\mathrm{a}}\gamma_{\mathrm{cr}}\varepsilon_{\mathrm{cr}}\right) - \alpha\varepsilon_{\mathrm{a},-}^2 + S_{\mathrm{inj}} \end{bmatrix}. \tag{4.3}$$

Here, we included another source term of Alfvén waves, denoted by S_{inj}. The reason for its presence is twofold: 1) it accounts for unresolved sources of Alfvén waves. The main example for these sources are SNRs, where CRs stream away from the shock and thus generate

Alfvén waves on a subgrid level, and 2) it prevents the Alfvén wave energy densities to become negligibly small by introducing an antagonist to the damping processes.

We can perform the spatial derivative in eq. (4.1) and get the transport equation in its advective form:

$$\frac{\partial \boldsymbol{U}}{\partial t} + \mathbf{A}(\boldsymbol{U})\frac{\partial \boldsymbol{U}}{\partial x} = \boldsymbol{S}(\boldsymbol{U}), \tag{4.4}$$

where the matrix $\mathbf{A}$ carries all the information about the transport of $\boldsymbol{U}$. We can formally decompose this matrix into its characteristic speeds by calculating its eigenvalues. With each of those speeds one characteristic component of $\boldsymbol{U}$ is transported. In general, this component is difficult to derive and not necessarily an entry of the vector $\boldsymbol{U}$ but a function of those. Mathematically we can calculate the characteristic speeds by calculating the eigenvalues of $\mathbf{A}$. In our case, the spectrum and hence the set of all eigenvalues, of $\mathbf{A}$ is given by:

$$\sigma_{\text{spec}}\left(\mathbf{A}(\boldsymbol{U})\right) = \left\{+v_{\text{a}}, -v_{\text{a}}, +\frac{c}{\sqrt{3}}, -\frac{c}{\sqrt{3}}\right\}. \tag{4.5}$$

We can associate the propagation of the corresponding wave energy to both Alfvén velocities. Whereas the characteristic speeds $\pm c/\sqrt{3}$ are associated with the relativistic transport of CRs. Here, the speeds are constant and do not depend on $\boldsymbol{U}$, which is in general not the case (see e.g., the equations of hydrodynamics where u and $u \pm c_{\text{s}}$ are the characteristic velocities, which depend on the local velocity u). The most important velocity of those is the characteristic velocity which has the largest magnitude. In mathematics this quantity is called the spectral radius and reads in our case:

$$\rho_{\text{spec}} = \rho_{\text{spec}}\left(\mathbf{A}(\boldsymbol{U})\right) = \frac{c}{\sqrt{3}}. \tag{4.6}$$

The spectral radius has a physical interpretation: it is the largest velocity with which localized information can be propagated. Hence, a point x has only a causal influence within the cone that is given by $x \pm \rho_{\text{spec}} t$. If ρ_{spec} depends on $\boldsymbol{U}$, this geometrical shape is more complicated but the qualitative result remains the same: only inside this causal region that is spanned by the fastest characteristic velocity the evolution can influence any physical quantity described by eq. (4.1).

The underlying idea of finite volume methods is to describe the state vector $\boldsymbol{U}$ not as a complicated function of space and time, but by spatial averages over specified regions at certain times t_n. The spatial average of $\boldsymbol{U}$ over an interval $[x_{i-\frac{1}{2}}, x_{i+\frac{1}{2}}]$ with length $\Delta x_i = x_{i+\frac{1}{2}} - x_{i-\frac{1}{2}}$ at time t_n is

$$\boldsymbol{U}_i^n = \frac{1}{\Delta x_i}\int_{x_{i-\frac{1}{2}}}^{x_{i+\frac{1}{2}}} \mathrm{d}x\, \boldsymbol{U}(x, t_n). \tag{4.7}$$

We call the interval $[x_{i-\frac{1}{2}}, x_{i+\frac{1}{2}}]$ a computational cell centered at $x_i = (x_{i-\frac{1}{2}} + x_{i+\frac{1}{2}})/2$ or just the cell i. Sometimes it is helpful to consider $\boldsymbol{U}_i^n$ as the value of $\boldsymbol{U}$ in x_i although this is not the case in general. In the special case where $\boldsymbol{U}$ is a linear function inside the cell i, this is true.

We can integrate eq. (4.1) over $[x_{i-\frac{1}{2}}, x_{i+\frac{1}{2}}]$ and $[t^n, t^{n+1}]$ to see how the averaged states evolve over a time step $\Delta t = t^{n+1} - t^n$. The result is:

$$\boldsymbol{U}_i^{n+1} = \boldsymbol{U}_i^n - \Delta t \frac{\boldsymbol{F}_{i+\frac{1}{2}} - \boldsymbol{F}_{i-\frac{1}{2}}}{\Delta x_i} + \Delta t \boldsymbol{S}_i, \tag{4.8}$$

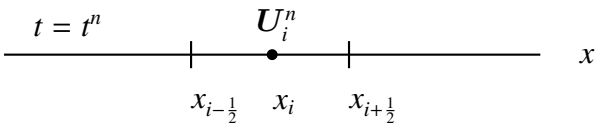

Figure 4.1.: Geometry of the finite volume method.

where we defined the averaged fluxes and sources as:

$$\boldsymbol{F}_{i+\frac{1}{2}} = \frac{1}{\Delta t}\int_{t^n}^{t^{n+1}} \mathrm{d}t\, \boldsymbol{F}(\boldsymbol{U}(x_{i+\frac{1}{2}}, t)), \tag{4.9}$$

$$\boldsymbol{S}_i = \frac{1}{\Delta t\, \Delta x_i}\int_{t^n}^{t^{n+1}} \mathrm{d}t \int_{x_{i-\frac{1}{2}}}^{x_{i+\frac{1}{2}}} \mathrm{d}x\, \boldsymbol{S}(\boldsymbol{U}(x,t)). \tag{4.10}$$

Eq. (4.8) is a trivial formal solution to eq. (4.1). At this point we cannot calculate the next state $\boldsymbol{U}_i^{n+1}$ based on the information given by the current $\boldsymbol{U}_i^n$, we would need to know the particular and full solution $\boldsymbol{U}(x,t)$ to calculate the occurring averages in eqs. (4.9) and (4.10). This problem is the starting point of so-called Godunov methods, which we will describe now. Here, we just state one possible Godunov method, which is straight forward to implement and versatile enough to use it for most problems. The general idea behind those methods is to approximate eq. (4.9) based on the states left and right of a cell interface ($\boldsymbol{U}_\mathrm{L}$ and $\boldsymbol{U}_\mathrm{R}$, respectively). In a first step, we evaluate the flux integral by its time-centered value

$$\boldsymbol{F}_{i+\frac{1}{2}} \approx \boldsymbol{F}\left(\boldsymbol{U}\left(x_{i+\frac{1}{2}}, t^n + \frac{\Delta t}{2}\right)\right), \tag{4.11}$$

and thus shift our task to finding an approximation for the state at the interface that is given at the half-step. The interface value $\boldsymbol{U}\left(x_{i+\frac{1}{2}}, t^n + \frac{\Delta t}{2}\right)$ may not be single-valued as the function $\boldsymbol{U}\left(x, t^n + \frac{\Delta t}{2}\right)$ may have a discontinuity at $x_{i+\frac{1}{2}}$. We thus have to find an appropriate replacement for $\boldsymbol{F}_{i+\frac{1}{2}}$. Riemann solvers are best suited for this task and calculate a flux based on the two values at the interface:

$$\boldsymbol{F}_{i+\frac{1}{2}} \approx F(\boldsymbol{U}_\mathrm{L}, \boldsymbol{U}_\mathrm{R}), \tag{4.12}$$

where $\boldsymbol{U}_{\mathrm{L,R}}$ are evaluated at $t = t^n + \Delta t/2$.

Step 1: Reconstruction The most obvious choices for the left- and right-sided states of an interface are the corresponding mean-values in the neighboring cells:

$$\boldsymbol{U}_\mathrm{L} = \boldsymbol{U}_i^n, \tag{4.13}$$

$$\boldsymbol{U}_\mathrm{R} = \boldsymbol{U}_{i+1}^n, \tag{4.14}$$

even at the half step. These completely valid choices lead to a stable numerical algorithm with a resulting L_1-error

$$\mathrm{error}_{L_1} = \sum_i |U_i - U(t, x_i)| \tag{4.15}$$

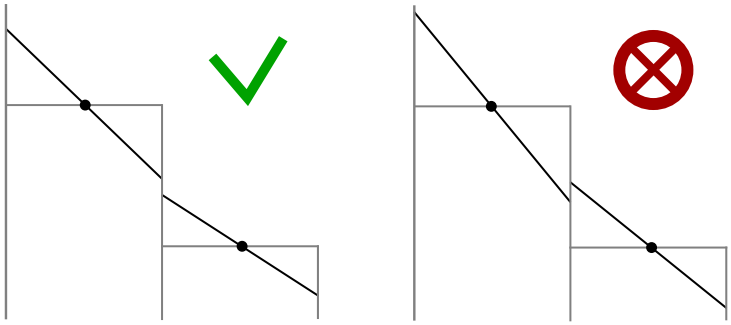

Figure 4.2.: Slope limiter of the finite volume method. The gradients on the left-hand side introduce no new extrema at the cell interface, whereas this is the case with the gradients on the right-hand side.

which behaves as $\text{error}_{L_1} \propto \Delta x$. We could proceed with this but refrain from doing so: the numerical solutions computed with this algorithm suffer from excessive numerical diffusion. All sharp features that are present in the solution are quickly spread. An algorithm that leads to a scheme with an error $\text{error}_{L_1} \propto \Delta x^2$ and preserves features is fundamentally rooted in the reconstruction of $U(x, t^n)$ based on the mean values U_i^n (Van Leer, 1997).

The basic idea is to strive for a better representation of the function $\boldsymbol{U}(x, t)$ inside a computational cell. To this end, we interpolate the function based on its averages over neighboring cells. If we evaluate a linear interpolation at the boundaries we have:

$$\boldsymbol{U}_{i,\pm}^n = \boldsymbol{U}_i^n \pm \frac{\Delta x_i}{2} \boldsymbol{\nabla} U_i^n, \tag{4.16}$$

where $\boldsymbol{\nabla} U_i^n$ is a suitable approximation of the actual gradient. Generally, there are many possible ways to calculate such an gradient. In order to construct a stable numerical scheme, it is necessary to chose $\boldsymbol{\nabla} U_i^n$ such that over-/undershoots at cell boundaries are avoided (see Fig. 4.2). This would introduce new extrema into the reconstruction and cast our algorithm more dispersive. In the worst case (e.g., for velocities near 0) this could lead to an erroneous inversion of the propagation direction. In order to prevent over-/undershoots, slope limiters are used. In their simplest form, which we use here, they calculate an approximation of the gradient that avoids over-/undershoots based on the left- and right-sided difference-approximation of the gradient. One of those is the *minmod*-limited gradient given by:

$$\boldsymbol{\nabla} U_i^n = \text{minmod}\left(\frac{\boldsymbol{U}_i^n - \boldsymbol{U}_{i-1}^n}{x_i - x_{i-1}}, \frac{\boldsymbol{U}_{i+1}^n - \boldsymbol{U}_i^n}{x_{i+1} - x_i} \right). \tag{4.17}$$

The minmod-function given for a scalar rads as:

$$\text{minmod}(a, b) = \frac{\text{sign}(a) + \text{sign}(b)}{2} \min(|a|, |b|), \tag{4.18}$$

while the minmod-function is evaluated component-wise for vector-arguments. This slope limiter picks the gradient with the smallest magnitude of the left- and right-sided gradients if both share the same sign.

The author studied several different slope limiters and found this to be the most robust limiter, while other theoretically valid slope limiters tend to fail in practice.

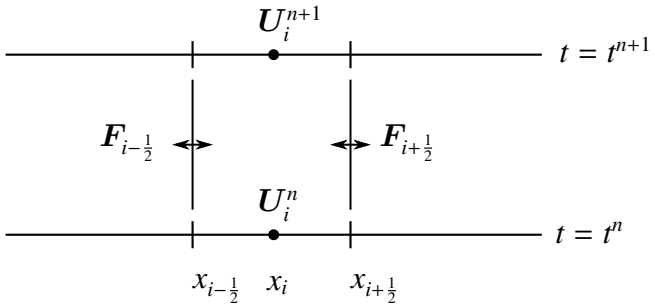

Figure 4.3.: Schematic representation of the flux exchange. To advance and simultaneously conserve $\int \mathrm{d}x\, \boldsymbol{U}$ in the simulation volume, the fluxes have to be defined on and shared with cells neighboring an interface.

Step 2: Space-Time Predictor To evaluate the flux at the half-step, we need to know what are the interface values at this time. For this we use the Hancock Space-Time Predictor, that evolves the extrapolated values as:

$$\boldsymbol{U}_{i,\pm}^{n+\frac{1}{2}} = \boldsymbol{U}_{i,\pm}^{n} - \frac{\Delta t}{2} \frac{\boldsymbol{F}(\boldsymbol{U}_{i,+}^{n}) - \boldsymbol{F}(\boldsymbol{U}_{i,-}^{n})}{\Delta x_i} + \frac{\Delta t}{2} S\left(\boldsymbol{U}_{i,\pm}^{n+\frac{1}{2}}\right). \tag{4.19}$$

In addition to the original version of the predictor we added the source terms in a implicit fashion. Note that although this predictor resembles eq. (4.8), it is manifestly different. Here, the state is updated using purely information attributed to a single cell. In contrast, the fluxes in eq. (4.8) are the same for neighboring cells. Based on this, our full scheme exchanges fluxes of conserved quantities between neighboring cells. This conserves physical quantities inside the computational domain, e.g., energy. However, this is not true for the predicted states in eq. (4.19).

In practice, it is advantageous to use a predictor, as it is purely local. This means that no values need to be communicated with neighboring cells.

By neglecting this step, our scheme would be formally accuarate to first order. Nevertheless, excessive numerical diffusion is already avoided by solely using the reconstructing described in the last step.

Step 3: Flux calculation We are now equipped to finally calculate the flux in eq. (4.8). Based on the states to the left and right of an interface, Riemann solvers calculate a flux as a solution of the emerging Riemann problem at the interface (denoted as if the interface was placed at $x = 0$):

$$\frac{\partial \boldsymbol{U}}{\partial t} + \frac{\partial \boldsymbol{F}(\boldsymbol{U})}{\partial x} = 0, \tag{4.20}$$

$$\begin{cases} U(x,0) = U_L, & x < 0, \\ U(x,0) = U_R, & x > 0 \end{cases} \tag{4.21}$$

In general, the solution can be complicated, which is the reason why approximative Riemann solvers are used in real-world applications. We choose the versatile HLLE Riemann solver:

$$\boldsymbol{F}_{i+\frac{1}{2}} = \boldsymbol{F}_{HLLE}\left(\boldsymbol{U}_{i,+}^{n+\frac{1}{2}}, \boldsymbol{U}_{i+1,-}^{n+\frac{1}{2}}\right), \tag{4.22}$$

$$\boldsymbol{F}_{i-\frac{1}{2}} = \boldsymbol{F}_{HLLE}\left(\boldsymbol{U}_{i-1,+}^{n+\frac{1}{2}}, \boldsymbol{U}_{i,-}^{n+\frac{1}{2}}\right), \tag{4.23}$$

where the flux is calculated using:

$$\boldsymbol{F}_{HLLE}(\boldsymbol{U}_L, \boldsymbol{U}_R) = \frac{S_R \boldsymbol{F}(\boldsymbol{U}_L) - S_L \boldsymbol{F}(\boldsymbol{U}_R)}{S_R - S_L} - \frac{S_L S_R}{S_R - S_L}\left(\boldsymbol{U}_L - \boldsymbol{U}_R\right). \tag{4.24}$$

The signal speeds $S_L \leq 0$ and $S_R \geq 0$ are given below. The first term is a linear combination of both left- and right-sided fluxes at the interface. It can be seen as a weighted mean between the two, which prefers the most dynamically important flux. The second term is the so-called diffusion term. It introduces numerical diffusion at places were the solution is discontinuous. This diffusion is necessary for convergence in a physical and mathematical sense. Physically, because it is responsible for convergence to an entropy-satisfying solution, i.e., where the second law of thermodynamics holds. Mathematically, as the small amount of diffusion smooths occurring oscillations that could prevent convergence to the solution.

In their original work, Harten et al. (1983) (HLL in HLLE) did not specify how to calculate both wave speeds. The introduced ambiguity is twofold: first, the true wave speeds are not known a priori and need to be calculated based on the Riemann problem. This requires a solution of the Riemann problem, which can be computationally expensive. Second, one can use estimates for the wave speeds. There are many estimates that result in stable and converging numerical algorithms. We stick to the Einfeldt (1988) (E in HLLE) wave speeds estimates which are given by:

$$S_L = \min\left(0, \min\sigma_{\text{spec}}\left(\mathbf{A}(\boldsymbol{U_L})\right), \min\sigma_{\text{spec}}\left(\mathbf{A}\left(\frac{\boldsymbol{U_L} + \boldsymbol{U_R}}{2}\right)\right)\right), \tag{4.25}$$

$$S_R = \max\left(0, \max\sigma_{\text{spec}}\left(\mathbf{A}(\boldsymbol{U_R})\right), \max\sigma_{\text{spec}}\left(\mathbf{A}\left(\frac{\boldsymbol{U_L} + \boldsymbol{U_R}}{2}\right)\right)\right). \tag{4.26}$$

Step 4: Final Time Advance With the calculated inter-cell fluxes, we can finalize the timestep of eq. (4.8):

$$\boldsymbol{U}_i^{n+1} = \boldsymbol{U}_i^n - \Delta t \frac{\boldsymbol{F}_{i+\frac{1}{2}} - \boldsymbol{F}_{i-\frac{1}{2}}}{\Delta x_i} + \Delta t S\left(\boldsymbol{U}_i^{n+1}\right), \tag{4.27}$$

where we approximate the source term in an implicit manner.

In order to get a stable numerical algorithm we have to restrict the admissible time steps Δt. For our hyperbolic scheme, we have to fulfill the local Courant-Friedrichs-Lewy (CFL) condition in its classical variant:

$$\frac{\Delta t_i}{\Delta x_i} = \text{CFL} \times \rho_{\text{spec}}\left(\mathbf{A}(\boldsymbol{U})\right), \tag{4.28}$$

where the condition

$$0 < \mathrm{CFL} < \frac{1}{2} \tag{4.29}$$

for CFL number must hold. This condition implies a global time step of:

$$\Delta t = \min_i \Delta t_i. \tag{4.30}$$

The CFL-condition has a physical interpretation. It ensures that the fastest wave can not be transported faster than one computational cell per timestep. If this condition would be violated, our flux calculation between neighboring cells becomes unphysical. In this case information could be transported from a cell to the cell after the next, while jumping over the actual neighboring cell. We did not account for this case in our flux calculation and thus have to obey to the CFL-condition to obtain plausible results.

4.2. Treatment of the Source Terms

Due to the high dynamical range of time scales in the source terms, an implicit implementation of them is necessary as shown in eqs. (4.27) and (4.19).

Inserting the actual source terms in eq. (4.3) renders these equations to become nonlinear. Hence, there can be no general solutions or the solution can be numerically expensive to compute. For the case of an existing solution there are different numerical techniques to calculate an approximative one. As the source terms themselves are straight forward to calculate, we use the Newton-Raphson method to approximate the solution of eqs. (4.19) and (4.27). The starting point of this method are equations of the form

$$\boldsymbol{F}(\boldsymbol{s}) = \boldsymbol{0}. \tag{4.31}$$

We can simply recast our eqs. (4.19) and (4.27) into this form by subtracting either the left-hand or the right-hand side.

The Newton-Raphson method calculates successively better estimates for the roots of a function $\boldsymbol{F}$ by iterating the following recursion formula:

$$\boldsymbol{s}_{k+1} = \boldsymbol{s}_k - [\mathrm{D}\boldsymbol{F}(\boldsymbol{s}_k)]^{-1}\boldsymbol{F}(\boldsymbol{s}_k), \tag{4.32}$$

where $\mathrm{D}\boldsymbol{F}$ is the Jacobian of the function. This iteration needs an initial guess $\boldsymbol{s}_0$. For implicit numerical differential equations such as eqs. (4.19) and (4.27), the state vector of the current time step is a good initial guess, as it is readily available and likely close to the root. We thus adopt the initial guess for the iterations of eq. (4.27) according to

$$\boldsymbol{s}_0 = \boldsymbol{U}_i^n. \tag{4.33}$$

To understand the Newton-Raphson method, we visualize it in the left-hand side of Fig. 4.4 for an one dimensional problem. Here, the method extrapolates a better guess for the root by walking down the gradient towards smaller values of F. As a result, this the iteration quickly converges towards the root. In higher dimensions, this is not the case (see right-hand side of

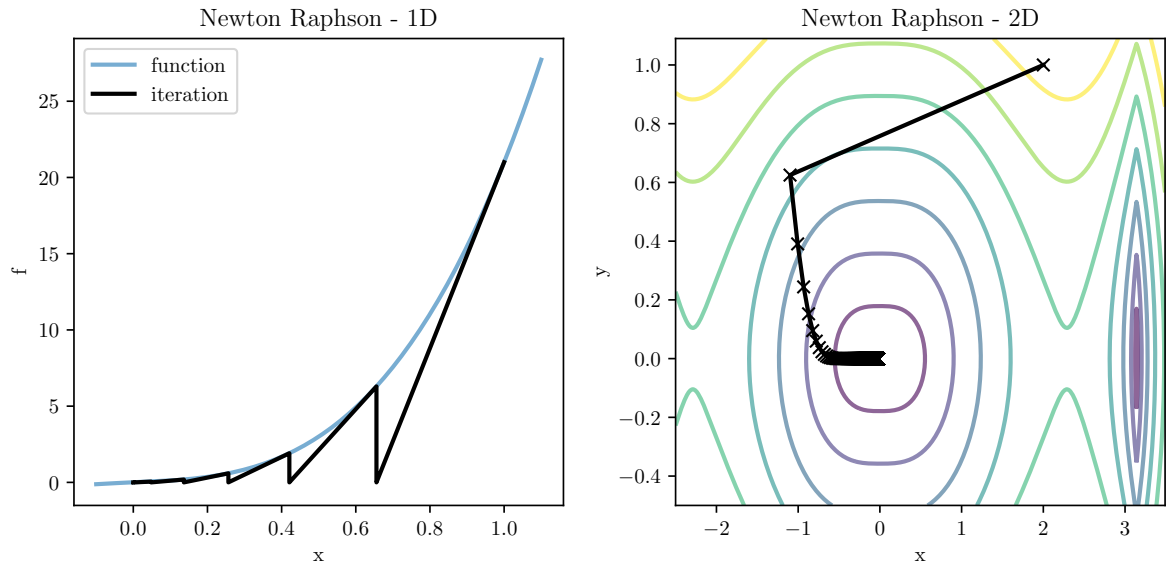

Figure 4.4.: Newton Raphson Method in multiple dimensions. *Left*: The one dimension case. We show the iteration of $f(s) = s - 20\,s^3$ with initial guess $s_0 = 1$ *Right*: The two dimension case with $\boldsymbol{F}(\boldsymbol{s}) = ((s_x - 1.5)\,\mathrm{abs}(\sin(x)) + 5 s_y^2,\, s_y^2)$ and initial guess $(2, 1)$. We display the first component of the function using equidistant contour lines.

Fig. 4.4). There, the step is in general not aligned with the gradient. This is apparent in the first step, which moves obliquely to the gradient of the first component of $\boldsymbol{F}$ (the gradient is always perpendicular to contour lines). Nevertheless, the iteration lowers $\boldsymbol{F}(\boldsymbol{s}_k)$ successively until it reaches the inner plateau of the function, where the root resides.

In principle the iteration aims at finding the correct root of $\boldsymbol{F}$, i.e., a $\boldsymbol{s}_k$ such that $\boldsymbol{F}(\boldsymbol{s}_k) = 0$. Because this is hard to achieve with floating point numbers that we used to implement the method on a computer and even computationally costly to achieve, we replace this formally correct end of the iteration by a softer criterion, i.e., instead we abort the iteration if

$$\|\boldsymbol{F}(\boldsymbol{s}_k)\| < 10^{-9}, \tag{4.34}$$

where $\|\cdot\|$ is some norm. In practice either the L^1-norm or the L^2-norm are used. We adopt the L^1-norm, as it avoids numerically expensive multiplications and can be quickly calculated. Note that no extra evaluation of $\boldsymbol{F}(\boldsymbol{s}_k)$ is needed, as it needs to be calculated for the next iteration step in eq. (4.32).

There are some caveats to the general use of the Newton-Raphson method. This method does not always converge. There are some popular examples of functions $\boldsymbol{F}$, where the method oscillates around a root but never converges. This can be cured by using a modified versions and replacing $[\mathrm{D}\boldsymbol{F}(\boldsymbol{s}_k)]^{-1}$ by $h\,[\mathrm{D}\boldsymbol{F}(\boldsymbol{s}_k)]^{-1}$ with relaxation parameter $h < 1$. This parameter allows for smaller jumps during an iteration, which can help to achieve convergence at the cost of a slower progress. For the case of CRHD we do not use this relaxation. Furthermore, the method iterates towards any root and there is no guarantee that it convergences to a physically admissible root. For our example, this could result e.g., in negative energies. However, because our source terms are mildly non-linear, obtaining negative energies is highly unlikely as we

Table 4.1.: Adopted numerical models for our simulations.

name	initial condition	c_{red}	χ	α	S_{inj}
`gauss`	gaussian	100	5×10^{7}	5×10^{10}	1×10^{-8}
`gauss_slow`	gaussian	10	5×10^{7}	5×10^{10}	1×10^{-8}
`low_damp`	gaussian	100	1×10^{6}	1×10^{11}	5×10^{-6}
`int_damp`	gaussian	100	1×10^{6}	5×10^{11}	5×10^{-6}
`hig_damp`	gaussian	100	1×10^{6}	1×10^{12}	5×10^{-6}
`box`	box	100	5×10^{7}	5×10^{10}	1×10^{-8}
`box_slow`	box	10	5×10^{7}	5×10^{10}	1×10^{-8}

start the iteration with a physically admissible state.

4.3. Exemplary Problems

With our numerical method in place, we now describe and discuss our actual simulations.

Instead of using fractions c/v_{a} that are realized in physical environments (under ISM conditions: $v_{\mathrm{a}} \sim 30\mathrm{km/s}$; under IGM conditions: $v_{\mathrm{a}} \sim 100\mathrm{km/s}$), we use a reduced-speed-of-light approximation (Gnedin and Abel, 2001; Gnedin, 2016). To this end, we adopt a reduced speed $c_{\mathrm{red}} \ll c$ for the physical speed of light c in eq. (4.2). We use this approximation since it can be justified as an asymptotic limit: as long as the order of time scales associated with Alfvén and light velocities remain the same for a reduced speed of light, the dynamics should not change. In our case, the equilibrium fluxes $f_{\mathrm{cr}} = \pm v_{\mathrm{a}}(\varepsilon_{\mathrm{cr}} + P_{\mathrm{cr}})$ must be realized faster than the time scale given by the Alfvén velocity: L/v_{a}, where L is a typical CR gradient length. More practically, this approximation reduces the computational costs dramatically because the time step in eq. (4.28) can be increased. Therefore, we need less iterations and thus less wallclock time of our numerical method to reach a certain time T. Nevertheless, we have to check if this unphysical approximation is applicable.

To start the simulation we use the two initial conditions:

$$\text{gaussian:} \begin{cases} g(x) & = \exp(-40x^2), \\ \varepsilon_{\mathrm{cr}}(x) & = 10 + g(x), \\ f_{\mathrm{cr}}(x) & = \gamma_{\mathrm{cr}} \mathrm{sgn}(x) g(x) \varepsilon_{\mathrm{cr}}(x), \\ \varepsilon_{\mathrm{a},\pm}(x) & = (1 + g(x)) \times 10^{-6}, \end{cases} \qquad \text{box:} \begin{cases} g(x) & = 1_{[-1/4,1/4]}(x), \\ \varepsilon_{\mathrm{cr}}(x) & = g(x), \\ f_{\mathrm{cr}}(x) & = \gamma_{\mathrm{cr}} \mathrm{sgn}(x) \varepsilon_{\mathrm{cr}}(x), \\ \varepsilon_{\mathrm{a},\pm}(x) & = (1 + g(x)) \times 10^{-6}, \end{cases} \tag{4.35}$$

where 1_A is the characteristic function of a set A.

Both initial conditions model a localized CR population that streams away from their symmetry axis with Alfvén velocity. We further assume that there is a constant pool of Alfvén waves of both propagation directions present while the populations are supported by an increased amount of Alfvén wave energy.

Throughout the rest of this section we use code units ($v_{\mathrm{a}} = 1$) and rewrite the diffusion

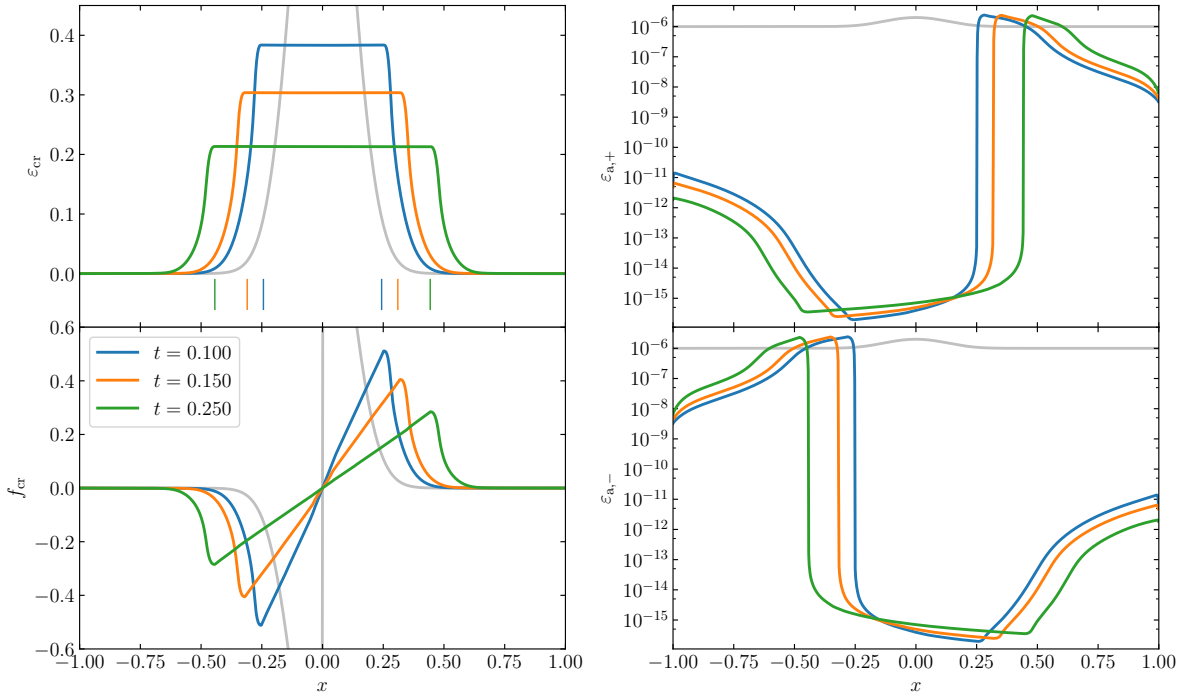

Figure 4.5.: Temporal evolution of a Gaussian defined in model `gauss` using our new theory. We show ε_{cr} and f_{cr} in the left panels and $\varepsilon_{a,+}$ and $\varepsilon_{a,-}$ in the right panels. The wings of the Gaussian are transported with the Alfvén velocity as indicated by the coloured vertical lines in the ε_{cr} panel. These lines are initially placed at the standard deviation of the initial Gaussian and moved outwards with velocity $\gamma_{cr} v_a$ in both directions. We display the initial conditions as grey lines. Figure from Thomas and Pfrommer (2018).

coefficients as:

$$\frac{1}{3\kappa_\pm} = \chi \varepsilon_{a,\pm}, \tag{4.36}$$

using eq. (3.55). We use a small suite of parameter combinations listed in Tab. 4.1. We use these models to test different aspects of CR transport by changing c_{red}, χ, and α to emphasize the dynamics of different terms in the transport equations. In general, these parameters are chosen such that $\varepsilon_{a,\pm}/\varepsilon_{cr} \sim 10^{-6}$. This corresponds to the expected $\delta B/B \sim 10^{-3}$ assuming pressure equilibrium between CRs and large scale magnetic fields.

Macroscopic transport In Fig. 4.5 we show evolution of the Gaussian model `gauss`.

The initially smooth Gaussian spreads such that an plateau develops. Inside this plateau the bulk of CRs are transported with sub-alfvénic velocities, as can be inferred from the f_{cr} panel in Fig. 4.5. Therein $f_{cr} \propto x$ holds such that $\partial_t \varepsilon_{cr} = \text{const.}$ which leads to an apparently coherent decrease in CR energy density. As CRs are transported sub-alfvénically no Alfvén waves can be driven by gyroresonant instability and only wave damping operates efficiently. The residual

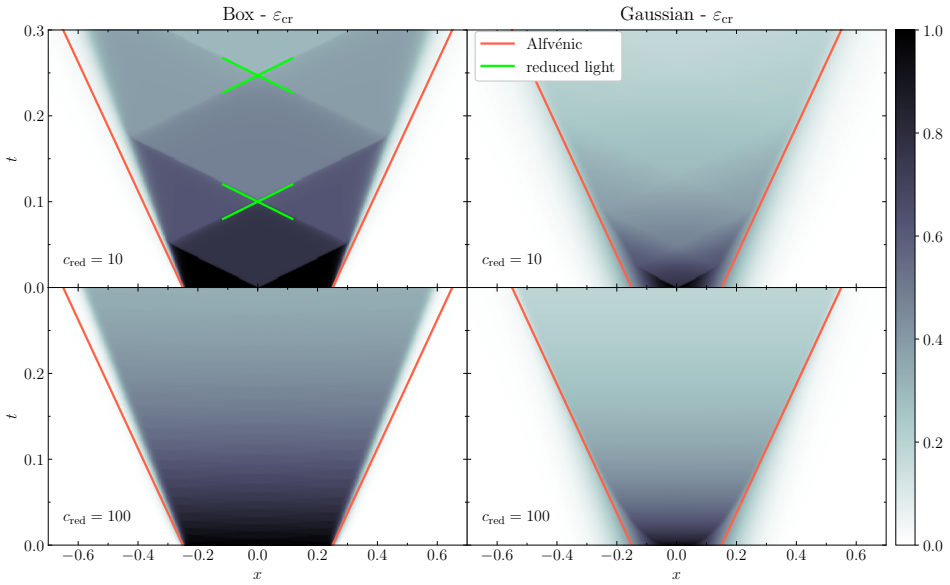

Figure 4.6.: x-t plot of the models `box_slow`, `box` (both on the left-hand side) and `gauss_slow`, `gauss` (both on the right-hand side). We draw coloured characteristics associated with the velocities of Alfvén waves (red) and light (green) and color-code ε_{cr} in the background. The CR population is confined by the Alfvén velocity for each choice of c_{red}. If the reduced speed of light is lowered to 10 times the Alfvén velocity light-like characteristics become visible. Figure from Thomas and Pfrommer (2018).

$\lesssim 10^{-15}$ wave energy densities are a dynamical lower limit of the counteracting injection of Alfvén wave energy by S_{inj} and damping caused by acceleration of CR and nonlinear Landau damping.

In the wings of the Gaussian, the gradient in ε_{cr} induces a small anisotropy by virtue of the Eddington-term which perturbs the streaming CRs. This anisotropy triggers the gyroresonant instability which decelerates CRs and transfers their energy into Alfvén waves. Hence, there is a strongly counteracting process to the wave damping, which results in wave energy densities of $\varepsilon_{a,\pm} \sim 10^{-6}$. These low energy densities scatter CRs on time scales $\lesssim 10^{-4}$ (in code units) such that scattering is efficient on the displayed time scales.

Characteristic speeds In Fig. 4.6 we show evolution of the Gaussian and box initial conditions with different values of c_{red} following the parameters `gauss`, `gauss_slow`, `box`, `box_slow`. The box initial conditions provide a stringent test, as the transition between the CR population and region outside is sharp. There is thus a strong gradient in ε_{cr}, which shifts the dynamics towards that directly induced by the Eddington-term.

These simulations exemplify the applicability of the reduced-speed-of-light approximation. In the cases of $c_{red}/v_a = 10$ the plots show multiple characteristics in ε_{cr} which can be associated with the lightlike velocities $\pm c_{red}/\sqrt{3}$. Reducing the speed of light is accompanied by a decrease in typical scattering time scales. Consider a parcel in which the characteristic resides at a fixed time. This characteristic should amplify Alfvén waves. Since no wave energy is present in the plateau of the CR distribution, these waves need to first grow and overcome

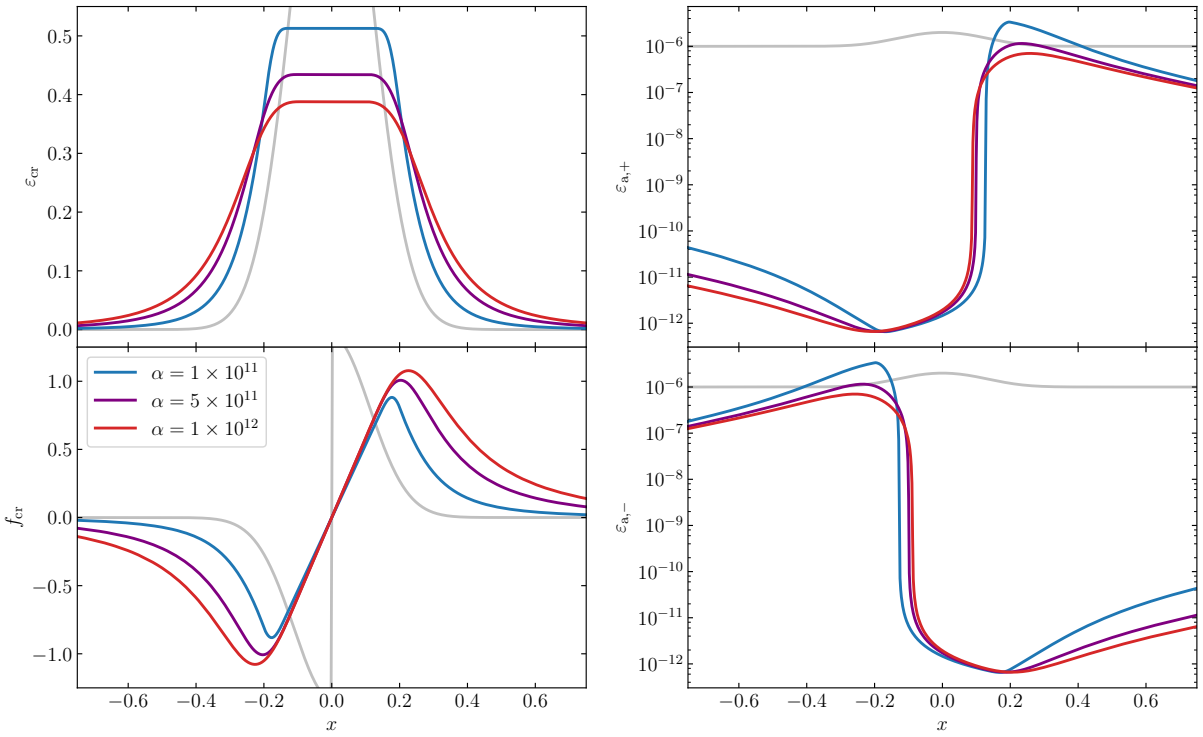

Figure 4.7.: Impact of varying damping coefficients. Increasing the damping coefficient α increases the diffusivity of CR transport. We display the initial conditions as grey lines. Figure from Thomas and Pfrommer (2018).

the damping. Even if the waves were sufficiently strong, the associated scattering times would be too slow and the characteristic would have already left the parcel. This leaves the features unscattered and makes them visible as small perturbations of the plateau.

Nevertheless, the evolution of wings of the CR distribution is invariant under a reasonable choice of $c_{\rm red}$. Even in the flawed case with $c_{\rm red} = 10$, the spatial extends of both distributions grow with velocities $\pm\gamma_{\rm cr} v_{\rm a}$ in both directions.

Varying diffusivity In Fig. 4.7 we investigate the impact of different damping coefficients on the transport of CRs using the models `low_damp`, `int_damp`, and `hig_damp`. We artificially increase the injection rate $S_{\rm inj}$ for presentation reasons. The presented results in $\varepsilon_{\rm cr}$ and $f_{\rm cr}$ do not depend on the particular choice of this rate. Merely the lower bound of $\varepsilon_{\rm a,\pm}$ is affected by this value.

Successively increasing the damping coefficients results in an increasingly diffusive component of the transport. CRs get less frequently scattered because the overall level of Alfvén wave energy is lower due to the stronger damping. The waves are incapable of capturing the bulk of CRs in their own frame. Hence, CRs can now stream with velocities that exceed the Alfvénic one. This increases the spatial extent of the evolving gaussians. The diffusivity increases especially in the outer parts of the wings, since there is even less CR energy available to transfer it into magnetic energy of the Alfvén waves, which in turn causes less scattering.

The choice of the damping coefficient has clear implications for the transport of CRs. It

regulates the reservoir of Alfvén wave energy, the scattering time scales and hence the diffusivity. Nevertheless, global features in the evolution of the CR distribution remain the same for varying damping coefficients.

5 Summary and Conclusion

In this work we derive a new macroscopic transport equation for CRs. Despite their low number densities, these particles are important feedback agents in different astrophysical environments. They can interact with the thermal gas and become dynamically important due to their large kinetic energy and their interaction with electromagnetic fields. Improving our understanding of CR transport enables us to better understand these astrophysical systems.

Jiang and Oh (2018) propose to map the CR transport equation on those of RHD. They do not provide a consistent derivation and argue through analogy between both relativistic fluids. Here, we extend their idea and derive our equations based on approximations of the CR-version of the Fokker-Planck equation. In this process we consider momentum and pitch-angle scattering of CRs by Alfvén waves. To overcome the emerging complexity of the Fokker-Planck equation, we use the moment-method known from RHD and approximate the spectrum of Alfvén wave energy by a simple powerlaw. The resulting macroscopic transport equations contain the energy equation that was used previously in the limit of rapid scattering.

Our treatment of pitch-angle scattering and momentum diffusion leads to Galilean invariant scattering terms in the limit $O(\bar{\nu} v_\mathrm{a}^2/v^2)$. This invariance is a physical necessity, as the scattering proceeds until the distribution isotropizes in the wave frame and is energy conserving in this frame. Any non-invariant terms would not be able to capture this properly as CRs are tied to the frame in which they evaluated. This result demonstrates that our derivation and, in particular, the used approximations are reasonable.

The scattering of CRs is regulated by the strength of the ambient Alfvénic turbulence. The energy contained in the associated waves can vary temporarily and spatially. In order to model this correctly, we recall how Alfvén waves are transported macroscopically and account for different processes affecting the energy contained in waves. Both, CRs and Alfvén waves are tightly coupled through the gyroresonant instability. This inverse process of momentum diffusion transfers energy between both agents of scattering. In our hydrodynamic limit, the gain of Alfvén wave energy by this process is exactly compensated by the loss of CR energy and vice versa, as required physically. Different damping mechanisms can transfer residual Alfvén wave energy into the thermal gas and heat it. We review the damping mechanisms and calculate corresponding hydrodynamic versions of Alfvén wave energy loss terms since this heating is an important feedback channel in different astrophysical systems.

We test our theory using numerical simulations of idealized test cases. We show that standard finite volume methods are sufficient to simulate CR streaming. Earlier attempts to do this that use previous formulations of the CR energy equation need to use mathematical regularizations and advanced numerical methods to solve the resulting nonlinear diffusion equation. Our results show the expected transport behavior for the bulk of CRs: if there is a sufficiently steep gradient in ε_cr, a small anisotropy is induced and Alfvén waves can grow and scatter CRs into their frame. This leads to an effective transport of CRs with the Alfvén velocity. Using a small parameter study, we show that a more diffusive propagation of CRs follows a increase in wave damping and subsequently a decrease in scattering.

In a next step, we will investigate the emerging dynamics of our theory using full 3D-MHD simulations. This will help us to asses its applicability and performance in actual astrophysical systems.

A Complete Calculation of Occurring Integrals

A.1. μ-Integrals for the Fluid Equations

Here, we calculate all necessary μ integrals to derive the transport eqs. (3.8) and eq. (3.9) term-by-term. As a reminder: we defined $f = f_0 + 3\mu f_1$ in our Eddington approximation. With this definition, only powers in μ appear in the transport equations. We multiply eq.(3.1) with 1 and integrate over th intervall $[-1, 1]$, which yields the first moment of the equation.

For the time derivative we have:

$$\begin{aligned}\frac{1}{2}\int_{-1}^{1} \mathrm{d}\mu\, 1 \frac{\partial f}{\partial t} &= \frac{1}{2}\int_{-1}^{1} \mathrm{d}\mu \left(\frac{\partial f_0}{\partial t} + 3\mu \frac{\partial f_1}{\partial t}\right) \\ &= \frac{1}{2}\int_{-1}^{1} \mathrm{d}\mu\, \frac{\partial f_0}{\partial t} \\ &= \frac{\partial f_0}{\partial t}. \end{aligned} \tag{A.1}$$

The moment of the advection term is:

$$\begin{aligned}\frac{1}{2}\int_{-1}^{1} \mathrm{d}\mu\, (\boldsymbol{u} + \mu v \boldsymbol{b}) \cdot \boldsymbol{\nabla} f &= \frac{1}{2}\int_{-1}^{1} \mathrm{d}\mu\, (\boldsymbol{u} + \mu v \boldsymbol{b}) \cdot \boldsymbol{\nabla} f_0 + 3(\mu \boldsymbol{u} + \mu^2 v \boldsymbol{b}) \cdot \boldsymbol{\nabla} f_1 \\ &= \frac{1}{2}\int_{-1}^{1} \mathrm{d}\mu\, \boldsymbol{u} \cdot \boldsymbol{\nabla} f_0 + 3\mu^2 v \boldsymbol{b} \cdot \boldsymbol{\nabla} f_1 \\ &= \boldsymbol{u} \cdot \boldsymbol{\nabla} f_0 + v \boldsymbol{b} \cdot \boldsymbol{\nabla} f_1. \end{aligned} \tag{A.2}$$

We split the pseudoforces in two separate terms depending on the particular derivatives of f. We obtain for the 1-moment of terms containing $\partial_p f$:

$$\begin{aligned}&\frac{1}{2}\int_{-1}^{1} \mathrm{d}\mu\, p \frac{\partial f}{\partial p}\left[\frac{1-3\mu^2}{2}(\boldsymbol{b} \cdot \boldsymbol{\nabla} \boldsymbol{u} \cdot \boldsymbol{b}) - \frac{1-\mu^2}{2}\boldsymbol{\nabla} \cdot \boldsymbol{u}\right] \\ &\quad = \frac{1}{2}\int_{-1}^{1} \mathrm{d}\mu \left[\frac{1-3\mu^2}{2}(\boldsymbol{b} \cdot \boldsymbol{\nabla} \boldsymbol{u} \cdot \boldsymbol{b}) - \frac{1-\mu^2}{2}\boldsymbol{\nabla} \cdot \boldsymbol{u}\right] p \frac{\partial f_0}{\partial p} \\ &\quad\quad + \frac{1}{2}\int_{-1}^{1} \mathrm{d}\mu\, 3\mu \left[\frac{1-3\mu^2}{2}(\boldsymbol{b} \cdot \boldsymbol{\nabla} \boldsymbol{u} \cdot \boldsymbol{b}) - \frac{1-\mu^2}{2}\boldsymbol{\nabla} \cdot \boldsymbol{u}\right] p \frac{\partial f_1}{\partial p} \\ &\quad = -\frac{1}{3}(\boldsymbol{\nabla} \cdot \boldsymbol{u}) p \frac{\partial f_0}{\partial p}, \end{aligned} \tag{A.3}$$

while for that containing $\partial_\mu f$ we obtain:

$$\begin{aligned}\frac{1}{2}\int_{-1}^{1}\mathrm{d}\mu\, 1\left[v\boldsymbol{\nabla}\cdot\boldsymbol{b}+\mu\boldsymbol{\nabla}\cdot\boldsymbol{u}-3\mu(\boldsymbol{b}\cdot\nabla\boldsymbol{u}\cdot\boldsymbol{u})\right]\frac{1-\mu^2}{2}\frac{\partial f}{\partial\mu}&\\ =\frac{1}{2}\int_{-1}^{1}\mathrm{d}\mu\, 3\left[v\boldsymbol{\nabla}\cdot\boldsymbol{b}+\mu\boldsymbol{\nabla}\cdot\boldsymbol{u}-3\mu(\boldsymbol{b}\cdot\nabla\boldsymbol{u}\cdot\boldsymbol{b})\right]\frac{1-\mu^2}{2}f_1&\\ =v(\boldsymbol{\nabla}\cdot\boldsymbol{b})f_1.&\end{aligned}\tag{A.4}$$

Adding those 1-moments yields eq. (3.8).

Next, we calculate the μ-moment. To this end, we multiply eq. (3.1) by μ and apply integrate over pitch-angle. The term that contains the time derivate evaluates to:

$$\begin{aligned}\frac{1}{2}\int_{-1}^{1}\mathrm{d}\mu\,\mu\frac{\partial f}{\partial t}=\frac{1}{2}\int_{-1}^{1}\mathrm{d}\mu\left(\mu\frac{\partial f_0}{\partial t}+3\mu^2\frac{\partial f_1}{\partial t}\right)&\\ =\frac{1}{2}\int_{-1}^{1}\mathrm{d}\mu\, 3\mu^2\frac{\partial f_1}{\partial t}&\\ =\frac{\partial f_1}{\partial t}.&\end{aligned}\tag{A.5}$$

Taking the μ-moment of the advection term yields:

$$\begin{aligned}\frac{1}{2}\int_{-1}^{1}\mathrm{d}\mu\,\mu(\boldsymbol{u}+\mu v\boldsymbol{b})\cdot\boldsymbol{\nabla}f=\frac{1}{2}\int_{-1}^{1}\mathrm{d}\mu\,(\mu\boldsymbol{u}+\mu^2 v\boldsymbol{b})\cdot\boldsymbol{\nabla}f_0+3(\mu^2\boldsymbol{u}+\mu^3 v\boldsymbol{b})\cdot\boldsymbol{\nabla}f_1&\\ =\frac{1}{2}\int_{-1}^{1}\mathrm{d}\mu\,\mu^2 v\boldsymbol{b}\cdot\boldsymbol{\nabla}f_0+3\mu^2\boldsymbol{u}\cdot\boldsymbol{\nabla}f_1&\\ =\frac{v}{3}\boldsymbol{b}\cdot\boldsymbol{\nabla}f_0+\boldsymbol{u}\cdot\boldsymbol{\nabla}f_1.&\end{aligned}\tag{A.6}$$

For the terms describing pseudoforces we have:

$$\begin{aligned}\frac{1}{2}\int_{-1}^{1}\mathrm{d}\mu\,\mu p\frac{\partial f}{\partial p}\left[\frac{1-3\mu^2}{2}(\boldsymbol{b}\cdot\boldsymbol{\nabla}\boldsymbol{u}\cdot\boldsymbol{b})-\frac{1-\mu^2}{2}\boldsymbol{\nabla}\cdot\boldsymbol{u}\right]&\\ =\quad\frac{1}{2}\int_{-1}^{1}\mathrm{d}\mu\quad\mu\left[\frac{1-3\mu^2}{2}(\boldsymbol{b}\cdot\boldsymbol{\nabla}\boldsymbol{u}\cdot\boldsymbol{b})-\frac{1-\mu^2}{2}\boldsymbol{\nabla}\cdot\boldsymbol{u}\right]p\frac{\partial f_0}{\partial p}&\\ +\frac{1}{2}\int_{-1}^{1}\mathrm{d}\mu\, 3\mu^2\left[\frac{1-3\mu^2}{2}(\boldsymbol{b}\cdot\boldsymbol{\nabla}\boldsymbol{u}\cdot\boldsymbol{b})-\frac{1-\mu^2}{2}\boldsymbol{\nabla}\cdot\boldsymbol{u}\right]p\frac{\partial f_1}{\partial p}&\\ =\left[-\frac{2}{5}(\boldsymbol{b}\cdot\boldsymbol{\nabla}\boldsymbol{u}\cdot\boldsymbol{b})-\frac{1}{5}\boldsymbol{\nabla}\cdot\boldsymbol{u}\right]p\frac{\partial f_1}{\partial p}&\end{aligned}\tag{A.7}$$

and

$$\begin{aligned}\frac{1}{2}\int_{-1}^{1}\mathrm{d}\mu\,\mu\left[v\boldsymbol{\nabla}\cdot\boldsymbol{b}+\mu\boldsymbol{\nabla}\cdot\boldsymbol{u}-3\mu(\boldsymbol{b}\cdot\nabla\boldsymbol{u}\cdot\boldsymbol{b})\right]\frac{1-\mu^2}{2}\frac{\partial f}{\partial\mu}&\\ =\frac{1}{2}\int_{-1}^{1}\mathrm{d}\mu\, 3\left[v\boldsymbol{\nabla}\cdot\boldsymbol{b}+\mu\boldsymbol{\nabla}\cdot\boldsymbol{u}-3\mu(\boldsymbol{b}\cdot\nabla\boldsymbol{u}\cdot\boldsymbol{b})\right]\mu\frac{1-\mu^2}{2}f_1&\\ =\left[\frac{1}{5}\boldsymbol{\nabla}\cdot\boldsymbol{u}-\frac{3}{5}(\boldsymbol{b}\cdot\nabla\boldsymbol{u}\cdot\boldsymbol{b})\right]f_1.&\end{aligned}\tag{A.8}$$

Again, combining the μ-moments results in eq. (3.9).

A.2. Integrals of the Scattering Operator

A.2.1. μ-Integrals of the scattering coefficient

For the grey-approximation of the scattering coefficient in eq. (3.47) we found $\nu_{\pm}(\mu) \propto |\mu \mp v_a/v|$. In order to calculate the macroscopic version of the scattering terms, the first three μ-moments of this scattering coefficient are required. We first calculate those moments for the modulus functions $|\mu \mp v_a/v|$ to simplify subsequent calculations.

We start with the two zeroth μ-moments. For the interaction with co-propagating waves, we will need:

$$\begin{aligned}\int_{-1}^{1} \mathrm{d}\mu\,(1-\mu^2)\left|\mu-\frac{v_a}{v}\right| &= \int_{-1}^{v_a/v} \mathrm{d}\mu\,(1-\mu^2)\left(-\mu+\frac{v_a}{v}\right)+\int_{v_a/v}^{1} \mathrm{d}\mu\,(1-\mu^2)\left(\mu-\frac{v_a}{v}\right)\\ &= \frac{1}{12}\left(3-\frac{v_a}{v}\right)\left(1+\frac{v_a}{v}\right)^3+\frac{1}{12}\left(3+\frac{v_a}{v}\right)\left(1-\frac{v_a}{v}\right)^3\\ &= \frac{1}{12}\left(6+12\frac{v_a^2}{v^2}-2\frac{v_a^4}{v^4}\right)\\ &= \frac{1}{2}+\frac{v_a^2}{v^2}+o\left(\frac{v_a^2}{v^2}\right),\end{aligned} \tag{A.9}$$

while the corresponding moment of the counter-propagating wave results by symmetry (or direct calculation):

$$\int_{-1}^{1} \mathrm{d}\mu\,(1-\mu^2)\left|\mu+\frac{v_a}{v}\right| = \frac{1}{2}+\frac{v_a^2}{v^2}+o\left(\frac{v_a^2}{v^2}\right). \tag{A.10}$$

We now calculate the next two μ-moments. In the subsequent calculations of scattering terms or growth rates only their order in v_a/v is of interest while their exact value is not needed. Nevertheless, we will show the full calculations and results for completeness. For the first μ-moment, we need the following integral:

$$\begin{aligned}\int_{-1}^{1} \mathrm{d}\mu\,(1-\mu^2)\mu\left|\mu-\frac{v_a}{v}\right| &= \int_{-1}^{v_a/v} \mathrm{d}\mu\,(1-\mu^2)\mu\left(-\mu+\frac{v_a}{v}\right)+\int_{v_a/v}^{1} \mathrm{d}\mu\,(1-\mu^2)\mu\left(\mu-\frac{v_a}{v}\right)\\ &= -\frac{1}{60}\left(1+\frac{v_a}{v}\right)^3\left(8-9\frac{v_a}{v}+3\frac{v_a^2}{v^2}\right)-\frac{1}{60}\left(1-\frac{v_a}{v}\right)^3\left(8+9\frac{v_a}{v}+3\frac{v_a^2}{v^2}\right)\\ &= \frac{1}{60}\left(-30\frac{v_a}{v}+20\frac{v_a^3}{v^3}-6\frac{v_a^5}{v^5}\right)\\ &= -\frac{1}{2}\frac{v_a}{v}+o\left(\frac{v_a^2}{v^2}\right),\end{aligned} \tag{A.11}$$

and its symmetric counterpart:

$$\int_{-1}^{1} \mathrm{d}\mu\,(1-\mu^2)\mu\left|\mu+\frac{v_a}{v}\right| = +\frac{1}{2}\frac{v_a}{v}+o\left(\frac{v_a^2}{v^2}\right). \tag{A.12}$$

Lastly, the μ^2-moment contains the following integral:

$$\begin{aligned}\int_{-1}^{1} \mathrm{d}\mu\,(1-\mu^2)\mu^2 \left|\mu - \frac{v_\mathrm{a}}{v}\right| &= \int_{-1}^{v_\mathrm{a}/v} \mathrm{d}\mu\,(1-\mu^2)\mu^2\left(-\mu + \frac{v_\mathrm{a}}{v}\right) + \int_{v_\mathrm{a}/v}^{1} \mathrm{d}\mu\,(1-\mu^2)\mu^2\left(\mu - \frac{v_\mathrm{a}}{v}\right)\\ &= -\frac{1}{60}\left(5 + 8\frac{v_\mathrm{a}}{v} + 5\frac{v_\mathrm{a}^4}{v^4} - 2\frac{v_\mathrm{a}^6}{v^6}\right) - \frac{1}{60}\left(5 - 8\frac{v_\mathrm{a}}{v} + 5\frac{v_\mathrm{a}^4}{v^4} - 2\frac{v_\mathrm{a}^6}{v^6}\right)\\ &= \frac{1}{60}\left(10 + 10\frac{v_\mathrm{a}^4}{v^4} + 4\frac{v_\mathrm{a}^6}{v^6}\right)\\ &= \frac{1}{6} + o\left(\frac{v_\mathrm{a}^2}{v^2}\right). \end{aligned} \tag{A.13}$$

The backward Doppler-shifted integral is given by symmetry:

$$\int_{-1}^{1} \mathrm{d}\mu\,(1-\mu^2)\mu^2 \left|\mu + \frac{v_\mathrm{a}}{v}\right| = \frac{1}{6} + o\left(\frac{v_\mathrm{a}^2}{v^2}\right). \tag{A.14}$$

A.2.2. Pitch-Angle Integrals for $\varepsilon_{\mathrm{cr}}$

We calculate phase-space moments of the scattering terms in eq. (3.18) by starting with their 1-moment in μ. We postpone the energy moments to the next subsection. Adding the results and calculating the energy-moments yields the right hand side of eq. (3.52).

We frequently use the definitions in eqs. (3.47) and (3.48) and calculate the scattering terms separately for $D_{\mu\mu}$, $D_{\mu p}$ and D_{pp}, where we further split the terms containing $D_{\mu p}$ in separate integrals:

$$\left.\frac{\partial f}{\partial t}\right|_{\mathrm{scatt}} = \left.\frac{\partial f}{\partial t}\right|_{\mathrm{scatt},D_{\mu\mu}} + \left.\frac{\partial f}{\partial t}\right|_{\mathrm{scatt},D_{\mu p}} + \left.\frac{\partial f}{\partial t}\right|_{\mathrm{scatt},D_{p\mu}} + \left.\frac{\partial f}{\partial t}\right|_{\mathrm{scatt},D_{pp}}, \tag{A.15}$$

where the subscript denotes the moment of the corresponding diffusion term in eq. (3.18). We further remind the reader that f_0 is of order $O(1)$ whereas f_1 exhibits order $O(v_\mathrm{a}/v)$.

The $\mu\mu$-integral reads

$$\begin{aligned}\int_{-1}^{1} \mathrm{d}\mu\ \left.\frac{\partial f}{\partial t}\right|_{\mathrm{scatt},D_{\mu\mu}} &= \int_{-1}^{1} \mathrm{d}\mu\,\frac{\partial}{\partial\mu}\left\{p\frac{v_\mathrm{a}}{v}\frac{1-\mu^2}{2}\left[\left(1-\mu\frac{v_\mathrm{a}}{v}\right)^2\nu_+ + \left(1+\mu\frac{v_\mathrm{a}}{v}\right)^2\nu_-\right]\frac{\partial f}{\partial\mu}\right\}\\ &= 0, \end{aligned} \tag{A.16}$$

while the μp integral

$$\begin{aligned}\int_{-1}^{1} \mathrm{d}\mu\ \left.\frac{\partial f}{\partial t}\right|_{\mathrm{scatt},D_{\mu p}} &= \int_{-1}^{1} \mathrm{d}\mu\,\frac{\partial}{\partial\mu}\left\{p\frac{v_\mathrm{a}}{v}\frac{1-\mu^2}{2}\left[\left(1-\mu\frac{v_\mathrm{a}}{v}\right)\nu_+ - \left(1+\mu\frac{v_\mathrm{a}}{v}\right)\nu_-\right]\frac{\partial f}{\partial p}\right\}\\ &= 0, \end{aligned} \tag{A.17}$$

vanishes by virtue of the fundamental theorem of calculus. The first non-vanishing 1-moment

derives from the second $D_{\mu p}$ term. We calculate:

$$\begin{aligned}
\int_{-1}^{1}\mathrm{d}\mu\ \left.\frac{\partial f}{\partial t}\right|_{\mathrm{scatt},D_{p\mu}} &= \int_{-1}^{1}\mathrm{d}\mu\ \frac{1}{p^2}\frac{\partial}{\partial p}\left\{p^2 p\frac{v_\mathrm{a}}{v}\frac{1-\mu^2}{2}\left[\left(1-\mu\frac{v_\mathrm{a}}{v}\right)\nu_+ - \left(1+\mu\frac{v_\mathrm{a}}{v}\right)\nu_-\right]\frac{\partial f}{\partial \mu}\right\}\\
&= \frac{1}{p^2}\frac{\partial}{\partial p}p^2 p\frac{v_\mathrm{a}}{v}\int_{-1}^{1}\mathrm{d}\mu\ \frac{1-\mu^2}{2}\left[\left(1-\mu\frac{v_\mathrm{a}}{v}\right)\nu_+ - \left(1+\mu\frac{v_\mathrm{a}}{v}\right)\nu_-\right]\frac{\partial f}{\partial \mu}\\
&= \frac{1}{p^2}\frac{\partial}{\partial p}p^2 p\frac{v_\mathrm{a}}{v}\frac{3}{2}\int_{-1}^{1}\mathrm{d}\mu\ \left(1-\mu^2\right)\left[\left(1-\mu\frac{v_\mathrm{a}}{v}\right)\nu_+ - \left(1+\mu\frac{v_\mathrm{a}}{v}\right)\nu_-\right]f_1\\
&= 2\frac{1}{p^2}\frac{\partial}{\partial p}p^2 p\frac{v_\mathrm{a}}{v}\frac{3}{4}\int_{-1}^{1}\mathrm{d}\mu\ \left(1-\mu^2\right)\left[\left(1-\mu\frac{v_\mathrm{a}}{v}\right)\nu_+ - \left(1+\mu\frac{v_\mathrm{a}}{v}\right)\nu_-\right]f_1\\
&= 2\frac{1}{p^2}\frac{\partial}{\partial p}p^2 p\frac{v_\mathrm{a}}{v}\frac{3}{4}\int_{-1}^{1}\mathrm{d}\mu\ \left(1-\mu^2\right)\left[\left(\nu_+-\nu_-\right)-\mu\frac{v_\mathrm{a}}{v}\left(\nu_++\nu_-\right)\right]f_1,
\end{aligned} \tag{A.18}$$

where the second term in the brackets is of order v_a^3/v^3 and thus vanishes. Finally, the result for this moment is:

$$\begin{aligned}
&= 2\frac{1}{p^2}\frac{\partial}{\partial p}p^2 p\frac{v_\mathrm{a}}{v}\frac{3}{4}\int_{-1}^{1}\mathrm{d}\mu\ \left(1-\mu^2\right)\left(\nu_+-\nu_-\right)f_1\\
&= 2\frac{1}{p^2}\frac{\partial}{\partial p}p^2 p\frac{v_\mathrm{a}}{v}\frac{3}{4}\pi\Omega'\frac{1/2}{\varepsilon_B}\int_{-1}^{1}\mathrm{d}\mu\ \left(1-\mu^2\right)\left(\varepsilon_{\mathrm{a},+}\left|\mu-\frac{v_\mathrm{a}}{v}\right|-\varepsilon_{\mathrm{a},-}\left|\mu+\frac{v_\mathrm{a}}{v}\right|\right)f_1\\
&= 2\frac{1}{p^2}\frac{\partial}{\partial p}p^2 p\frac{v_\mathrm{a}}{v}\frac{3}{4}\pi\Omega'\frac{1/2}{\varepsilon_B}\left[\varepsilon_{\mathrm{a},+}\left(\frac{1}{2}+\frac{v_\mathrm{a}^2}{v^2}\right)-\varepsilon_{\mathrm{a},-}\left(\frac{1}{2}+\frac{v_\mathrm{a}^2}{v^2}\right)\right]f_1\\
&= 2\frac{1}{p^2}\frac{\partial}{\partial p}p^2 p\frac{v_\mathrm{a}}{v}(\bar{\nu}_+-\bar{\nu}_-)f_1.
\end{aligned} \tag{A.19}$$

The last term contributing to the ε_cr equation is a D_{pp} term. We calculate its moment to:

$$\begin{aligned}
\int_{-1}^{1}\mathrm{d}\mu\ \left.\frac{\partial f}{\partial t}\right|_{\mathrm{scatt},D_{pp}} &= \int_{-1}^{1}\mathrm{d}\mu\ \frac{1}{p^2}\frac{\partial}{\partial p}\left\{p^2 p^2\frac{v_\mathrm{a}^2}{v^2}\frac{1-\mu^2}{2}\left(\nu_++\nu_-\right)\frac{\partial f}{\partial p}\right\}\\
&= \int_{-1}^{1}\mathrm{d}\mu\ \frac{1}{p^2}\frac{\partial}{\partial p}\left\{p^2 p^2\frac{v_\mathrm{a}^2}{v^2}\frac{1-\mu^2}{2}\left(\nu_++\nu_-\right)\frac{\partial\left(f_0+3f_1\right)}{\partial p}\right\}
\end{aligned} \tag{A.20}$$

since f_1 is of order v_a/v, we can neglect its contribution to this integral.

$$
\begin{aligned}
&= \int_{-1}^{1} \mathrm{d}\mu \, \frac{1}{p^2}\frac{\partial}{\partial p}\left\{ p^2 p^2 \frac{v_\mathrm{a}^2}{v^2}\frac{1-\mu^2}{2}\left(\nu_+ + \nu_-\right)\frac{\partial f_0}{\partial p}\right\} \\
&= \frac{1}{p^2}\frac{\partial}{\partial p} p^2 p^2 \frac{v_\mathrm{a}^2}{v^2}\int_{-1}^{1}\mathrm{d}\mu\,\frac{1-\mu^2}{2}\left(\nu_+ + \nu_-\right)\frac{\partial f_0}{\partial p} \\
&= \frac{2}{3}\frac{1}{p^2}\frac{\partial}{\partial p} p^2 p^2 \frac{v_\mathrm{a}^2}{v^2}\frac{3}{4}\int_{-1}^{1}\mathrm{d}\mu\,\left(1-\mu^2\right)\left(\nu_+ + \nu_-\right)\frac{\partial f_0}{\partial p} \\
&= \frac{2}{3}\frac{1}{p^2}\frac{\partial}{\partial p} p^2 p^2 \frac{v_\mathrm{a}^2}{v^2}\frac{3}{4}\pi\Omega'\frac{1/2}{\varepsilon_B}\int_{-1}^{1}\mathrm{d}\mu\,\left(1-\mu^2\right)\left(\varepsilon_{\mathrm{a},+}\left|\mu - \frac{v_\mathrm{a}}{v}\right| + \varepsilon_{\mathrm{a},-}\left|\mu + \frac{v_\mathrm{a}}{v}\right|\right)\frac{\partial f_0}{\partial p} \\
&= \frac{2}{3}\frac{1}{p^2}\frac{\partial}{\partial p} p^2 p^2 \frac{v_\mathrm{a}^2}{v^2}\frac{3}{4}\pi\Omega'\frac{1/2}{\varepsilon_B}\left[\varepsilon_{\mathrm{a},+}\left(\frac{1}{2}+\frac{v_\mathrm{a}^2}{v^2}\right) + \varepsilon_{\mathrm{a},-}\left(\frac{1}{2}+\frac{v_\mathrm{a}^2}{v^2}\right)\right]\frac{\partial f_0}{\partial p} \\
&= \frac{2}{3}\frac{1}{p^2}\frac{\partial}{\partial p} p^2 p^2 \frac{v_\mathrm{a}^2}{v^2}\left(\bar{\nu}_+ + \bar{\nu}_-\right)\frac{\partial f_0}{\partial p}.
\end{aligned}
\tag{A.21}
$$

A.2.3. Momentum Integrals for $\varepsilon_{\mathrm{cr}}$

To finalize the phase-space moments for the scattering terms in the energy equation, we need to apply the definition

$$
\int \mathrm{d}^3 p T(p) = \int_0^\infty \mathrm{d}p\, 2\pi p^2 T(p) \int_{-1}^{1}\mathrm{d}\mu \tag{A.22}
$$

to every term in eq. (A.15). Because we have already calculated the μ integral, we simply insert the derived results from the the last subsection. Starting with the two trivial moments (using eq. (A.16))

$$
\begin{aligned}
\left.\frac{\partial \varepsilon_{\mathrm{cr}}}{\partial t}\right|_{\mathrm{scatt},D_{\mu\mu}} &= \int_0^\infty \mathrm{d}p\, 2\pi p^2 T(p) \int_{-1}^{1}\mathrm{d}\mu\, \left.\frac{\partial f}{\partial t}\right|_{\mathrm{scatt},D_{\mu\mu}} \\
&= 0,
\end{aligned}
\tag{A.23}
$$

and, using eq. (A.17);

$$
\begin{aligned}
\left.\frac{\partial \varepsilon_{\mathrm{cr}}}{\partial t}\right|_{\mathrm{scatt},D_{\mu p}} &= \int_0^\infty \mathrm{d}p\, 2\pi p^2 T(p) \int_{-1}^{1}\mathrm{d}\mu\, \left.\frac{\partial f}{\partial t}\right|_{\mathrm{scatt},D_{\mu p}} \\
&= 0,
\end{aligned}
\tag{A.24}
$$

we calculate the energy moment of the second $D_{\mu p}$ term based on eq. (A.19) to:

$$\begin{aligned}
\left.\frac{\partial \varepsilon_{\mathrm{cr}}}{\partial t}\right|_{\mathrm{scatt},D_{p\mu}} &= \int_0^\infty \mathrm{d}p\, 2\pi p^2 T(p) \int_{-1}^1 \mathrm{d}\mu \left.\frac{\partial f}{\partial t}\right|_{\mathrm{scatt},D_{p\mu}} \\
&= \int_0^\infty \mathrm{d}p\, 4\pi T(p) \frac{\partial}{\partial p} p^2 p \frac{v_\mathrm{a}}{v} (\bar{\nu}_+ - \bar{\nu}_-) f_1 \\
&= -\int_0^\infty \mathrm{d}p\, 4\pi v p^2 p \frac{v_\mathrm{a}}{v} (\bar{\nu}_+ - \bar{\nu}_-) f_1 \\
&= -3 \int_0^\infty \mathrm{d}p\, 4\pi p^2 \frac{vp}{3} \frac{v_\mathrm{a}}{v} (\bar{\nu}_+ - \bar{\nu}_-) f_1 \\
&= -3 \frac{v_\mathrm{a}}{c^2} (\bar{\nu}_+ - \bar{\nu}_-) \int_0^\infty \mathrm{d}p\, 4\pi p^2 \frac{vp}{3} v f_1 \\
&= -3 \frac{v_\mathrm{a}}{c^2} (\bar{\nu}_+ - \bar{\nu}_-) K_{\mathrm{cr}}.
\end{aligned} \tag{A.25}$$

For the contribution of momentum diffusion to the energy balance, we obtain:

$$\begin{aligned}
\left.\frac{\partial \varepsilon_{\mathrm{cr}}}{\partial t}\right|_{\mathrm{scatt},D_{pp}} &= \int_0^\infty \mathrm{d}p\, 2\pi p^2 T(p) \int_{-1}^1 \mathrm{d}\mu \left.\frac{\partial f}{\partial t}\right|_{\mathrm{scatt},D_{pp}} \\
&= \int_0^\infty \mathrm{d}p\, 2\pi p^2 T(p) \frac{2}{3} \frac{1}{p^2} \frac{\partial}{\partial p} p^2 p^2 \frac{v_\mathrm{a}^2}{v^2} (\bar{\nu}_+ + \bar{\nu}_-) \frac{\partial f_0}{\partial p} \\
&= \int_0^\infty \mathrm{d}p\, \frac{4}{3}\pi T(p) \frac{\partial}{\partial p} p^4 \frac{v_\mathrm{a}^2}{v^2} (\bar{\nu}_+ + \bar{\nu}_-) \frac{\partial f_0}{\partial p} \\
&= -\int_0^\infty \mathrm{d}p\, \frac{4}{3}\pi v p^4 \frac{v_\mathrm{a}^2}{v^2} (\bar{\nu}_+ + \bar{\nu}_-) \frac{\partial f_0}{\partial p} \\
&= -\frac{v_\mathrm{a}^2}{c^2} (\bar{\nu}_+ + \bar{\nu}_-) \int_0^\infty \mathrm{d}p\, \frac{4}{3}\pi v p^4 \frac{\partial f_0}{\partial p} \\
&= 4 \frac{v_\mathrm{a}^2}{c^2} (\bar{\nu}_+ + \bar{\nu}_-) \int_0^\infty \mathrm{d}p\, \frac{4}{3}\pi v p^3 f_0 \\
&= 4 \frac{v_\mathrm{a}^2}{c^2} (\bar{\nu}_+ + \bar{\nu}_-) \int_0^\infty \mathrm{d}p\, 4\pi p^2 \frac{pv}{3} f_0 \\
&= 4 \frac{v_\mathrm{a}^2}{c^2} (\bar{\nu}_+ + \bar{\nu}_-) P_{\mathrm{cr}},
\end{aligned} \tag{A.26}$$

using eq. (A.21).

A.2.4. Pitch-Angle Integrals for f_{cr}

We apply the same procedure for calculating the μ and energy moments of eq. (3.18). This results in their contribution to eq. (3.54). For the μ-moments, we multiply each scattering term in eq. (A.15) by μ and integrate over μ for each term. Starting with the $\mu\mu$ pitch-angle scattering term, we have:

$$\begin{aligned}\int_{-1}^{1}\mathrm{d}\mu\,\mu\left.\frac{\partial f}{\partial t}\right|_{\mathrm{scatt},D_{\mu\mu}} &= \int_{-1}^{1}\mathrm{d}\mu\,\mu\frac{\partial}{\partial\mu}\left\{\frac{1-\mu^2}{2}\left[\left(1-\mu\frac{v_\mathrm{a}}{v}\right)^2\nu_+ + \left(1+\mu\frac{v_\mathrm{a}}{v}\right)^2\nu_-\right]\frac{\partial f}{\partial\mu}\right\}\\ &= -\int_{-1}^{1}\mathrm{d}\mu\left\{\frac{1-\mu^2}{2}\left[\left(1-\mu\frac{v_\mathrm{a}}{v}\right)^2\nu_+ + \left(1+\mu\frac{v_\mathrm{a}}{v}\right)^2\nu_-\right]\frac{\partial f}{\partial\mu}\right\}\\ &= -\frac{3}{2}\int_{-1}^{1}\mathrm{d}\mu\left(1-\mu^2\right)\left[\left(1-\mu\frac{v_\mathrm{a}}{v}\right)^2\nu_+ + \left(1+\mu\frac{v_\mathrm{a}}{v}\right)^2\nu_-\right]f_1.\end{aligned}$$

Directly expanding the quadratic terms results in $(1-\mu^2)$, $(1-\mu^2)\mu$ and $(1-\mu^2)\mu^2$ moments of the scattering coefficient. Since the $(1-\mu^2)\mu$ moment is of order v_a/v, we can neglect it because it is multiplied with f_1 and a factor from the binomial formula, both of order v_a/v. The same is true for the term $(1-\mu^2)\mu^2$ because it is accompanied by a factor v_a^2/v^2 resulting from the quadratic expansion. We obtain:

$$\begin{aligned}&= -\frac{3}{2}\int_{-1}^{1}\mathrm{d}\mu\left(1-\mu^2\right)(\nu_+ + \nu_-)\,f_1\\ &= -\frac{3}{2}\pi\Omega'\frac{1/2}{\varepsilon_B}\int_{-1}^{1}\mathrm{d}\mu\left(1-\mu^2\right)\left(\varepsilon_{\mathrm{a},+}\left|\mu-\frac{v_\mathrm{a}}{v}\right| + \varepsilon_{\mathrm{a},-}\left|\mu+\frac{v_\mathrm{a}}{v}\right|\right)f_1\\ &= -\frac{3}{2}\pi\Omega'\frac{1/2}{\varepsilon_B}\left[\varepsilon_{\mathrm{a},+}\left(\frac{1}{2}+\frac{v_\mathrm{a}^2}{v^2}\right) + \varepsilon_{\mathrm{a},-}\left(\frac{1}{2}+\frac{v_\mathrm{a}^2}{v^2}\right)\right]f_1\\ &= -2(\bar{\nu}_+ + \bar{\nu}_-)f_1.\end{aligned} \tag{A.27}$$

The next moment results from a $D_{p\mu}$-term, which we evaluate to:

$$\begin{aligned}\int_{-1}^{1}\mathrm{d}\mu\,\mu\left.\frac{\partial f}{\partial t}\right|_{\mathrm{scatt},D_{p\mu}} &= \int_{-1}^{1}\mathrm{d}\mu\,\mu\frac{1}{p^2}\frac{\partial}{\partial p}\left\{p^2 p\frac{v_\mathrm{a}}{v}\frac{1-\mu^2}{2}\left[\left(1-\mu\frac{v_\mathrm{a}}{v}\right)\nu_+ - \left(1+\mu\frac{v_\mathrm{a}}{v}\right)\nu_-\right]\frac{\partial f}{\partial\mu}\right\}\\ &= \frac{1}{p^2}\frac{\partial}{\partial p}p^2 p\frac{v_\mathrm{a}}{v}\int_{-1}^{1}\mathrm{d}\mu\,\mu\left\{\frac{1-\mu^2}{2}\left[\left(1-\mu\frac{v_\mathrm{a}}{v}\right)\nu_+ - \left(1+\mu\frac{v_\mathrm{a}}{v}\right)\nu_-\right]\frac{\partial f}{\partial\mu}\right\}\\ &= \frac{3}{p^2}\frac{\partial}{\partial p}p^2 p\frac{v_\mathrm{a}}{v}\int_{-1}^{1}\mathrm{d}\mu\,\mu\left\{\frac{1-\mu^2}{2}\left[\left(1-\mu\frac{v_\mathrm{a}}{v}\right)\nu_+ - \left(1+\mu\frac{v_\mathrm{a}}{v}\right)\nu_-\right]f_1\right\}.\end{aligned}$$

No term will remain from this integral because: the terms proportional to 1 in the parenthesis is a $(1-\mu^2)\mu$ moment of the scattering coefficient and thus of order v_a/v, which is entirely of order v_a^3/v^3. This derives from with the v_a/v factor in front of the integral and the fact that f_1 is of order v_a/v. The remaing term in the parenthesis is directly proportional to v_a/v and vanishes by the same argument as before. We thus have:

$$\int_{-1}^{1}\mathrm{d}\mu\,\mu\left.\frac{\partial f}{\partial t}\right|_{\mathrm{scatt},D_{p\mu}} = 0. \tag{A.28}$$

We calculate the other $D_{p\mu}$ term by starting with the term:

$$\begin{aligned}
\int_{-1}^{1} \mathrm{d}\mu\, \mu \left.\frac{\partial f}{\partial t}\right|_{\mathrm{scatt},D_{\mu p}} &= \int_{-1}^{1} \mathrm{d}\mu\, \mu \frac{\partial}{\partial \mu}\left\{ p\frac{v_\mathrm{a}}{v}\frac{1-\mu^2}{2}\left[\left(1-\mu\frac{v_\mathrm{a}}{v}\right)\nu_+ - \left(1+\mu\frac{v_\mathrm{a}}{v}\right)\nu_-\right]\frac{\partial f}{\partial p}\right\} \\
&= -\int_{-1}^{1} \mathrm{d}\mu \left\{ p\frac{v_\mathrm{a}}{v}\frac{1-\mu^2}{2}\left[\left(1-\mu\frac{v_\mathrm{a}}{v}\right)\nu_+ - \left(1+\mu\frac{v_\mathrm{a}}{v}\right)\nu_-\right]\frac{\partial f}{\partial p}\right\} \\
&= -p\frac{v_\mathrm{a}}{v}\frac{1}{2}\int_{-1}^{1} \mathrm{d}\mu \left(1-\mu^2\right)\left[\left(1-\mu\frac{v_\mathrm{a}}{v}\right)\nu_+ - \left(1+\mu\frac{v_\mathrm{a}}{v}\right)\nu_-\right]\frac{\partial f}{\partial p} \\
&= -p\frac{v_\mathrm{a}}{v}\frac{1}{2}\int_{-1}^{1} \mathrm{d}\mu \left(1-\mu^2\right)\left[\left(1-\mu\frac{v_\mathrm{a}}{v}\right)\nu_+ - \left(1+\mu\frac{v_\mathrm{a}}{v}\right)\nu_-\right]\frac{\partial}{\partial p}(f_0 + 3f_1\mu)
\end{aligned}$$

Next, we check which terms will remain from this integral:

- f_0 combined with the 1-term from the parenthesis results in a $(1-\mu^2)$ moment of the scattering coefficient and is thus of first order and remains,
- f_0 combined with the μ-term from the parenthesis results in a $(1-\mu^2)\mu$ moment of the scattering coefficient and is thus of third order and vanishes,
- f_1 combined with the 1-term from the parenthesis results in a $(1-\mu^2)\mu$ moment of the scattering coefficient and is thus of third order and vanishes,
- f_1 combined with the μ-term from the parenthesis results in a $(1-\mu^2)\mu^2$ moment of the scattering coefficient and is thus of third order and vanishes.

Removing the vanishing terms from the integral yields:

$$\begin{aligned}
&= -p\frac{v_\mathrm{a}}{v}\frac{1}{2}\int_{-1}^{1} \mathrm{d}\mu \left(1-\mu^2\right)(\nu_+ - \nu_-)\frac{\partial f_0}{\partial p} \\
&= -p\frac{v_\mathrm{a}}{v}\frac{1}{2}\pi\Omega'\frac{1/2}{\varepsilon_B}\int_{-1}^{1} \mathrm{d}\mu \left(1-\mu^2\right)\left(\varepsilon_{\mathrm{a},+}\left|\mu - \frac{v_\mathrm{a}}{v}\right| - \varepsilon_{\mathrm{a},-}\left|\mu + \frac{v_\mathrm{a}}{v}\right|\right)\frac{\partial f_0}{\partial p} \\
&= -p\frac{v_\mathrm{a}}{v}\frac{1}{2}\pi\Omega'\frac{1/2}{\varepsilon_B}\left[\varepsilon_{\mathrm{a},+}\left(\frac{1}{2}+\frac{v_\mathrm{a}^2}{v^2}\right) - \varepsilon_{\mathrm{a},-}\left(\frac{1}{2}+\frac{v_\mathrm{a}^2}{v^2}\right)\right]\frac{\partial f_0}{\partial p} \\
&= -p\frac{v_\mathrm{a}}{v}\frac{2}{3}\frac{3}{4}\pi\Omega'\frac{1/2}{\varepsilon_B}\left[\varepsilon_{\mathrm{a},+}\left(\frac{1}{2}+\frac{v_\mathrm{a}^2}{v^2}\right) - \varepsilon_{\mathrm{a},-}\left(\frac{1}{2}+\frac{v_\mathrm{a}^2}{v^2}\right)\right]\frac{\partial f_0}{\partial p} \\
&= -p\frac{v_\mathrm{a}}{v}\frac{2}{3}\left(\bar{\nu}_+ - \bar{\nu}_-\right)\frac{\partial f_0}{\partial p}
\end{aligned} \tag{A.29}$$

The momentum-scattering term yields:

$$\begin{aligned}
\int_{-1}^{1} \mathrm{d}\mu\, \mu \left.\frac{\partial f}{\partial t}\right|_{\mathrm{scatt},D_{pp}} &= \int_{-1}^{1} \mathrm{d}\mu\, \mu \frac{1}{p^2}\frac{\partial}{\partial p}\left[p^2 p^2 \frac{v_\mathrm{a}^2}{v^2}\frac{1-\mu^2}{2}\left(\nu_+ + \nu_-\right)\frac{\partial f}{\partial p}\right] \\
&= \frac{1}{p^2}\frac{\partial}{\partial p}p^2 p^2 \frac{v_\mathrm{a}^2}{v^2}\int_{-1}^{1} \mathrm{d}\mu\, \mu \frac{1-\mu^2}{2}\left(\nu_+ + \nu_-\right)\frac{\partial f}{\partial p} \\
&= \frac{1}{p^2}\frac{\partial}{\partial p}p^2 p^2 \frac{v_\mathrm{a}^2}{v^2}\int_{-1}^{1} \mathrm{d}\mu\, \mu \frac{1-\mu^2}{2}\left(\nu_+ + \nu_-\right)\frac{\partial}{\partial p}(f_0 + 3f_1\mu)
\end{aligned}$$

The contribution from the f_0 term vanishes because it results in a $(1-\mu^2)\mu$ moment of the scattering coefficient which adds an additional v_a/v to the factor v_a^2/v^2 in front of the integral

and is thus of third order and negligible. The terms containing f_1 also vanish, as f_1 is of order v_a/v and is of third order because of the same factor as before. We finally obtain:

$$\int_{-1}^{1} \mathrm{d}\mu\, \mu \left.\frac{\partial f}{\partial t}\right|_{\mathrm{scatt},D_{p\mu}} = 0 \tag{A.30}$$

A.2.5. Momentum Integrals for f_cr

Equipped with the first pitch-angle moments of all diffusion coefficients, we are now able to calculate the corresponding momentum moments. We again write:

$$\left.\frac{\partial f_\mathrm{cr}}{\partial t}\right|_\mathrm{scatt} = \left.\frac{\partial f_\mathrm{cr}}{\partial t}\right|_{\mathrm{scatt},D_{\mu\mu}} + \left.\frac{\partial f_\mathrm{cr}}{\partial t}\right|_{\mathrm{scatt},D_{\mu p}} + \left.\frac{\partial f_\mathrm{cr}}{\partial t}\right|_{\mathrm{scatt},D_{p\mu}} + \left.\frac{\partial f_\mathrm{cr}}{\partial t}\right|_{\mathrm{scatt},D_{pp}} . \tag{A.31}$$

Starting with the pitch-angle diffusion and using eq. (A.27), we have:

$$\begin{aligned}
\left.\frac{\partial f_\mathrm{cr}}{\partial t}\right|_{\mathrm{scatt},D_{\mu\mu}} &= \int_0^\infty \mathrm{d}p\, 2\pi p^2 T(p) v \int_{-1}^{1} \mathrm{d}\mu\, \mu \left.\frac{\partial f}{\partial t}\right|_{\mathrm{scatt},D_{\mu\mu}} \\
&= -\int_0^\infty \mathrm{d}p\, 2\pi p^2 T(p) v 2(\bar{\nu}_+ + \bar{\nu}_-) f_1 \\
&= -(\bar{\nu}_+ + \bar{\nu}_-) \int_0^\infty \mathrm{d}p\, 4\pi p^2 T(p) v f_1 \\
&= -(\bar{\nu}_+ + \bar{\nu}_-) f_\mathrm{cr}.
\end{aligned} \tag{A.32}$$

The $p\mu$-diffusion contribution to the evolution of the flux vanishes by means of eq. (A.28):

$$\begin{aligned}
\left.\frac{\partial f_\mathrm{cr}}{\partial t}\right|_{\mathrm{scatt},D_{p\mu}} &= \int_0^\infty \mathrm{d}p\, 2\pi p^2 T(p) v \int_{-1}^{1} \mathrm{d}\mu\, \mu \left.\frac{\partial f}{\partial t}\right|_{\mathrm{scatt},D_{p\mu}} \\
&= 0.
\end{aligned} \tag{A.33}$$

The next and non-vanishing term results from eq. (A.29) and is given by:

$$\begin{aligned}
\left.\frac{\partial f_\mathrm{cr}}{\partial t}\right|_{\mathrm{scatt},D_{\mu p}} &= \int_0^\infty \mathrm{d}p\, 2\pi p^2 T(p) v \int_{-1}^{1} \mathrm{d}\mu\, \mu \left.\frac{\partial f}{\partial t}\right|_{\mathrm{scatt},D_{\mu p}} \\
&= -\int_0^\infty \mathrm{d}p\, 2\pi p^2 T(p) v p \frac{v_\mathrm{a}}{v} \frac{2}{3} (\bar{\nu}_+ - \bar{\nu}_-) \frac{\partial f_0}{\partial p} \\
&= -\int_0^\infty \mathrm{d}p\, 4\pi \frac{p^3}{3} T(p) v \frac{v_\mathrm{a}}{v} (\bar{\nu}_+ - \bar{\nu}_-) \frac{\partial f_0}{\partial p} \\
&= -v_\mathrm{a} (\bar{\nu}_+ - \bar{\nu}_-) \int_0^\infty \mathrm{d}p\, 4\pi \frac{p^3}{3} T(p) \frac{\partial f_0}{\partial p} \\
&= v_\mathrm{a} (\bar{\nu}_+ - \bar{\nu}_-) \int_0^\infty \mathrm{d}p\, 4\pi \left(\frac{p^3 v}{3} + p^2 T(p) \right) f_0 \\
&= v_\mathrm{a} (\bar{\nu}_+ - \bar{\nu}_-) (\varepsilon_\mathrm{cr} + P_\mathrm{cr}) .
\end{aligned} \tag{A.34}$$

The last remaining term is the contribution from the momentum diffusion, which vanishes by virtue of eq. (A.30):

$$\left.\frac{\partial f_{\mathrm{cr}}}{\partial t}\right|_{\mathrm{scatt},D_{pp}} = \int_0^\infty \mathrm{d}p\, 2\pi p^2 T(p) v \int_{-1}^{1} \mathrm{d}\mu\, \mu \left.\frac{\partial f}{\partial t}\right|_{\mathrm{scatt},D_{pp}} = 0. \tag{A.35}$$

A.3. Growth Rate of Alfvén Waves

Here, we calculate the energy density growth of the Alfvén waves. We adopt the same general methods to approximate the complete equation to order v_{a}^2/v^2, as used before during the calculation of the scattering terms for the CRs transport equation. We start with:

$$\begin{aligned}
&\int_0^\infty \mathrm{d}k\, \Gamma_{\mathrm{gri},\pm}(k) R_\pm(k) \\
&\quad = \pm\frac{\pi}{2}\frac{\Omega^2 v_{\mathrm{a}}}{\boldsymbol{B}^2/4\pi} \int \mathrm{d}^3 p \frac{1-\mu^2}{2} p \left(\frac{\partial f}{\partial \mu} + \frac{\boldsymbol{b}\cdot\boldsymbol{u}_\pm}{v} p \frac{\partial f}{\partial p}\right) \int_0^\infty \mathrm{d}k\, \delta\left((\mu v \mp v_{\mathrm{a}})k - \Omega\right) R_\pm(k) \\
&\quad = \pm\frac{\pi}{2}\frac{\Omega^2 v_{\mathrm{a}}}{\boldsymbol{B}^2/4\pi} \int \mathrm{d}^3 p \frac{1-\mu^2}{2} p \left(\frac{\partial f}{\partial \mu} + \frac{\boldsymbol{b}\cdot\boldsymbol{u}_\pm}{v} p \frac{\partial f}{\partial p}\right) \frac{1}{|\mu v \mp v_{\mathrm{a}}|} R_\pm(k_{\mathrm{res}}) \\
&\quad = \pm\frac{\pi}{2}\frac{\Omega v_{\mathrm{a}}}{\boldsymbol{B}^2/4\pi} \int \mathrm{d}^3 p \frac{1-\mu^2}{2} p \left(\frac{\partial f}{\partial \mu} + \frac{\boldsymbol{b}\cdot\boldsymbol{u}_\pm}{v} p \frac{\partial f}{\partial p}\right) |k_{\mathrm{res}}| R_\pm(k_{\mathrm{res}}) \\
&\quad = \pm v_{\mathrm{a}} \int \mathrm{d}^3 p \frac{1-\mu^2}{2} p \left(\frac{\partial f}{\partial \mu} + \frac{\boldsymbol{b}\cdot\boldsymbol{u}_\pm}{v} p \frac{\partial f}{\partial p}\right) \nu_\pm(p,\mu).
\end{aligned} \tag{A.36}$$

We calculate this integral by splitting it into contributions from both derivatives of f. First, the integral containing $\partial_\mu f$ evaluates to:

$$
\begin{aligned}
\pm v_\mathrm{a} \int \mathrm{d}^3p\, \frac{1-\mu^2}{2} p \frac{\partial f}{\partial \mu} \nu_\pm(p,\mu) = \\
&= \pm v_\mathrm{a} \frac{3}{2} \int_0^\infty \mathrm{d}p\, 2\pi p^3 \int_{-1}^1 \mathrm{d}\mu\, (1-\mu^2) \nu_\pm(p,\mu) f_1 \\
&= \pm v_\mathrm{a} \frac{3}{2} \pi\Omega' \frac{\varepsilon_{\mathrm{a},\pm}/2}{\varepsilon_B} \int_0^\infty \mathrm{d}p\, 2\pi p^3 \int_{-1}^1 \mathrm{d}\mu\, (1-\mu^2) \left|\mu \mp \frac{v_\mathrm{a}}{v}\right| f_1 \\
&= \pm v_\mathrm{a} \frac{3}{2} \pi\Omega' \frac{\varepsilon_{\mathrm{a},\pm}/2}{\varepsilon_B} \int_0^\infty \mathrm{d}p\, 2\pi p^3 \left(\frac{1}{2} + \frac{v_\mathrm{a}^2}{v^2}\right) f_1 \\
&= \pm v_\mathrm{a} \frac{3}{4} \pi\Omega' \frac{\varepsilon_{\mathrm{a},\pm}/2}{\varepsilon_B} \int_0^\infty \mathrm{d}p\, 4\pi p^3 \left(\frac{1}{2} + \frac{v_\mathrm{a}^2}{c^2}\right) f_1 \\
&= \pm v_\mathrm{a} \bar{\nu}_\pm \int_0^\infty \mathrm{d}p\, 4\pi p^3 f_1 \\
&= \pm 3 \frac{v_\mathrm{a} \bar{\nu}_\pm}{c^2} \int_0^\infty \mathrm{d}p\, 4\pi p^2 \frac{pv}{3} v f_1 \\
&= \pm 3 \frac{v_\mathrm{a} \bar{\nu}_\pm}{c^2} K_\mathrm{cr} \\
&= \pm \frac{v_\mathrm{a} \bar{\nu}_\pm}{c^2} f_\mathrm{cr}
\end{aligned}
\tag{A.37}
$$

The integral containing the p-derivative of f reads:

$$
\begin{aligned}
\pm v_\mathrm{a} \int \mathrm{d}^3p\, \frac{1-\mu^2}{2} p^2 \frac{\boldsymbol{b}\cdot\boldsymbol{u}_\pm}{v} \frac{\partial f}{\partial p} \nu_\pm(p,\mu) = \\
&= v_\mathrm{a}^2 \int \mathrm{d}^3p\, \frac{1-\mu^2}{2} p^2 \frac{1}{v} \frac{\partial f}{\partial p} \nu_\pm(p,\mu) \\
&= v_\mathrm{a}^2 \pi\Omega' \frac{\varepsilon_{\mathrm{a},\pm}/2}{\varepsilon_B} \int_0^\infty \mathrm{d}p\, 2\pi p^2 p^2 \frac{1}{v} \int_{-1}^1 \mathrm{d}\mu\, \frac{1-\mu^2}{2} \left|\mu \mp \frac{v_\mathrm{a}}{v}\right| \frac{\partial f}{\partial p} \\
&= v_\mathrm{a}^2 \pi\Omega' \frac{\varepsilon_{\mathrm{a},\pm}/2}{\varepsilon_B} \int_0^\infty \mathrm{d}p\, 2\pi p^4 \frac{1}{v} \int_{-1}^1 \mathrm{d}\mu\, \frac{1-\mu^2}{2} \left|\mu \mp \frac{v_\mathrm{a}}{v}\right| \frac{\partial f}{\partial p} \\
&= \frac{v_\mathrm{a}^2}{c^2} \pi\Omega' \frac{\varepsilon_{\mathrm{a},\pm}/2}{\varepsilon_B} \int_0^\infty \mathrm{d}p\, \pi p^4 v \int_{-1}^1 \mathrm{d}\mu\, \left(1-\mu^2\right) \left|\mu \mp \frac{v_\mathrm{a}}{v}\right| \frac{\partial f}{\partial p}
\end{aligned}
$$

Again, we can nelgect the contribution of f_1 because it yields a third order contribution to this integral. We proceed with:

$$
\begin{aligned}
&= \frac{v_\mathrm{a}^2}{c^2}\pi\Omega' \frac{\varepsilon_{\mathrm{a},\pm}/2}{\varepsilon_B} \int_0^\infty \mathrm{d}p\, \pi p^4 v \frac{\partial f_0}{\partial p} \int_{-1}^1 \mathrm{d}\mu \left(1-\mu^2\right) \left|\mu \mp \frac{v_\mathrm{a}}{v}\right| \\
&= \frac{v_\mathrm{a}^2}{c^2}\pi\Omega' \frac{\varepsilon_{\mathrm{a},\pm}/2}{\varepsilon_B} \int_0^\infty \mathrm{d}p\, \pi p^4 v \frac{\partial f_0}{\partial p} \left(\frac{1}{2} + \frac{v_\mathrm{a}^2}{v^2}\right) \\
&= \frac{v_\mathrm{a}^2}{c^2}\pi\Omega' \frac{\varepsilon_{\mathrm{a},\pm}/2}{\varepsilon_B} \left(\frac{1}{2} + \frac{v_\mathrm{a}^2}{c^2}\right) \int_0^\infty \mathrm{d}p\, \pi p^4 v \frac{\partial f_0}{\partial p} \\
&= -4\frac{3}{4}\frac{v_\mathrm{a}^2}{c^2}\pi\Omega' \frac{\varepsilon_{\mathrm{a},\pm}/2}{\varepsilon_B} \left(\frac{1}{2} + \frac{v_\mathrm{a}^2}{c^2}\right) \int_0^\infty \mathrm{d}p\, 4\pi p^2 \frac{pv}{3} f_0 \\
&= -4\frac{v_\mathrm{a}^2}{c^2}\bar{\nu}_\pm \int_0^\infty \mathrm{d}p\, 4\pi p^2 \frac{pv}{3} f_0 \\
&= -4\frac{v_\mathrm{a}^2}{c^2}\bar{\nu}_\pm P_\mathrm{cr} \\
&= -\frac{v_\mathrm{a}^2}{c^2}\bar{\nu}_\pm (\varepsilon_\mathrm{cr} + P_\mathrm{cr}).
\end{aligned}
\tag{A.38}
$$

Combing both contributions results in a final wave energy density growth due to the interaction with CRs:

$$
\begin{aligned}
\int_0^\infty \mathrm{d}k\, \Gamma_{\mathrm{gri},\pm}(k) R_\pm(k) &= \pm\frac{v_\mathrm{a}\bar{\nu}_\pm}{c^2} f_\mathrm{cr} - \frac{v_\mathrm{a}^2}{c^2}\bar{\nu}_\pm(\varepsilon_\mathrm{cr} + P_\mathrm{cr}) \\
&= \pm\frac{v_\mathrm{a}}{c^2}\bar{\nu}_\pm \left(f_\mathrm{cr} \mp v_\mathrm{a}(\varepsilon_\mathrm{cr} + P_\mathrm{cr})\right) \\
&= \pm\frac{v_\mathrm{a}}{3\kappa_\pm} \left(f_\mathrm{cr} \mp v_\mathrm{a}(\varepsilon_\mathrm{cr} + P_\mathrm{cr})\right).
\end{aligned}
\tag{A.39}
$$

Bibliography

A. Achterberg. The ponderomotive force due to cosmic ray generated Alfven waves. A&A, 98:195–197, May 1981.

F. Aharonian, R. Yang, and E. de Oña Wilhelmi. Massive Stars as Major Factories of Galactic Cosmic Rays. ArXiv e-prints, April 2018.

R. Aloisio, P. Blasi, and P. D. Serpico. Nonlinear cosmic ray Galactic transport in the light of AMS-02 and Voyager data. A&A, 583:A95, November 2015. doi: 10.1051/0004-6361/201526877.

P. Blasi. Origin of Galactic Cosmic Rays. Nuclear Physics B Proceedings Supplements, 239: 140–147, June 2013. doi: 10.1016/j.nuclphysbps.2013.05.023.

P. Blasi and E. Amato. Diffusive propagation of cosmic rays from supernova remnants in the Galaxy. I: spectrum and chemical composition. J. Cosmology Astropart. Phys., 1:010, January 2012. doi: 10.1088/1475-7516/2012/01/010.

C. M. Booth, O. Agertz, A. V. Kravtsov, and N. Y. Gnedin. Simulations of Disk Galaxies with Cosmic Ray Driven Galactic Winds. ApJ, 777:L16, November 2013. doi: 10.1088/2041-8205/777/1/L16.

S. I. Braginskii. Transport Processes in a Plasma. Reviews of Plasma Physics, 1:205, 1965.

D. Breitschwerdt, J. F. McKenzie, and H. J. Völk. Galactic winds. I - Cosmic ray and wave-driven winds from the Galaxy. A&A, 245:79–98, May 1991.

D. Breitschwerdt, J. F. McKenzie, and H. J. Völk. Galactic winds. II - Role of the disk-halo interface in cosmic ray driven galactic winds. A&A, 269:54–66, March 1993.

J. R. Buchler. Radiation hydrodynamics in the fluid frame. J. Quant. Spec. Radiat. Transf., 22: 293–300, September 1979. doi: 10.1016/0022-4073(79)90119-5.

A. C. Cummings, E. C. Stone, B. C. Heikkila, N. Lal, W. R. Webber, G. Jóhannesson, I. V. Moskalenko, E. Orlando, and T. A. Porter. Galactic Cosmic Rays in the Local Interstellar Medium: Voyager 1 Observations and Model Results. ApJ, 831:18, November 2016. doi: 10.3847/0004-637X/831/1/18.

R. L. Dewar. Interaction between Hydromagnetic Waves and a Time-Dependent, Inhomogeneous Medium. Physics of Fluids, 13:2710–2720, November 1970. doi: 10.1063/1.1692854.

L. O. Drury and J. H. Völk. Hydromagnetic shock structure in the presence of cosmic rays. ApJ, 248:344–351, August 1981. doi: 10.1086/159159.

R. Dung and R. Schlickeiser. The influence of the Alfvenic cross and magnetic helicity on the cosmic ray transport equation. I - Isospectral slab turbulence. A&A, 240:537–540, December 1990.

J. A. Earl. Diffusion of Charged Particles in a Random Magnetic Field. ApJ, 180:227–238, February 1973. doi: 10.1086/151957.

B. Einfeldt. On Godunov-Type Methods for Gas Dynamics. SIAM Journal on Numerical Analysis, 25:294–318, April 1988. doi: 10.1137/0725021.

A. J. Farmer and P. Goldreich. Wave Damping by Magnetohydrodynamic Turbulence and Its Effect on Cosmic-Ray Propagation in the Interstellar Medium. ApJ, 604:671–674, April 2004. doi: 10.1086/382040.

E. A. Foote and R. M. Kulsrud. Hydromagnetic waves in high Beta plasmas. ApJ, 233:302–316, October 1979. doi: 10.1086/157391.

P. Girichidis, T. Naab, S. Walch, M. Hanasz, M.-M. Mac Low, J. P. Ostriker, A. Gatto, T. Peters, R. Wünsch, S. C. O. Glover, R. S. Klessen, P. C. Clark, and C. Baczynski. Launching Cosmic-Ray-driven Outflows from the Magnetized Interstellar Medium. ApJ, 816:L19, January 2016. doi: 10.3847/2041-8205/816/2/L19.

N. Y. Gnedin. On the Proper Use of the Reduced Speed of Light Approximation. ApJ, 833:66, December 2016. doi: 10.3847/1538-4357/833/1/66.

N. Y. Gnedin and T. Abel. Multi-dimensional cosmological radiative transfer with a Variable Eddington Tensor formalism. New A, 6:437–455, October 2001. doi: 10.1016/S1384-1076(01)00068-9.

P. Goldreich and S. Sridhar. Toward a theory of interstellar turbulence. 2: Strong alfvenic turbulence. ApJ, 438:763–775, January 1995. doi: 10.1086/175121.

F. Guo and S. P. Oh. Feedback heating by cosmic rays in clusters of galaxies. MNRAS, 384:251–266, February 2008. doi: 10.1111/j.1365-2966.2007.12692.x.

M. Hanasz, H. Lesch, T. Naab, A. Gawryszczak, K. Kowalik, and D. Wóltański. Cosmic rays can drive strong outflows from gas-rich high-redshift disk galaxies. ApJ, 777(2):L38, 2013.

Amiram Harten, Peter D. Lax, and Bram van Leer. On upstream differencing and godunov-type schemes for hyperbolic conservation laws. SIAM Review, 25(1):35–61, 1983. doi: 10.1137/1025002.

Joseph V. Hollweg. Nonlinear Landau Damping of Alfvén Waves. Phys. Rev. Lett., 27:1349–1352, November 1971. doi: 10.1103/PhysRevLett.27.1349.

P. A. Isenberg. A hemispherical model of anisotropic interstellar pickup ions. J. Geophys. Res., 102:4719–4724, March 1997. doi: 10.1029/96JA03671.

S. Jacob and C. Pfrommer. Cosmic ray heating in cool core clusters - I. Diversity of steady state solutions. MNRAS, 467:1449–1477, May 2017. doi: 10.1093/mnras/stx131.

S. A. Jacques. Momentum and energy transport by waves in the solar atmosphere and solar wind. ApJ, 215:942–951, August 1977. doi: 10.1086/155430.

Y.-F. Jiang and S. P. Oh. A New Numerical Scheme for Cosmic-Ray Transport. ApJ, 854:5, February 2018. doi: 10.3847/1538-4357/aaa6ce.

T. W. Jones. Alfven wave transport effects in the time evolution of parallel cosmic-ray-modified shocks. ApJ, 413:619–632, August 1993. doi: 10.1086/173031.

A. J. Klimas and G. Sandri. Foundation of the Theory of Cosmic-Ray Transport in Random Magnetic Fields. ApJ, 169:41, October 1971. doi: 10.1086/151116.

C.-M. Ko. A note on the hydrodynamical description of cosmic ray propagation. A&A, 259: 377–381, June 1992.

R. Kulsrud and W. P. Pearce. The Effect of Wave-Particle Interactions on the Propagation of Cosmic Rays. ApJ, 156:445, May 1969. doi: 10.1086/149981.

R. M. Kulsrud. Plasma Physics for Astrophysics. Princeton University Press, 2004. doi: 10.1017/S0022112005006737.

A. Lazarian and A. Beresnyak. Cosmic ray scattering in compressible turbulence. MNRAS, 373:1195–1202, December 2006. doi: 10.1111/j.1365-2966.2006.11093.x.

J. A. le Roux and G. M. Webb. A Focused Transport Approach to the Time-dependent Shock Acceleration of Solar Energetic Particles at a Fast Traveling Shock. ApJ, 746:104, February 2012. doi: 10.1088/0004-637X/746/1/104.

Martin A. Lee and Heinrich J. Völk. Damping and Non-Linear Wave-Particle Interactions of Alfvén-Waves in the Solar Wind. Ap&SS, 24:31–49, September 1973. doi: 10.1007/BF00648673.

I. Lerche. Unstable Magnetosonic Waves in a Relativistic Plasma. ApJ, 147:689, February 1967. doi: 10.1086/149045.

Yoram Lithwick and Peter Goldreich. Compressible Magnetohydrodynamic Turbulence in Interstellar Plasmas. ApJ, 562:279–296, November 2001. doi: 10.1086/323470.

Y. E. Litvinenko and P. L. Noble. A Numerical Study of Diffusive Cosmic-Ray Transport with Adiabatic Focusing. ApJ, 765:31, March 2013. doi: 10.1088/0004-637X/765/1/31.

Y. E. Litvinenko and P. L. Noble. Comparison of the telegraph and hyperdiffusion approximations in cosmic-ray transport. Physics of Plasmas, 23(6):062901, June 2016. doi: 10.1063/1.4953564.

Y. E. Litvinenko and R. Schlickeiser. The telegraph equation for cosmic-ray transport with weak adiabatic focusing. A&A, 554:A59, June 2013. doi: 10.1051/0004-6361/201321327.

R. B. Lowrie, J. E. Morel, and J. A. Hittinger. The coupling of radiation and hydrodynamics. The Astrophysical Journal, 521(1):432, 1999.

M. A. Malkov and R. Z. Sagdeev. Cosmic Ray Transport with Magnetic Focusing and the Telegraph Model. ApJ, 808:157, August 2015. doi: 10.1088/0004-637X/808/2/157.

J. F. McKenzie and R. A. B. Bond. The role of non-linear Landau damping in cosmic ray shock acceleration. A&A, 123:111–117, June 1983.

C. D. Meyer, D. S. Balsara, and T. D. Aslam. A stabilized Runge-Kutta-Legendre method for explicit super-time-stepping of parabolic and mixed equations. Journal of Computational Physics, 257:594–626, January 2014. doi: 10.1016/j.jcp.2013.08.021.

D. Mihalas and R. I. Klein. On the Solution of the Time-Dependent inertial-Frame Equation of radiative Transfer in Moving Media to O(v/c). Journal of Computational Physics, 46(1): 97 – 137, 1982. ISSN 0021-9991. doi: https://doi.org/10.1016/0021-9991(82)90007-9.

D. Mihalas and B. Weibel Mihalas. Foundations of radiation hydrodynamics. Oxford University Press, 1984.

J. A. Miller. Magnetohydrodynamic turbulence dissipation and stochastic proton acceleration in solar flares. ApJ, 376:342–354, July 1991. doi: 10.1086/170284.

M. Padovani and D. Galli. Cosmic-Ray Propagation in Molecular Clouds. In D. F. Torres and O. Reimer, editors, Cosmic Rays in Star-Forming Environments, volume 34 of Astrophysics and Space Science Proceedings, page 61, 2013. doi: 10.1007/978-3-642-35410-6_6.

P. P. Papadopoulos, W.-F. Thi, F. Miniati, and S. Viti. Extreme cosmic ray dominated regions: a new paradigm for high star formation density events in the Universe. MNRAS, 414: 1705–1714, June 2011. doi: 10.1111/j.1365-2966.2011.18504.x.

E. N. Parker. The Dynamical State of the Interstellar Gas and Field. ApJ, 145:811, September 1966. doi: 10.1086/148828.

C. Pfrommer, R. Pakmor, K. Schaal, C. M. Simpson, and V. Springel. Simulating cosmic ray physics on a moving mesh. MNRAS, 465:4500–4529, March 2017. doi: 10.1093/mnras/stw2941.

M. S. Potgieter. Solar Modulation of Cosmic Rays. Living Reviews in Solar Physics, 10:3, June 2013. doi: 10.12942/lrsp-2013-3.

S. Recchia, P. Blasi, and G. Morlino. Cosmic ray driven Galactic winds. MNRAS, 462:4227–4239, November 2016. doi: 10.1093/mnras/stw1966.

L. F. S. Rodrigues, G. R. Sarson, A. Shukurov, P. J. Bushby, and A. Fletcher. The Parker Instability in Disk Galaxies. ApJ, 816:2, January 2016. doi: 10.3847/0004-637X/816/1/2.

M. Salem and G. L. Bryan. Cosmic ray driven outflows in global galaxy disc models. MNRAS, 437:3312–3330, February 2014. doi: 10.1093/mnras/stt2121.

R. Schlickeiser. Cosmic-ray transport and acceleration. I - Derivation of the kinetic equation and application to cosmic rays in static cold media. II - Cosmic rays in moving cold media with application to diffusive shock wave acceleration. ApJ, 336:243–293, January 1989. doi: 10.1086/167009.

J. Seo, H. Kang, and D. Ryu. The Contribution of Stellar Winds to Cosmic Ray Production. Journal of Korean Astronomical Society, 51:37–48, April 2018. doi: 10.5303/JKAS.2018.51.2.37.

A. Shalchi. Second-order quasilinear theory of cosmic ray transport. Physics of Plasmas, 12 (5):052905–052905, May 2005. doi: 10.1063/1.1895805.

A. Shalchi, editor. Nonlinear Cosmic Ray Diffusion Theories, volume 362 of Astrophysics and Space Science Library, 2009. doi: 10.1007/978-3-642-00309-7.

A. Shalchi and R. Schlickeiser. Evidence for the Nonlinear Transport of Galactic Cosmic Rays. ApJ, 626:L97–L99, June 2005. doi: 10.1086/431905.

P. Sharma, P. Colella, and D. F. Martin. Numerical implementation of streaming down the gradient: Application to fluid modeling of cosmic rays and saturated conduction. SIAM Journal on Scientific Computing, 32(6):3564–3583, 2010. doi: 10.1137/100792135.

J. Skilling. Cosmic Rays in the Galaxy: Convection or Diffusion? ApJ, 170:265, December 1971. doi: 10.1086/151210.

J. Skilling. Cosmic ray streaming. I - Effect of Alfven waves on particles. MNRAS, 172: 557–566, September 1975. doi: 10.1093/mnras/172.3.557.

Roberto Soler, Jaume Terradas, Ramon Oliver, and Jose Luis Ballester. The role of Alfvén wave heating in solar prominences. A&A, 592, July 2016. doi: 10.1051/0004-6361/201628722.

P. A. Sturrock. Plasma Physics: An Introduction to the Theory of Astrophysical, Geophysical and Laboratory Plasmas. Cambridge University Press, 1994. doi: 10.1017/CBO9781139170598.

R. C. Tautz and I. Lerche. Application of the three-dimensional telegraph equation to cosmic-ray transport. Research in Astronomy and Astrophysics, 16:162, October 2016. doi: 10.1088/1674-4527/16/10/162.

R. C. Tautz and A. Shalchi. On the widespread use of the Corrsin hypothesis in diffusion theories. Physics of Plasmas, 17:122313, December 2010. doi: 10.1063/1.3530185.

R. C. Tautz, A. Shalchi, and R. Schlickeiser. Semi-Quasi-Linear Description of Cosmic-Ray Perpendicular Transport. ApJ, 672:642–649, January 2008. doi: 10.1086/524126.

R. C. Tautz, A. Dosch, F. Effenberger, H. Fichtner, and A. Kopp. Pitch-angle scattering in magnetostatic turbulence. I. Test-particle simulations and the validity of analytical results. A&A, 558:A147, October 2013. doi: 10.1051/0004-6361/201322142.

A. Teufel and R. Schlickeiser. Analytic calculation of the parallel mean free path of heliospheric cosmic rays. I. Dynamical magnetic slab turbulence and random sweeping slab turbulence. A&A, 393:703–715, October 2002. doi: 10.1051/0004-6361:20021046.

T Thomas and C. Pfrommer. Cosmic-ray hydrodynamics: Alfvén-wave regulated transport of cosmic rays. ArXiv e-prints, art. arXiv:1805.11092, May 2018.

M. Uhlig, C. Pfrommer, M. Sharma, B. B. Nath, T. A. Enßlin, and V. Springel. Galactic winds driven by cosmic ray streaming. MNRAS, 423:2374–2396, July 2012. doi: 10.1111/j.1365-2966.2012.21045.x.

B. Vaidya, D. Prasad, A. Mignone, P. Sharma, and L. Rickler. Scalable explicit implementation of anisotropic diffusion with Runge-Kutta-Legendre super-time stepping. MNRAS, 472:3147–3160, December 2017. doi: 10.1093/mnras/stx2176.

B. Van Leer. Towards the ultimate conservative difference scheme. Journal of Computational Physics, 135(2):229–248, 1997.

H. J. Völk and J. F. McKenzie. Characteristics of cosmic ray shocks in the presence of wave dissipation. International Cosmic Ray Conference, 9:246–249, January 1981.

G. B. Whitham. Group velocity and energy propagation for three dimensional waves. Communications on Pure and Applied Mathematics, 14(3):675–691, 1961. doi: 10.1002/cpa.3160140337.

J. Wiener, S. P. Oh, and F. Guo. Cosmic ray streaming in clusters of galaxies. MNRAS, 434:2209–2228, September 2013. doi: 10.1093/mnras/stt1163.

J. Wiener, C. Pfrommer, and S. P. Oh. Cosmic ray-driven galactic winds: streaming or diffusion? MNRAS, 467:906–921, May 2017. doi: 10.1093/mnras/stx127.

H. Yan and A. Lazarian. Cosmic Ray Transport Through Gyroresonance Instability in Compressible Turbulence. ApJ, 731:35, April 2011. doi: 10.1088/0004-637X/731/1/35.

G. P. Zank. Transport Processes in Space Physics and Astrophysics, volume 877 of Lecture Notes in Physics, Berlin Springer Verlag. Berlin Springer Verlag, 2014. doi: 10.1007/978-1-4614-8480-6.

G. P. Zank, J. Y. Lu, W. K. M. Rice, and G. M. Webb. Transport of energetic charged particles in a radial magnetic field. Part 1. Large-angle scattering. Journal of Plasma Physics, 64:507–541, November 2000. doi: 10.1017/S0022377800008709.

E. G. Zweibel. The microphysics and macrophysics of cosmic raysa). Physics of Plasmas, 20(5):055501, May 2013. doi: 10.1063/1.4807033.

E. G. Zweibel. The basis for cosmic ray feedback: Written on the wind. Physics of Plasmas, 24(5):055402, May 2017. doi: 10.1063/1.4984017.

Selbstständigkeitserklärung

Hiermit versichere ich, dass ich diese Arbeit selbständig verfasst und keine anderen als die von mir angegebenen Quellen und Hilfsmittel genutzt habe.

Timon Thomas